Insight into Quantitation of Solid-phase Microextraction

by

Md. Nazmul Alam

A thesis

presented to the University of Waterloo

in fulfillment of the

thesis requirement for the degree of

Doctor of Philosophy

in

Chemistry

Waterloo, Ontario, Canada, 2016

Author's Declaration

I hereby declare that I am the sole author of this thesis. This is a true copy of the thesis, including any required final revisions, as accepted by my examiners.

I understand that my thesis may be made electronically available to the public.

Abstract

Solid-phase microextraction (SPME) is a well-known sampling and sample preparation technique used for a wide variety of analytical applications. As there are various complex processes taking place at the time of extraction that influence the parameters of optimum extraction, a mathematical model and computational simulation describing the SPME process is required for experimentalists to understand and implement the technique without performing multiple costly and time-consuming experiments in the laboratory. In this thesis, a mechanistic mathematical model for the processes occurring in SPME extraction of analyte(s) from an aqueous sample medium is presented. The proposed mechanistic model was validated with experimental data. Several key factors that affect the extraction kinetics, such as sample agitation, fiber coating thickness, and presence of a binding matrix component, are discussed. More interestingly, for the first time, shorter or longer equilibrium times in the presence of a binding matrix component were explained with the help of an asymptotic analysis. Parameters that contribute to the variation of the equilibrium times are discussed, with the assumption that one binding matrix component is present in a static sample. Numerical simulation results show that the proposed model captures the phenomena occurring in SPME, leading to a clearer understanding of this process. Therefore, the currently presented model can be used to identify optimum experimental parameters without the need to perform a large number of experiments in the laboratory.

A calibration approach based on standard chemicals loaded onto an extraction phase (calibrant-loaded extraction phase, CL-EP) has gained popularity in various areas of sample analysis, such as environmental, toxicological, and tissue sampling research areas. In this thesis, the kinetics of calibrant release and analyte uptake between the sample and extraction phase with

a finite-element analysis (FEA) using COMSOL Multiphysics® software package. Effect of finite and infinite sample volume conditions, as well as various sample environment parameters such as fluid flow velocity, temperature, and presence of a binding matrix component were investigated in detail with the model in relation to the performance of the calibration. The simulation results demonstrate the suitability of the CL-EP method for analysis of samples at various sample environments. The calibrant-loaded approach can provide both total and free concentrations from a single experiment based on whether the K_{es} value being used is measured in a matrix-matched sample or in a matrix-free sample, respectively. Total concentrations can also be obtained by utilizing CL-EP in combination with external matrix-matched calibration, which can be employed to automate the sampling process and provide corrections for variations in sample preparation, matrix effects, and detection processes. This approach is also suitable for very small volumes of sample, where addition of an internal standard in the sample is either troublesome or can change the sample characteristics. Although the outcome of this study is applicable to any sampler based on calibrant-loaded liquid or solid extraction phase method, experimental data using a solid-phase microextraction (SPME) sampler was used to fit our simulation results. The numerical results are in very good agreement with the experimental data reported previously. Moreover, the computational model and numerical simulation presented will aid in the optimization of sampler design and sampling parameters prior to laboratory experiments, which will translate into savings in terms of time and expensive chemicals.

Despite the prevalence of porous-particle based coatings used for microextraction techniques, there is inadequate understanding of how extraction parameters influence the extracted amount and quantification of analytes. This is particularly important when extraction is performed with

these solid coatings under pre-equilibrium conditions, for instance, with diffusion based rapid calibration approach which is a popular technique for on-site chemical analysis for not requiring any calibration method or internal standards. This study presents a computational model for porous particle-based coatings used in solid phase microextraction. Although the model describes extraction behavior of analytes for both kinetic and equilibrium regime of extraction profile, the critical parameters for the diffusion based rapid sampling were studied using the developed model. Simulations are conducted under variations in both mass transfer and adsorptive surface binding constants, coating capacity, constrained by real-world experimental conditions of finite and infinite sample volume. The model simulation results demonstrated excellent correlation with previously reported experimental data and superior to previous semi-empirical models.

In the last chapter of the thesis, a novel SPME coating functionalized with a DNA aptamer for selective enrichment of a low abundance protein from diluted human plasma is described. This approach is based on the covalent immobilization of an aptamer ligand on electrospun microfibers made with the hydrophilic polymer poly(acrylonitrile-co-maleic acid) (PANCMA) on stainless steel rods. A plasma protein, human alpha-thrombin, was employed as a model protein for selective extraction by the developed Apt-SPME probe, and the detection was carried out with liquid chromatography/ tandem mass spectrometry (LC–MS/MS). The SPME probe exhibited highly selective capture, good binding capacity, high stability and good repeatability for the extraction of thrombin. The protein selective probe was employed for direct extraction of thrombin from 20-fold diluted human plasma samples without any other purification. The Apt-SPME method coupled with LC–MS/MS provided a good linear dynamic range of 0.5–50 nM in diluted human plasma with a good correlation coefficient ($R^2 = 0.9923$), and the detection limit of the proposed

method was found to be 0.30 nM. Finally, the Apt-SPME coupled with LC–MS/MS method was successfully utilized for the determination of thrombin in clinical human plasma samples. One shortcoming of the method is its reduced efficiency in undiluted human plasma compared to the standard solution. Nevertheless, this new aptamer affinity-based SPME probe opens up the possibility of selective enrichment of a given targeted protein from complex sample either in vivo or ex vivo.

Acknowledgements

First of all, I am grateful to the Almighty Creator and Sustainer for helping me all the way to accomplish this thesis.

I would like to thank my supervisor, Professor Janusz Pawliszyn, for his guidance throughout my PhD studies with an interesting and challenging project.

I am thankful to all my committee members, Professor Mario A. Monteiro, Professor Michael Tam, Dr. Juewen Liu for their effort to improve my research journey by providing thoughtful suggestions. I would also like to thank my external examiner, Professor Steve Weber of university of Pittsburgh, and internal examiner, Dr. Luis Ricardez Sandoval, for their constructive suggestion to improve the thesis.

I would also like to thank my colleagues in Prof. Pawliszyn's group for their support and help. Finally, I would like to thank my wife, Munira Hoque, and sons, Musaid Aldin, Muaz Alam, Mahir Alam and Mahad Alam for their love, care, support, prayer and encouragement.

Dedication

To my grandparents:

Mazharul Islam; Meher-un-nesa

&

Parents:

Md. Abdul Matin; Nurjahan begum

The care, guidance, patience and love that help me to shape who I am today.

Table of content

List of figures

List of abbreviations

BSA	Bovine serum albumin
CA	Concentration of free analyte
CB	Concentration of free binding
CE	Collision-induced dissociation energies
DP	Declustering potential
EIC	Extract ion chromatogram
EP	Entrance potential
FEA	Finite-element analysis
FEM	Finite element method
GC	Gas chromatograph
HPLC	High pressure liquid chromatography
HSA	Human serum albumin
LBL	Lampire Biological Laboratories
MA	Maleic acid
MRM	Multiple reaction monitoring
PAH	Polycyclic aromatic hydrocarbons
PBS	Phosphate buffered saline
RSD	Relative standard deviations
SEM	Scanning electron microscope
SPMD	Semipermeable Membrane Device
TWA	Time-weighted average

List of symbols

Symbol	Name
M	Stiff-spring velocity
$C_A{}^s$	Analyte concentration in solution
k_a	Association rate constant
K_d	Dissociation rate constant
K_{es}	Partition coefficient
$D_A{}^s$	Diffusion coefficient of analyte in solution
$D_A{}^f$	Diffusion coefficient of analyte in fiber
C_B	Bound analyte concentration
D_{BS}	Diffusion coefficient of the complex in solution
B	Diameter of the fiber core
A	Thickness of the fiber coating
P	Density of water
μ	Dynamic viscosity of water
R	Radius of the magnetic stirrer
L	Radius of the sample container

Chapter 1   **General introduction**

1.1   Solid-phase microextraction (SPME)

SPME presents many advantages over conventional sampling and sample preparation methods by combining sampling, sample preparation, and direct transfer of the analytes into a standard gas chromatograph (GC) or directly to a mass spectrometry.[1-3] Since its introduction in the early 1990s, SPME has been successfully applied to various applications, such as bioanalysis, environmental analysis,[4] food analysis etc.[5-7]

The fundamental of the SPME technique is based on exposing a small amount of extraction phase (extractant) to a sample for a predetermined length of time. The transport of analytes from the sample matrix to the extractant occurs immediately after contact between the two phases (Figure 1-1). The transport is mainly governed by the preferential affinity of the analytes to the extractant.[8] The higher the affinity the analyte has for the extractant relative to the sample matrix, the greater the uptake amount of analyte. If the SPME extractant is exposed for long enough to attain a concentration equilibrium between the extractant and sample, the net uptake amount remains unchanged after the equilibration is reached. Therefore, in SPME, the goal is not to extract 100% of the analyte from a sample unlike other conventional sample preparation techniques.
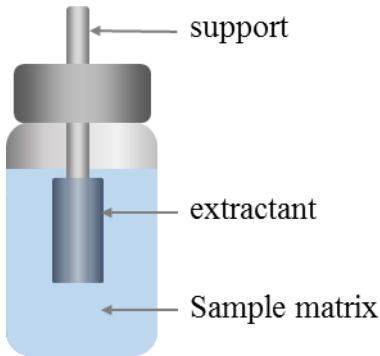
Figure 1-1. Schematic representation of a basic format of SPME technique.

The time to reach the extraction equilibrium is dependent on the sample agitation conditions, physicochemical properties of the sample matrix, partition coefficient of analyte between the extractant and sample matrix, and the physical dimensions of the sample matrix and the extractant.[9]

The partitioning is a thermodynamic phenomenon defined as the distribution of a chemical between two immiscible solvents, such as aqueous and organic phases, at equilibrium.[10] The partitioning coefficient P can be expressed as:

$$P = \frac{C_{org.}}{C_{aq.}} \qquad \text{1-1}$$

where $C_{org.}$ and $C_{aq.}$ are the concentration of a given chemical in the organic and aqueous phase, at the organic-aqueous interface. In practice, partitioning of chemicals is studied in the octanol/water system and is expressed by a logarithm of P, log$P$. In general, log$P$ is a measure of hydrophobicity or lipophilicity of compounds. This partitioning concept is employed in the SPME and can be described as:

2

$$K_{es} = \frac{C_e^{eq}}{C_s^{eq}} \qquad\qquad 1\text{-}2$$

where K_{es} is the partition coefficient or distribution coefficients utilized in the SPME, $C_e{}^{eq}$ and $C_s{}^{eq}$ are the equilibrium concentrations of a given analyte in the extractant and sample solution, respectively.

A typical profile obtained for the extraction amount by the extractant with respect to the exposure time is shown in Figure 1-2 . The profile can be distinguished into three regimes: (I) the amount of analyte extracted increases linearly with time, which is generally consider to obtain within 50% of equilibrium extracted amount, (II) the extracted amount increases significantly but not linearly, which is considered as the kinetic part of the profile, and (III) the extraction is assumed to reach at equilibrium.
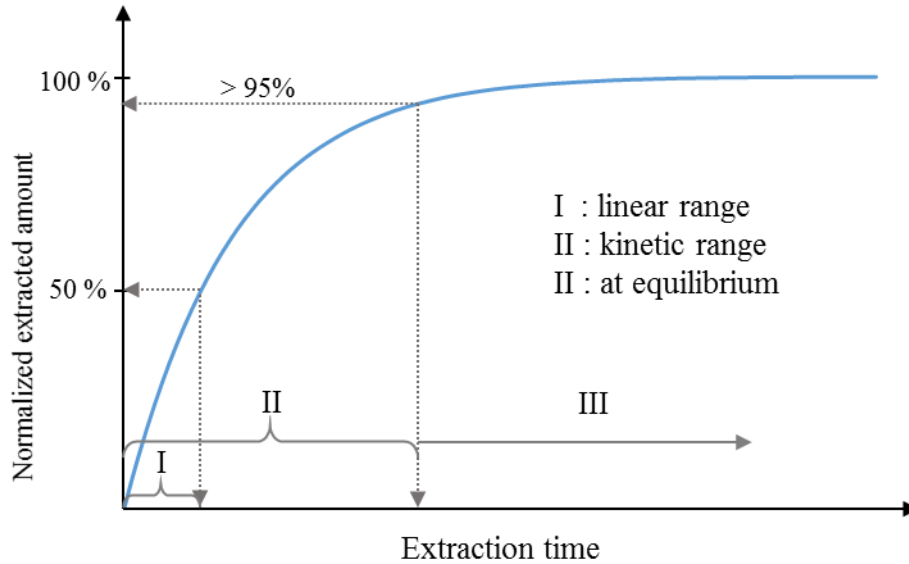
Figure 1-2. A typical extraction time profile obtained from an SPME device.

1.2 Equilibrium Extraction

If the SPME extractant is exposed into a sample matrix for enough time so as to reach a concentration equilibrium, the mass balance in a simple two phase system (see Figure 1-1) can be described by as:

$$C_s^0 V_s = C_s^{eq} V_s + C_e^{eq} V_e \qquad \qquad \text{1-3}$$

where C_s^0 is the initial concentration of an analyte in the sample, V_s is the sample volume, V_e is the volume of extraction phase, C_s^{eq} is the equilibrium concentration of the analyte in the sample and C_e^{eq} is the equilibrium concentration of the analyte in the extraction phase. Combination of eq. 1-2 and eq. 1-3 results in:

$$n^{eq} = \frac{K_{es}V_eV_s}{K_{es}V_e + V_s}C_s^0 \qquad\qquad 1\text{-}4$$

where n^{eq} is the quantity (mole or gram) of analyte extracted by the extraction phase. As shown in eq. 1-4, the n^{eq} is linearly proportional to the analyte concentration in the sample (C_s^0), which is the analytical basis for quantification at the equilibration stage of a SPME method.

For in vivo or on site application,[11-13] where the analyte sample volume is very large compared to the extraction phase, $V_s >> K_{es}V_e$, eq. 1-4 can be written as:

$$n^{eq} = K_{es}V_eC_s^0 \qquad\qquad 1\text{-}5$$

This equation describes two important features of SPME methods. The first one is the extraction phase can be exposed directly to the ambient air, water, production stream, etc. without necessary to collect definite amount of sample. Secondly, by knowing the K_{es}, the concentration of analyte can be determined by the amount extracted at equilibrium. This mode of quantification does not require any external calibrations that slow down the analytical process, and introduce additional errors. This feature of SPME is highly desirable for field analysis.

1.3   Pre-equilibrium Extraction: controlled by only diffusion of analyte in the boundary layer

The equilibrium mode of extraction provides the highest sensitivity of a SPME method by extracting maximum amount of analyte from the sample. However, if sensitivity is not a major concern of an analysis, extraction can be stopped before reaching the equilibrium.[14] At this pre-equilibrium condition, analyte quantification is only possible if the uptake amount of analyte is directly proportional to its initial concentration in a sample matrix. To investigate whether the

relationship between the extracted amount and initial concentration is linear in pre-equilibrium situations, the dynamic process of the SPME needs to be studied. Mathematical models developed to describe the linear relationship is discussed in the next sections.

1. 3. 1. Diffusion based model

A theoretical description of the dynamic process of SPME was first reported by Louch et al.[15] The model assumed a cylindrical extraction phases coated onto a solid support and analyte migration occurs only owing to their diffusion from the bulk sample matrix to the SPME coating and inside the coating.[15-18] The rate of analyte transport to the coating surface should be balanced by an equal rate of diffusion from the coating surface to the inner layer of the coating. This diffusion-based extraction dynamics can be described by Fick's Second law expressed as[19,20]:

$$\frac{\partial C(r,t)}{\partial t} = D \frac{1}{r}\left[\frac{\partial}{\partial r}\left(r\frac{\partial C(r,t)}{\partial r}\right)\right] \qquad 1\text{-}6$$

where D is the diffusion coefficient of the analyte in the sample matrix (D_s) or in the extractant (D_e), $\partial C/\partial x$ is the concentration gradient and C_s and C_e are concentrations of the analyte in the sample matrix and extractant, respectively. The solutions of the diffusion equations were obtained under two different extreme and one practical boundary conditions. In one extreme condition, the convection in the sample phase is so rapid that, the kinetic of extraction is determined entirely by the diffusion of the analyte in the extraction phase. Under this condition, the equilibration time, t_{eq}, corresponds to:

$$t_{eq} \approx t_{95\%} = \frac{2L^2}{D_e} \qquad 1\text{-}7$$

where L is the thickness of the coating, and D_e is the analyte diffusion coefficient in the extraction phase. The other extreme condition assumes that there is no convection in the sample so that the analytes must diffuse through an ever-broadening analytes-depleted layer in the sample phase and through the fiber coating.[21,22] In this case, the equilibrium time is significantly longer because the mass transfer of analytes from the progressively thicker boundary layer to the fiber coating determines overall extraction speed. In a practical agitation condition, it was assumed that there is always a thin layer of concentration boundary layer around the fiber in which no convection occurs. However, this is not a realistic condition since flow velocity gradient is always present at the proximity of a surface under an agitated environment.[23][24]When the extraction rate is determined by the diffusion in the boundary layer, equilibration time can be estimated from the equation below:

$$t_{eq} \approx t_{95\%} = \frac{3\delta_s K_{es} L}{D_s}$$

1-8

where δ_s is the thickness of the aqueous boundary layer, K_{es} is the partition coefficient. The thickness of the boundary layer (δ_s) is a function of some factors such as, the geometric configuration of the extractant, the sample agitation condition, temperature, and D_s of analyte. The average value of δ_s for a cylindrical SPME fiber geometry can be calculated by using eq. 1-9, originally developed for heat transfer model[25]:

$$\delta_s = 9.52(\frac{b}{Re^{0.62}Sc^{0.38}})$$

1-9

7

where Re is the Reynolds number (equal to $2ub/v$, $\mathbf{u}$ is the linear sample velocity, v is the kinematic viscosity of the matrix, b is the outside radius of the fiber coating), and Sc is the Schmidt number $= v/D_s$.

Although the model described extraction time profiles of SPME processes, a mathematical expression that relates the amount of analyte extracted by the coating and its initial concentration (the relationship is called "calibration") in the sample matrix was not presented.

1. 3. 2. Interface model

Koziel et al.,[26] developed the first calibration model based on the initial regime of extraction profile (I, in Figure 1-2), where the rate of analyte uptake is determined only by the diffusion coefficients of analytes through the boundary layer around the extractant. The schematic representation of mass transfers is illustrated in Figure 1-3 for a cylindrical geometry of the extraction phase coated on the supporting rod.
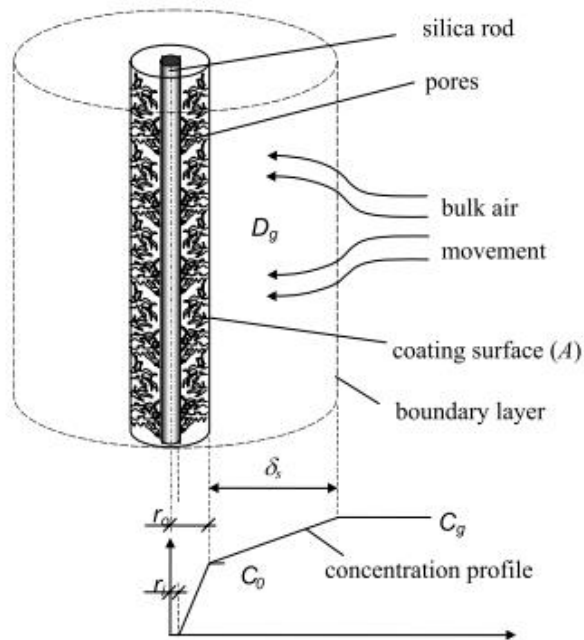
Figure 1-3. Schematic diagram of the calibration model based on diffusion through the boundary layer. Reprinted with permission from[26]. Copyright (2000) American Chemical Society.

The model assumes that analyte concentration in the bulk of the sample is constant during the short sampling time and there is a constant convective supply of analyte. In addition, the volume of the sample is considered much greater than the volume of the extractant so that the analyte uptake does not affect the bulk sample concentration. The extractant is also assumed to behave like a "perfect sink", which means the extraction is instantaneous and essentially irreversible. This perfect sink condition can only be satisfied when analyte concentration on the coating is such a low value compared to the equilibrium amount that this can be assumed to be negligible.[27-29] The

function describing the extracted amount of analyte with the sampling time can be derived by the following equation:

$$n = \frac{BAD_s}{\delta_s} \int_0^t C_s(t)dt \qquad \qquad 1\text{-}10$$

where n is the extracted amount (ng) of analyte at time t, D_s is the diffusion coefficient of a given analyte in sample, A is the outer surface area of the coating, δ_s is the thickness of the aqueous boundary layer, B is a geometric factor is a geometric factor referring to the geometry extractant, for a cylindrical geometry, the value is 3, and C_s is the analyte concentration in the sample. Since, the analyte concentration is assumed to be constant for very short sampling times, eq. 1-10 can be reduced to:

$$n = \frac{BAD_s}{\delta_s} C_s^0 t \qquad \qquad 1\text{-}11$$

Equation 1-11 shows that the extracted amount is proportional to the sampling time (t), diffusivity (D_s) for each analyte, and the bulk sample concentration (C_s^0) and inversely proportional to δ_s. Therefore, an analyte with a greater D_s will transport faster through the interface and reach the extractant. It should be noted that the values of D_s for the target analytes can be found in the literature or estimated from physicochemical properties. The above model enables quantitative analysis at the first linear regime of the pre-equilibrium extraction profile in SPME.

However, the effective thickness of the boundary layer in eq. 1-9 is an average estimate that does not account for changes with respect to the formation of wakes behind the extraction phase for unidirectional fluid flow.[30-32] Moreover, the boundary layer thickness decreases by increasing the sample flow velocity or by increasing the sample temperature. Increasing the temperature will,

however, reduce the partition coefficient (K_{es}).[33] As a result, the extractant might not be able to extract all of the analyte molecules reaching its surface, which means the extractant is no longer a "perfect sink" for all of the analytes.

1. 3. 3. Cross-flow Model

Chen et al[34] proposed another diffusion-based calibration model by considering actual swirl flow around the extraction phase shown in Figure 1-4.
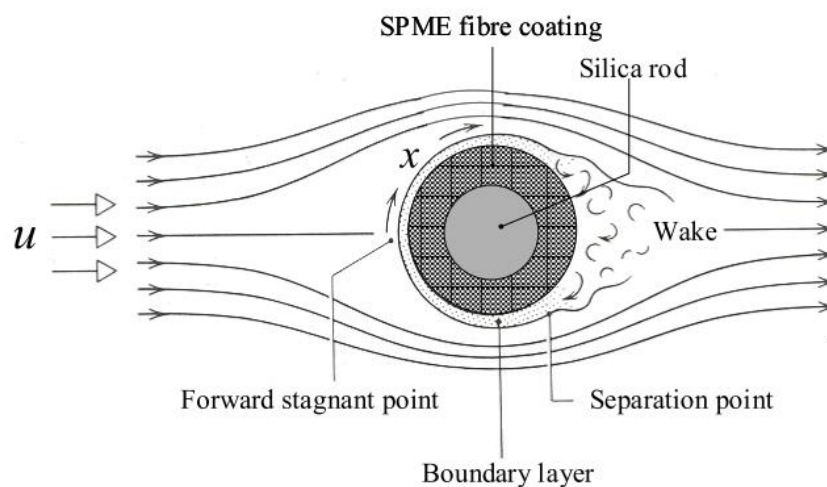
Figure 1-4. Schematic of linear flow of the sample in the direction normal to the cylindrical extractant, assumed in the cross flow model. Reprinted with permission from[34] Copyright (2003) American Chemical Society.

With this model, the target analyte concentration is related to the extracted amount of analyte by the eq.1-12[35]:

$$C_s^0 = \frac{n}{k_m A t} = \frac{nb}{E Re^m Sc^{1/3} A D_s t} \qquad \text{1-12}$$

where n the extracted amount at sampling time t, A is the surface area of the cylindrical extractant (fiber), D_s the diffusion coefficient of the analyte in sample, k_m the average mass-transfer coefficient, b the outer diameter of the fibre, Re the Reynolds number and Sc is the Schmidt number. Constants E and m are dependent on the Reynolds number and are available in the literature. An important constraints of diffusion based calibration technique is that the flow velocity or agitation of the sample matrix must be controlled so as to maintain a fixed diffusion layer thickness.[36] Sometimes additional equipment such as hand-held-drill is used to control the sample convection.

1. 3. 4. *Fixed diffusion path model*

The extraction phase is retracted a known distance of Z into a housing (a narrow tube or needle) as shown in Figure 1-5. In this configuration, there is no convective flow within the tube (in the Z region) and transport of analytes in this region is controlled by diffusion as described in eq.1-13. If the extractant behaves "perfect sink" for the target analyte, the concentrations of analyte in the sample can be calculated with eq.1-13[26].

$$n = D_s \frac{A}{Z} \int C_s(t)dt \qquad\qquad \text{1-13}$$

where n is the amount of the analyte extracted during time t, C_s is the analyte concentration in sample, A the cross[37]-sectional area of the extractant housing, and D_s the diffusion coefficient of the target analyte in the sample. Because of the presence of a long diffusion path the rate of analyte extraction is very slow in this approach. Thus, this approach is capable of generating a response proportional to the integral of the analyte concentration over time and space. Integrating eq.1-13 for a long period of sampling time provides the following equation:

$$\bar{C} = \frac{nZ}{AD_s t} \qquad\qquad 1\text{-}14$$

where $\bar{C}$ is the time-weighted average (TWA) concentration of the target analyte in the sample. Therefore, the presence of a well-defined diffusion path allows the sampler to utilize the Fick's first law of diffusion directly for calibration and the calculation of $\bar{C}$. Similar to the Interface model and Cross-flow model, the extracted amount is proportional to the molecular diffusion coefficient (D_s).
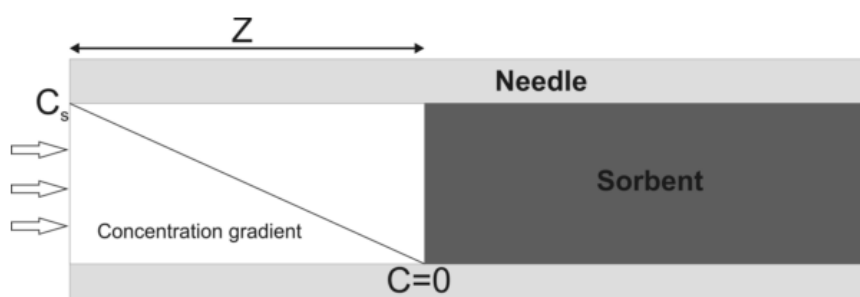
Figure 1-5. Fixed diffusion path model in SPME. Adapted with permission from [38]. Copyright (2003) American Chemical Society.

The fixed diffusion path samplers are mainly used for air or water sampling, since the diffusion coefficients of the analytes are either easy to find in the literature or easy to calculate with empirical equations. Another advantage of this sampler is that the analyte quantification is independent of the face velocity. This technique is very useful for field sampling where the convection conditions of water are very difficult to measure and calibrate.

The analyte extraction rate is much higher for the Interface or Cross-flow models than with the retracted devices since the diffusion boundary layers of the former sampling methods are much

thinner than that of the retracted devices. Thus, the Interface and Cross-flow models are more suitable for fast sampling and impractical to employ for TWA sampling.

In all these three approaches, the quantification is diffusion-based which means no calibration curves or internal standards are needed.[37] This characteristic makes this method especially suitable for on-site analysis where the construction of calibration curves or the addition of internal standards is known to be very difficult.

1.4   Pre-equilibrium extraction: controlled by diffusion and partition

The kinetics of the extraction process determines the speed of extractions. Kinetic theory identifies extraction rate "bottlenecks" in any extraction technique and therefore indicates strategies for increasing the speed of extractions. Besides the SPME approaches, mathematical models have been developed for analysis of the extraction kinetics in other sampling methods such as polyethylene passive samplers,[39] semipermeable membrane devices (SPMDs),[40,41], Chemcatchers[42,43], silicon rubber[44], etc. Theoretical analysis for the effect of fluid velocity,[45-47] temperature,[41] sample volume,[48] thickness of the extractant,[49] have been studied. In all of the models, however, the analyte transport was assumed by the Ficks law by considering one or two compartments. Although, these models are simple to use for simple sample environment, they are far from the real multiphase interaction that occurs between fluid movement, binding phenomena that present in real complex sample matrix.

1. 4. 1. Two compartment model for SPME

Since diffusion alone is a very slow mass transport process, analyte transport in the sample matrix is generally accelerated by agitation or forced convection by various means, such as stirrer

bars and ultrasounds. As a result, a stagnant layer of sample solution parallel and adjacent to the coating surface is developed in which analyte transfer can occur only by diffusion (Figure 1-6).[50,51] This layer is known as a boundary layer or diffusion layer. To solve the eq. 1-6 analytically,[37,52] a steady-state mass transfer is assumed to be established within a constant boundary layer when sufficient convective mass transport is applied in the sample matrix.[53] On the other hand, the steady-state mass transfer is valid within the coating where the diffusion layer thickness is equal to the coating thickness, as the coatings are generally very thin, generally in the range of a few micrometers (7-100 um).
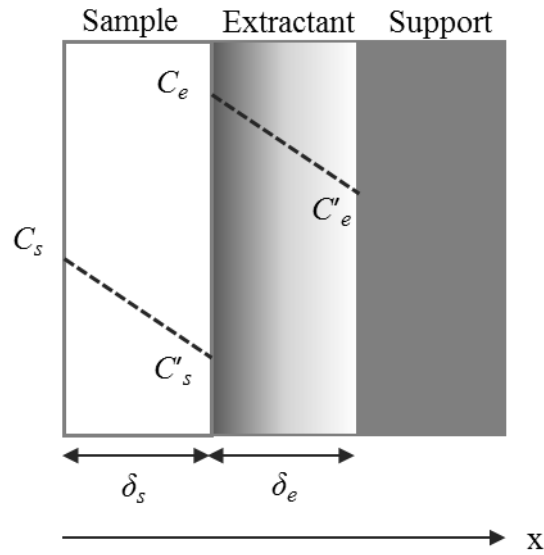
Figure 1-6. Schematics of mass transfer through the two compartment model. At practical agitation condition, a steady-state diffusion is considered. The concentration gradient in the coating is assumed to be linear. Adapted with permission from [53]. Copyright (1997) American Chemical Society.

The abovementioned assumptions provide the following rate of diffusion of analytes, from the edge of the boundary layer to the coating surface, and from the coating surface to the coating's inner layer:

$$\frac{1}{A}\frac{\partial n}{\partial t} = \frac{D_s}{\delta_s}(C_s - C'_s) = \frac{D_e}{\delta_e}(C_e - C'_e) \qquad \text{1-15}$$

where C_s is the analyte concentration at the edge of the boundary layer (bulk concentration), C_s' is the concentration of the analyte at the surface, δ_s is the boundary layer thickness in the sample matrix, δ_e is the thickness of the coating, C_e is the analyte concentration at the coating surface within the coating, and C_e' is the analyte concentration at the innermost layer of the coating. The diffusion rate in eq. 1-15 can be re-expressed with the use of a mass transfer coefficient (k):

16

$$\frac{1}{A}\frac{\partial n}{\partial t} = k_s(C_s - C_s') = k_e(C_e - C_e') \qquad\qquad \text{1-16}$$

where k_s and k_e are the mass-transfer coefficients of the analyte in the sample matrix and extractant, respectively. This mass transfer coefficient, based on a first-order kinetic model for mass transfer of analytes to the SPME coating, is similar to the model used for other passive sampling devices, such as Semipermeable Membrane Device (SPMD) or Polyethylene (PE) -based samplers.[54] It should be emphasized that the concept of diffusion within the coating that is used in the above equations is generally applied for liquid polymeric coatings such as polydimethylsiloxane (PDMS) and PE. However, for solid coatings, for example, PDMS-DVB, and CW-PDMS, the overall sorption is governed by the diffusive mass transfer in the boundary layer coupled with reversible sorption on the coating surface. The overall uptake rate has been empirically shown to be controlled by the diffusive mass transport with the following rate equation:[55]

$$\frac{1}{A}\frac{\partial n}{\partial t} = k_s(C_s - C_s') \qquad\qquad \text{1-17}$$

Solving either of the eq. 1-16 or eq. 1-17 with the initial conditions of $C_s = 0$ at time $(t) = 0$ and by incorporating the concept of partition coefficient (discussed in section 1.1) results in the following non-linear equation:

$$n = [1 - \exp(-a_e t)]\frac{K_{es}V_e V_s}{K_{es}V_e + V_s}C_s^0 \qquad\qquad \text{1-18}$$

where n is the amount of analyte extracted at time t is the extraction time, and a_e is the extraction rate constant that describes how fast equilibrium can be attained. The parameters outside of the third bracket of eq. 1-18 is identical to the eq. 1-4. Therefore, the eq. 1-18 can be simplified to

$$\frac{n}{n^{eq}} = 1 - \exp(-a_e t) \qquad \text{1-19}$$

where n^{eq} is the extracted amount (ng) at equilibrium, and is determined by the mass-transfer coefficients, the distribution constant, as well as the physical dimensions of the sample matrix and the SPME sampler. At equilibrium eq. 1-18 converts to eq. 1-4. Therefore, at pre-equilibrium extraction, the amount of analyte extracted is still a linear with the analyte concentration C_s^0, under the condition that the agitation, the extraction time, and the extraction temperature remain constant.

The model can explain the influence of stirring or agitation on the uptake kinetics and it can also be applied to predict kinetics based on parameters such as the fiber-water partition coefficient, diffusion coefficient, and diffusion layer thickness. A layer thickness for this model can be estimated by assuming that the flow around the SPME fiber is steady and laminar. However, the layer thickness estimate requires additional parameters such as the speed of the fluid at the fiber surface, the fluid's kinematic velocity, and the diffusion coefficient of the analyte in the medium. The disadvantage of the model is that for other agitation conditions such as ultrasound agitation, or agitation by fiber itself, the accelerated flow regimes do not fulfill the requirements for estimating the stagnant layer thickness.

1. 4. 2. One compartment model

Instead of assuming that mass transfer from bulk medium to extractant is controlled by an explicitly modeled stagnant layer around fiber, Vaes et al[56] have introduced the concept that mass

18

transfer is governed by the concentration difference between bulk medium and outer fiber surface. The model assumed a one-compartment system and first-order kinetics and proposed that the concentration on the extractant (C_e) is directly proportional to the sample concentration (C_s), according to

$$\frac{dC_e}{dt} = k_1 C_s - k_2 C_e \qquad\qquad 1\text{-}20$$

Where k_1 and k_2 are the uptake and elimination rate constants, respectively. At equilibrium ($dC_e/dt = 0$), the eq.1-20 turns to

$$\frac{C_e}{C_s} = \frac{k_1}{k_2} = K_{es} \qquad\qquad 1\text{-}21$$

Therefore, the concentration on the SPME fiber at equilibrium can be described by the eq. 1-5. The model was proposed in a sampling condition where the extractant extracts only a negligible amount of the total analyte present in the sample matrix. The advantage of such an approach is its simplicity. The disadvantage is that the model is not explicitly based on processes like diffusion and partitioning of the analyte and on the experimental conditions like medium volume and fiber geometry. Therefore, the model hampers the development of a more fundamental understanding of the experimental data which can be used to optimize experimental conditions.

1. 4. 3. Standard on extraction phase based calibration

The kinetics of desorption of the calibrant from the SPME coating and to the sample matrix follows the same model shown in equation 1-16, but in the opposite manner. In other words, the calibrant diffuses within the coating and migrates to the sample matrix by diffusion through the

boundary layer at steady-state conditions. Therefore, the nonlinear form of the equation for calibrant desorption is as follows:

$$\frac{q}{q_0} = 1 - \exp(-a_d t) \qquad \text{1-22}$$

where q is the amount of calibrant desorbed from the coating at time t, q_0 is the amount of calibrant impregnated onto the coating, a_d is the desorption rate constant. Since the amount of calibrant that remains on the coating after deployment can be quantified, equation 1-22 can be modified as:

$$\frac{Q}{q_0} = \exp(-a_d t) \qquad \text{1-23}$$

where Q ($= q_0\text{-}q$) is the amount of calibrant remaining on the coating after retraction of the coating from the sample matrix. The extraction and desorption kinetics shown in equations 5 and 7, respectively, are applicable for both liquid and solid coatings by assuming that the overall rate is controlled by the diffusion in the boundary layer in the sample matrix. Calibration techniques based on the desorption of standards from coatings rely on the fundamental principle that the symmetrical relationship between equation 5 and 7 holds true. This relationship can be represented as equation 1-24:

$$\frac{n}{n_e} + \frac{Q}{q_0} = 1 \qquad \text{1-24}$$

Alternatively, the symmetry can be justified if the extraction rate constant, a_e, is the same as that for desorption, a_d. For pre-equilibrium kinetic calibration, the n_e can be calculated by eq. 1-24. However, at any time of the sampling period (in situ extraction and desorption), the concentration of target analyte in the sample can be obtained from the following equation:

$$C_s = \frac{n}{K_{es}V_e(1 - \frac{Q}{q_0})}$$

1-25

1.5 Thesis Objectives

Solid phase microextraction (SPME) has already been recognized by the scientific and industrial community as a powerful alternative sampling and sample preparation technique to technologies such as liquid-liquid or solid phase extraction, as is evidenced by its rapid growth over the past decades.[57] The amounts of the analytes extracted at equilibrium can be predicted by simplified mathematical models. However, SPME measurements are often performed under non-equilibrium conditions, in particular for hydrophobic chemicals, in which equilibration times can be very long. It would be very useful to have a computational model to predict extracted amount on the extractant as a function of time. In addition, in complex samples, the presence of binding matrix components or hydrophobic phases may strongly influence the extraction efficiency and complicate the calibration procedure. Understanding the mechanism of the possible influence of a binding matrix component on the uptake kinetics of analytes into the extractant is particularly important when considering SPME measurements performed under non-equilibrium conditions. Despite all the efforts of SPME modeling and simulation, there is still a need to develop simple and accurate models not only for liquid coating, but for solid coating as well. Increasing computation capabilities and advancements in the application of numerical techniques make it possible to include all transport steps in kinetic modeling and simulation. Therefore, the prime objectives of this thesis are follows:

I. Development of a computational model with a Finite Element Method (FEM) based software Comsol Multiphysics by coupling all the transport and sorption phenomena occurs in a SPME method.

II. Elucidate the mechanism of the influence of a binding matrix components on the uptake kinetics.

III. Justification of the kinetic calibration approaches with the developed computational model and experimental data.

IV. Insight into the diffusion based calibration applied both for rapid environmental analysis.

V. Development of a selective extraction phase to extract a protein from human plasma.

Chapter 2 **Computational modeling of SPME**

2.1 Preamble

This chapter has been published as a part of the paper: Md. Nazmul Alam, Luis Ricardez-Sandoval, and Janusz Pawliszyn; *Numerical Modeling of Solid-Phase Microextraction: Binding Matrix Effect on Equilibrium Time*, **Anal. Chem., 2015,** 87 (19), pp 9846–9854. The contributions of Luis Ricardez-Sandoval, the co-author, involved modeling suggestions and manuscript revision. All tables and figures were reprinted from this publication with permission from American Chemical Society.

2.2 Introduction

The theory and practice of SPME have been examined in considerable detail in recent years in order to facilitate the processes of learning and application of this relatively new technique.[58] When a SPME coating is exposed to an analytical sample for a period of time, the extraction yield is primarily dependent on the partitioning of analyte(s) between the sample bulk phase and the supported extraction phase. The partitioning is, in turn, dominated by physicochemical factors related to the analyte, the sample matrix (i.e., the part of sample other than the analyte), and the extraction phase. As described in Chapter 1, based on the total residence time of the extraction phase in the sample solution, two extraction methods are used: (i) equilibrium extraction, which refers to extractions that take place when the extraction amount does not change significantly or when partition equilibrium is reached, and (ii) non-equilibrium extraction, which is the extracted amount at any given time before a state of equilibrium is reached. The extraction processes in

SPME consist of several physical domains with several processes occurring simultaneously: diffusion, convection, matrix binding, and adsorption or absorption.[59]

Different research groups have proposed slightly different approaches to model the kinetics of the absorption process for SPME. For example, some groups[60,56] considered the SPME fiber as a one-compartment, first-order kinetic model, whereas our group[58] divided the uptake process into two parts: intrafiber molecular diffusion in the coating domain and mass transfer around the fiber, which is governed by intralayer molecular diffusion over a stagnant layer with a finite thickness. Hermens and co-workers[61] modified the latter approach by introducing the mass transfer coefficient as a leading force due to the concentration gradient between bulk medium and fiber surface. Nevertheless, all these models have been simplified such that an analytical solution for the proposed model can be obtained; this can cause difficulties for experimentalists seeking to implement them in developing practical SPME methods that can be realistically applied to actual systems

In spite of all the developments achieved in different aspects of SPME, from creation of different formats to expansion of applications, it still remains a challenge for experimentalists to readily determine suitable experimental conditions that can provide acceptable (optimal) extraction amounts at low analyte concentrations.[62] As such, the development of a computational model will help increase our current knowledge of SPME methods by providing insight into the nature and dynamic characteristics of the extraction process.[63,64] In addition, the utilization of a computational model would significantly decrease the time and labor needed to develop and test several SPME designs as compared to the current practice of performing multiple (expensive) experiments.[65,66]

In this work, a computational-based mechanistic model for the absorption processes occurring in SPME has been developed by use of the finite element analysis software Comsol Multiphysics. Several common SPME experimental parameters, such as effect of agitation, fiber coating thickness, and presence of a binding matrix component, were considered and tested with the proposed model.

2.3   Mathematical model development

The present model involves three simultaneous and coupled processes: fluid flow past the SPME fiber dipped in the sample to be analyzed, mass transport to and from the fiber coating, and absorption of analyte by the fiber coating. Each of the domains considered in the present model is described next.

In the present mechanistic model, a typical geometry of SPME sampling was set up based on the experimental configurations reported by Louch et al.,[15] where the sample was placed in a vial stirred with a magnetic stirrer, which provided convective flow, and the SPME fiber was inserted through the vial cap. A schematic representation of the sample vial and SPME fiber, along with the corresponding modeling domain, is depicted in Figure 2-1a.
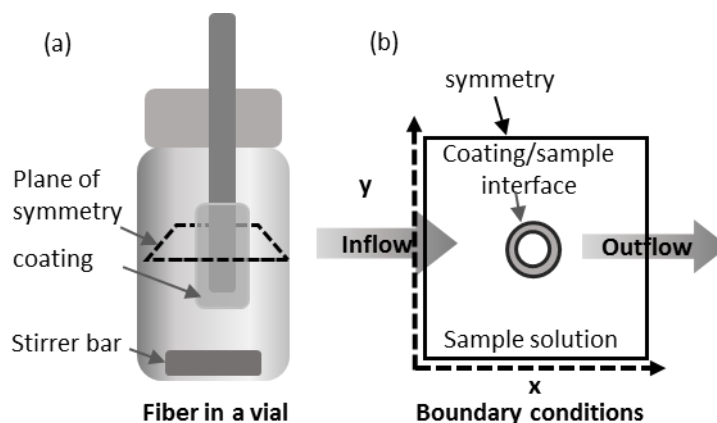
Figure 2-1. Schematic representation of the SPME/sample configuration. Experimental geometry based on Louch et al. containing a magnetic stirrer mediated convection, (a).[15] Here, a silica rod is used as a support for the coating, which is immersed in a sample solution for direct extraction. The 2D geometry with the boundary conditions used in the model, (b).

The fiber was located away from the center of the vial in order to avoid the central vortex region and to satisfy the assumption that the fluid flows past the fiber with a velocity normal to the fiber axis. The present analysis assumes a simple 2D geometry (Figure 2-1b) for simplicity of modeling and in order to reduce the amount of necessary calculations. The xy plane is set to be the cross section of the sample container, whereas the x-axis is set to be along the direction of flow. The governing equations for fluid flow, mass transport, and matrix effect are described next.

2. 3. 1. Fluid Flow Equations

Since the flow in the sampling container of SPME is in a low Reynolds number condition, it is assumed to be a laminar flow. The Navier−Stokes equation was employed to model the fluid

flow in the sampling container.[23] The conservation of momentum for incompressible fluid flow in a 2D geometry can be formulated as follows:

$$\rho \frac{\partial u}{\partial t} + \rho \left(u \frac{\partial u}{\partial x} + v \frac{\partial u}{\partial y} \right) - \mu \nabla^2 u + \frac{\partial p}{\partial x} = 0 \qquad \text{2-1}$$

$$\rho \frac{\partial v}{\partial t} + \rho \left(u \frac{\partial v}{\partial x} + v \frac{\partial v}{\partial y} \right) - \mu \nabla^2 v + \frac{\partial p}{\partial y} = 0 \qquad \text{2-2}$$

where u and v are the velocity components in the x and y directions, respectively; ρ is fluid density, p is pressure, and μ is fluid viscosity. For incompressible fluid flows, the following continuity equation is also considered:[67]

$$\frac{\partial u}{\partial x} + \frac{\partial v}{\partial y} = 0 \qquad \text{2-3}$$

The boundary conditions for the fluid flow model are shown in Figure 2-1b. Symmetry conditions ($\partial u/\partial x = \partial v/\partial y = 0$) were set at the two edges (Figure 2-1b). The boundary condition at the outlet was set to $p = 0$. A linear velocity was set at the inlet of the geometry. In order to obtain the linear velocity from stirring the solution with a magnetic stir bar, the following equation was employed:.[58,68]

$$u(x) = 0.575 \, \pi N R^2 \frac{1}{x} \qquad \text{2-4}$$

where R is the radius of the stir bar and N represents the revolutions per second. However, this equation provides velocity in one direction as opposed to the real flow patter around the cylindrical fiber. Therefore, if experimental data is available, the Comsol model was used to fit one set of experimental data to find out the linear velocity.

2. 3. 2. Mass Transport Equations

The analyte is transported by diffusion and convection in the bulk solution, whereas diffusion is the only transport mechanism occurring in the fiber coating. According to Fick's law, the following mass balances can be formulated to describe the time-dependent mass transport model for the present system:[69]

$$\frac{\partial C_A^s}{\partial t} + \nabla.(-D_A^s \nabla C_A^s + C_A^s \vec{u}) = 0 \qquad \text{2-5}$$

$$\frac{\partial C_A^e}{\partial t} + \nabla.(-D_A^e \nabla C_A^e) = 0 \qquad \text{2-6}$$

where $C_A{}^s$ and $C_A{}^e$ denote the concentrations (moles per cubic meter) of analyte A in solution phase and fiber coating, respectively. $D_A{}^s$ and $D_A{}^e$ are the diffusivity coefficients (square meters per second) in solution phase and in the fiber coating, respectively, while $\vec{u}$ denotes the velocity field, which can be obtained from the Navier−Stokes model described in the section 2. 3. 1. Equation 2-5) is valid for the solution side where convection is applied, whereas eq 2-6 is for the fiber's domain, where only diffusion is assumed to occur.

2. 3. 3. Boundary condition at coating/solution interface

At the coating/solution boundary, the conditions that ensure continuity of the dependent variables in the fiber coating and aqueous solution were specified. This specification is needed due to the nature of the analyte concentrations found at these two sites; while there is normally a movement of mass flux across the boundary, the overall concentration is most often discontinuous, since the individual concentrations on the coating and in the solution are different from each other. To circumvent this issue, two separate concentrations, i.e. concentration on the solution side ($C_A{}^s$)

and on the extraction phase ($C_A{}^e$), have been specified (shown in Figure 2-2). Then, the concentrations are coupled using an equilibrium relationship, i.e., a partition coefficient ($K_{es} = C_A{}^e/C_A{}^s$). In the present analysis, the value of the stiff-spring velocity term, k, was considered as 1000 m/s, since it provided sufficient mass exchange at the coating/solution interface.
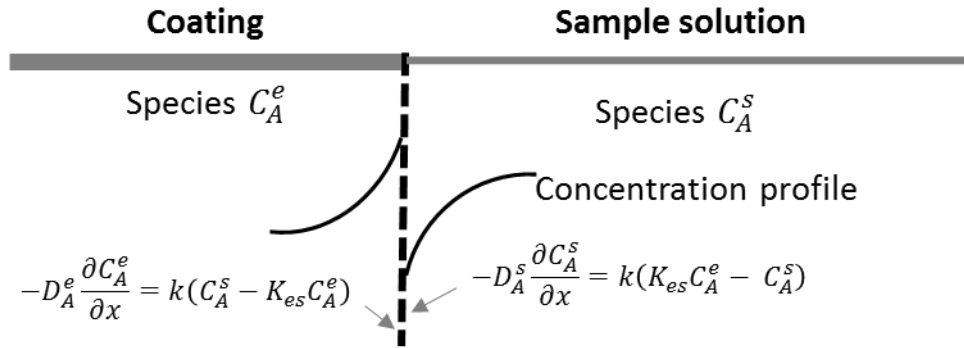
Figure 2-2. Boundary conditions used for mass transport in the coating/solution interface. Here, k is stiff-spring velocity term, K_{es} is the fiber-solution partition coefficient, $D_A{}^e$ and $D_A{}^s$ are the diffusivity coefficient of analyte (A) in fiber and solution phase, respectively.

At the coating/solution boundary, the conditions that ensure continuity of the dependent variables in the two regions, that is, fiber coating and aqueous solution, need to be specified.[70] Therefore, the fluxes at the boundary are coupled by use of Newton's law-type expressions:

$$-D_A^e \frac{\partial C_A^e}{\partial x} = k(C_A^s - K_{es}C_A^e) \qquad \text{2-7}$$

$$-D_A^s \frac{\partial C_A^s}{\partial x} = k(K_{es}C_A^e - C_A^s) \qquad \text{2-8}$$

where k is an arbitrary parameter called the stiff-spring velocity term, which should be of a large enough value so that a considerable mass exchange between the two regions can be established.

This technique has been used in previous studies that consider mass transfer between two different media.[71] K_{es} is called the partition coefficient. When a liquid phase is in contact with a solid phase, K_{es} can be defined as the ratio of concentration of a species in the solid phase to that in the liquid phase where they come in contact ($K_{es} = C_A^e/C_A^s$). A specified inlet concentration equal to the initial concentration was set at the inlet boundary ($C_A^s = C_A^s$, 0) and vanishing of $\partial C_A^s/\partial x^2$ at the outlet. The following equality of the mass flux of the analyte was considered at the sample vessel wall:

$$(C_A^s \vec{u} - D_A^s \nabla C_A^s) = 0 \qquad\qquad 2\text{-}9$$

2.4   Static Sample

2. 4. 1. Finite or small sample volume

At first, the absorption profile of an unstirred, small volume of benzene solution (100 µl) by a 56 µm thick PDMS coated fiber obtained by the present numerical simulation was compared with the previous study. As shown in Figure 2-3, the extraction profile obtained from this numerical solution predicts the expected behavior as reported in a previous experimental study. The extracted amounts of benzene at the equilibration time were almost same for both the experimental and simulated results. The numerical model is validated with a previous work performed by our group based an analytical solution where the result was verified with experimental work.

Generally the SPME fiber diameter is very small, within 100 to 500 µm, compared to the diameter of the solution container, which is often more than 2 mm. Moreover, the large diameter

of the sample container has a negligible effect on the extraction rate since the extraction amount is usually negligible with respect to the total amount of analyte present in sample solution.
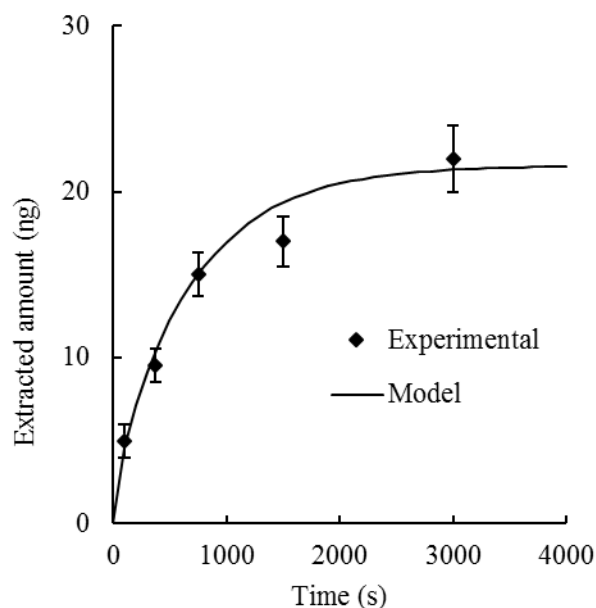
Figure 2-3. The computational model simulation results were fitted with the experimental data obtained from the absorption profile of an unstirred (static conditions), small volume of benzene solution (100 µl) by a 56 µm thick PDMS coated fiber reported by Louch et al.[1] Here, $D_A{}^s$: 1.08×10^{-9} m^2/s, $D_A{}^e$: 2.8×10^{-10} m^2/s, $C_A{}^s$:0.0128 mol/m^3, K_{es}: 125. The error bars represent standard deviations (n=3).

2. 4. 2. Effect of diffusion coefficient in solution

Under static sample condition, it was necessary to confirm that the extraction kinetics of analyte was influenced by mass transport through the boundary layer. One method to test for diffusion limitations is to increase the diffusivity of analyte in solution and look for concomitant changes in the extraction time profile. It is seen that increasing the analyte diffusivity in solution

from 1×10^{-9} to 5×10^{-6} m^2 s^{-1} yielded substantially faster uptake rate. Figure 2-4 depicts the predicted extracted amount as a function of time when the analyte diffusion coefficient is 10^{-6}, 10^{-7}, 10^{-8}, and 10^{-9} m^2 s^{-1}. As D_s increases, the Damkohler number D_a decreases, and the diffusion in the coating becomes progressively more uptake rate limited.[72] This results demonstrated the diffusion controlled kinetics in SPME.
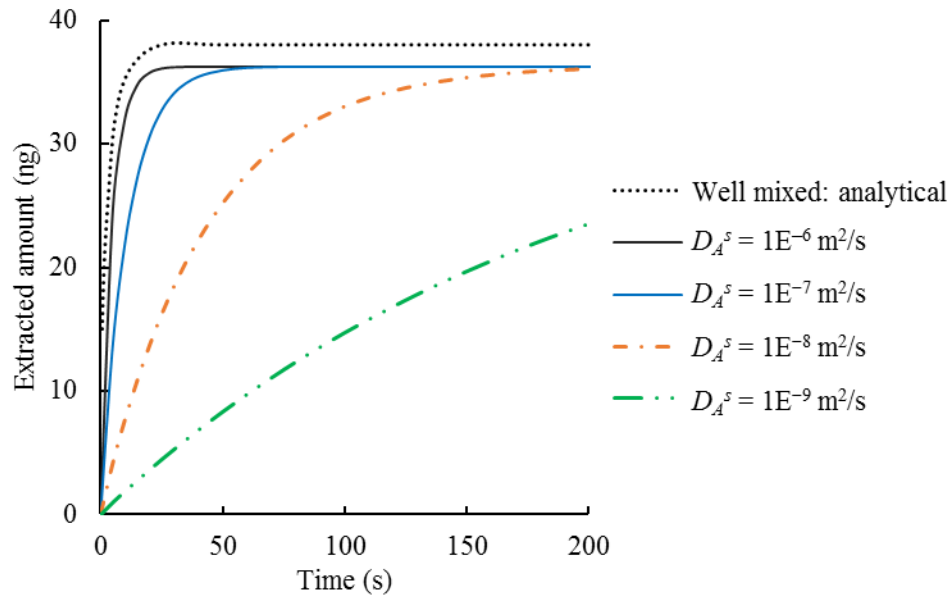
Figure 2-4. The extracted amount of benzene in fiber coating as a function of time for various values of the analyte diffusion coefficients ($D_A{}^s = 1\times10^{-6}$ to 1×10^{-9}) in sample solution. The equilibration time obtained for the $D_A{}^s = 1\times10^{-9}$ provided similar equilibration time obtained from the well-mixed case of exact solution described by Louch et al.[1] Here, $D_A{}^e$: 2.8×10^{-10} m^2/s, $C_A{}^s$:0.0128 mol/m^3, K_{es}: 125 and the coating thickness was 56 µm. For the present simulation, the convection was set zero (static conditions).

2. 4. 3. Flow profiles in a stirred sample vial

Convection in the SPME extraction can be applied in different ways such as agitation of the sample with a stirrer or flowing sample over the extraction phase. The geometrical domain used for the simulation was set up based on the experimental configurations reported by Louch et al,[15] where the sample was in a vial stirred with a magnetic stirrer, which provided convective flow, and the SPME fiber was inserted through the vial cap shown in Figure 2-5.

33
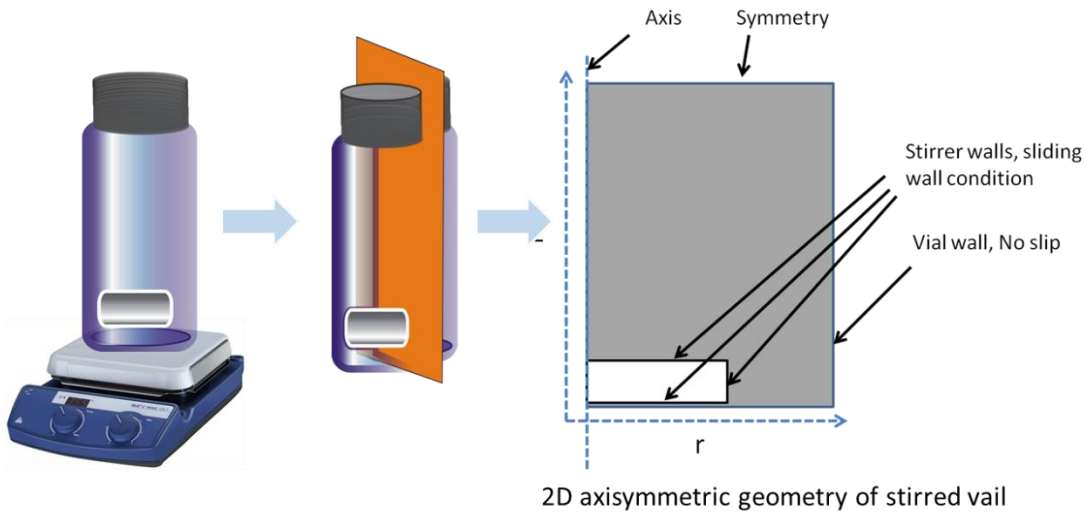
Figure 2-5. Geometry for modeling fluid velocity in the vial. A 2D axisymmetric geometry is considered for the modeling.

In order to find out the mass transfer profile in a sampling container the fluid velocity should be accessible. This velocity is highly dependent on the geometry and stirring conditions. To find out the effect of these parameters on the fluid velocity inside the container a few sets of simulation have be run. At first, the height and the width of the sample vial was varied to study the effect of the vial size.

Figure 2-6 shows the result for angular velocity profiles in the vial for two different heights. The surface plot shows the magnitude of the velocity where the white lines present streamlines of the velocity field. As shown in Figure 2-6, both the vial geometry and stir size have effect on the fluid velocity. Also, stirring speed have been changed to see the effect of operating condition in fixed pressure and temperature on flow patterns. The stirring speeds, 500 to 1000 rpm, provides laminar flow shown in Figure 2-9. As it can be expected with increasing the stirring speed, higher amount of Reynolds number achieved.

34
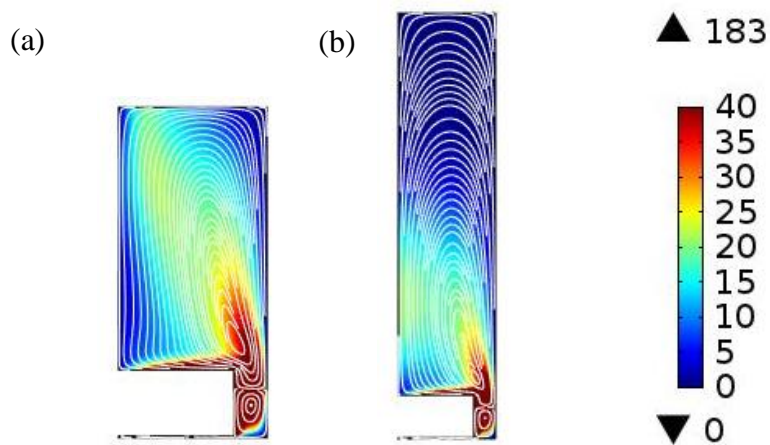
Figure 2-6. Effect of the vial height (*H*) on velocity magnetude (mm/s). (a) *H* = 10 mm; (b), H = 20 mm. stirring speed is 500 rpm with a stirrer of 7 mm long and 2 mm wide and vial diameter is 9 mm. All other conditions are the same.
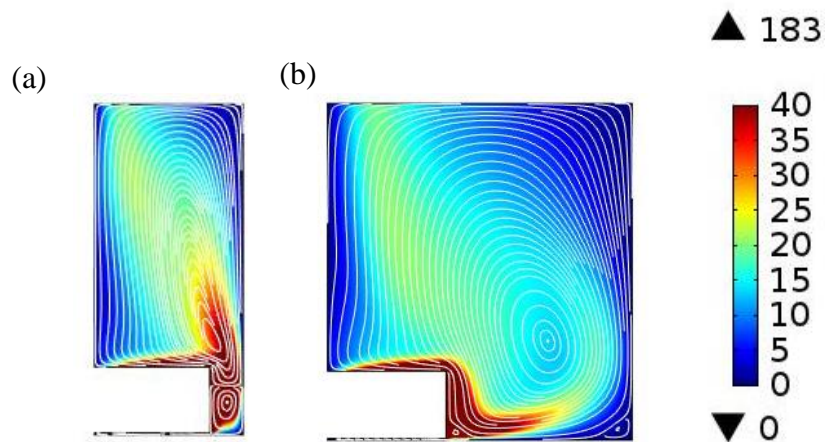
Figure 2-7. Effect of the vial width (*W*) on velocity magnetude (mm/s). (a) vail width is 9 mm; (b) vial width is 18 mm. Height of the vial is 10 mm. Stirrer is of 7 mm long and 2 mm wide. All other conditions are the same.
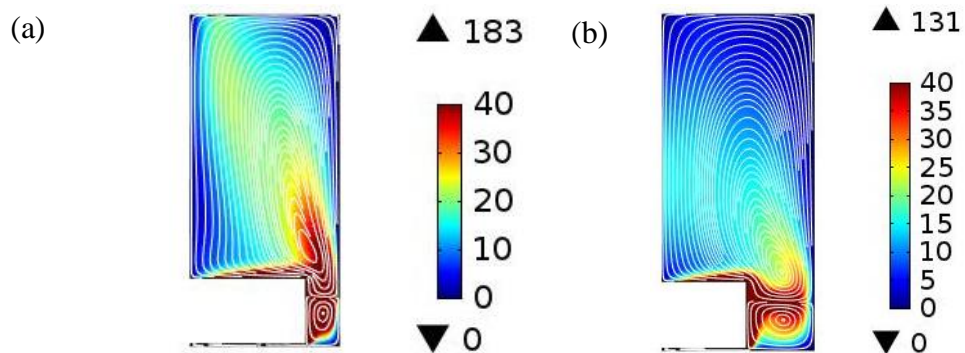
Figure 2-8. Effect of length of the stirr bar (*L*) on velocity magnetudes (mm/s). (a) *L* is of 7 mm; (b) *L* is of 5 mm. Hight of the vial is 10 mm, width of the vial is 9 mm, stirring speed is 500 rpm. All other conditions are the same.
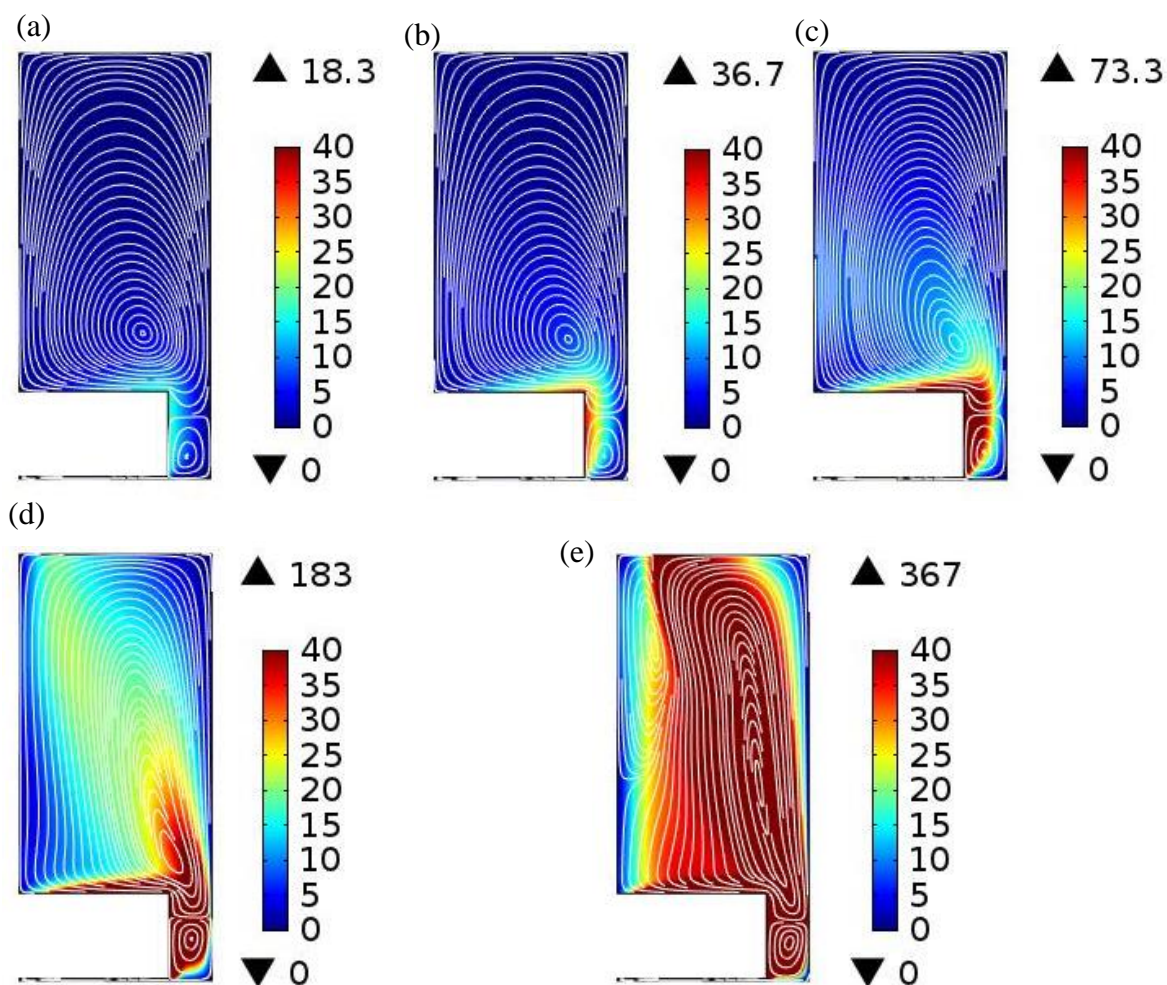
Figure 2-9. Effect of the stirring speed (rpm) on Reynolds number. Speed was set as; (a) 50 rpm, (b)100 rpm, (c) 200 rpm, (d) 500 rpm, (e) 1000 rpm. Vial height is 10 mm, Vial width is 9 mm, stirrer length is 7 mm, stirrer width is 2 mm. All other conditions are the same.

2. 4. 4. *Effect of stirring on equilibrium time*

The mechanistic model developed in this study has been validated with previous experimental work performed by our group for the extraction of benzene from an aqueous solution by a polydimethylsiloxane (PDMS) coating.[15] The model developed in this study can predict the

37

equilibration time with the absence or presence of stirring in the sample solution (shown in Figure 2-10).The model slightly underestimates the extracted amount for the static condition.
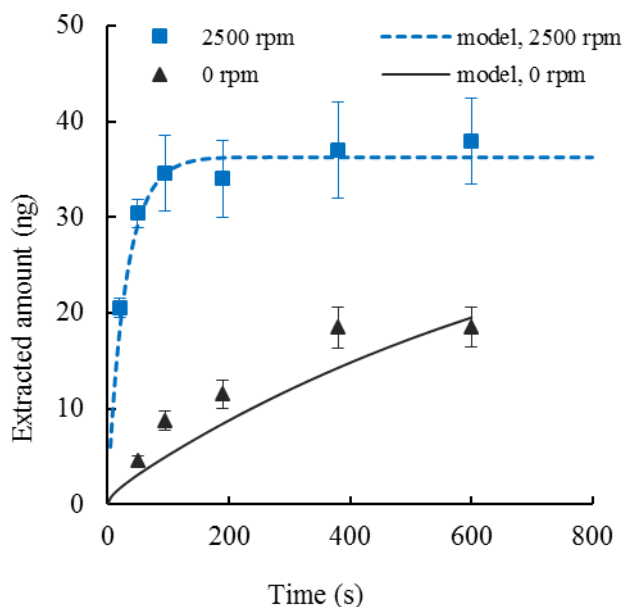
Figure 2-10. Effect of stirring on the extraction profile of 1 ppm benzene in water extracted with a 56 µm thick PDMS coating Here, $D_A{}^s$: 1.08×10^{-9} m^2/s, $D_A{}^e$: 2.8×10-10 m^2/s, $C_A{}^s$:0.0128 mol/m^3, K_{es}: 125. The error bars represent standard deviations (n=3).

Unavoidable convection due to fiber or solution movement might contribute to the higher experimental extracted amount at each time point. The equilibration time, 100 s, predicted by the present model is in agreement with the experimental data presented in a previous study for stirring speed of 2500 rpm. The good fitting of the experimental data indicates the coupling between solution and coating phases in the mathematical model for both agitated and nonagitated sample systems.

2.5   Dynamic sample

2. 5. 1. Dynamic flow through system

The second geometry was chosen based on the on-site sampling systems where there is a stream of fluid flowing from one side to the other and the SPME fiber is inserted into the stream.[34] The 2 D geometry shown in Figure 2-11 (b) was considered for simplicity of modeling and in order to reduce the calculations. The xy plane is set to be the cross-section of the sample container whereas the x-axis is set to be along the direction of flow. The governing equations for the fluid flow, the mass transport and the matrix effect are given below.
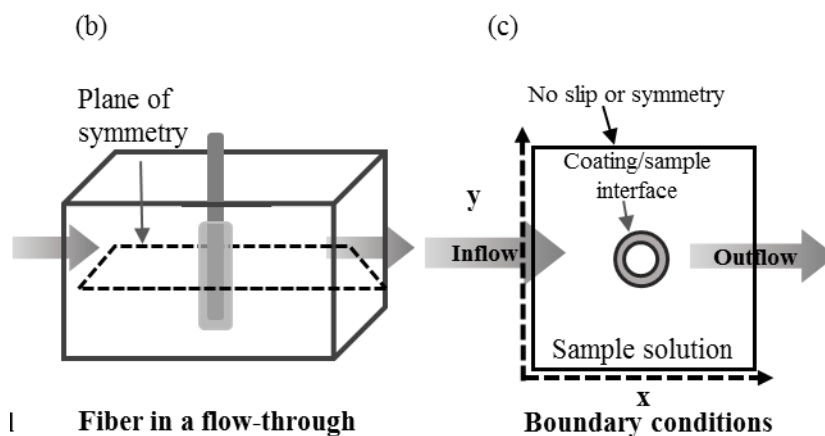
Figure 2-11. Simple graphical representation of the SPME/sample configuration. Here, a silica rod is a support for the coating which is immersed in a sample solution for direct extraction. Geometrical configuration based on Chen *et. al.*[34] with a flow through system, (a). The 2D geometry with the boundary conditions used in the model (b).

2. 5. 2. Flow profile in a flow through system

The fluid velocity field and concentration gradient due to the two different initial fluid velocities (1 cm/s and 50 cm/s) was shown in Figure 2-12. We can see that the concentration in the bulk around the coating does not vary significantly in the vial except at the vicinity of the coating surface. Furthermore, the highest concentration at the coating surface, which is found at the left side of the coating is about 4 µM. This means that even when the fluid first makes contact with the coating at the left side of the coating, there is a mass transport boundary layer where the concentration varies by about 9 µM (= 13-4). The concentration difference between the bulk and the surface of the sphere varies around the coating of the fiber.
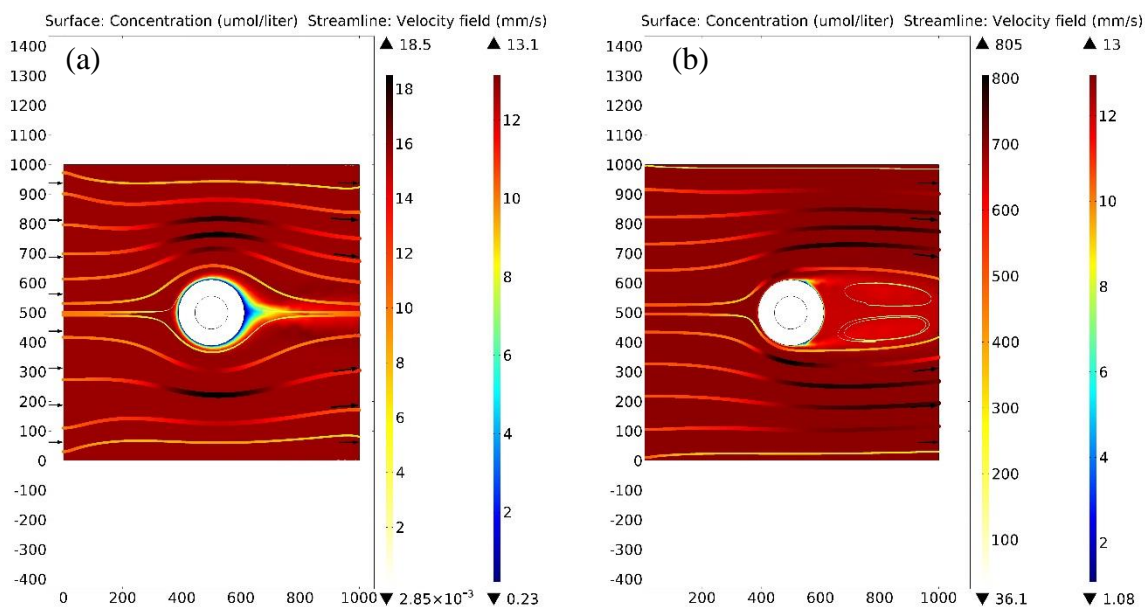
Figure 2-12. The figure shows the results of simulation of the flow around the fiber coating and the concentration of the reactant at two different initial flow rate, (a) flow rate = 1 cm/s, (b) flow rate = 50 cm/s. The surface plot shows the concentration of the analyte that extracts on the coating, (a) t= 2 s , (b) t = 0.01 s. The streamlines show the velocity field.

Due to the container's small dimensions, the Reynolds number of the flow is small (Re << 100), and the flow stays laminar in most of the area. The swirls are restricted to a small area behind the coating. The size and location of the swirls depend on the magnitude of the inflow velocity.

2. 5. 3. *Effect of flow velocity on equilibrium*

After inserting the SPME fiber to the analyte solution, the fiber coating starts to absorb analyte(s) and a concentration gradient develops in the vicinity of coating/liquid interface. In the absence of convection at zero stirring speed, the depletion zone starts relatively small/flat at the initial times until it extends indefinitely up to the container's walls. Therefore, steady state is never

reached because the depletion zone grows larger, diffusive flux becomes smaller and extraction becomes slower (Figure 2-13a). One way of reducing the growth of the depletion layer is to introduce a convection mechanism into the system such as agitation or stirring. As shown in Figure 2-13b, convection stops this growth in the depletion zone, giving a steady zone with a definite thickness for the target flux delivered by convection to balance the diffusive flux through the upstream depletion. In the zone of reduced analyte concentration which is often called the diffusion boundary layer; the analyte is assumed to migrate only by diffusion.[73]
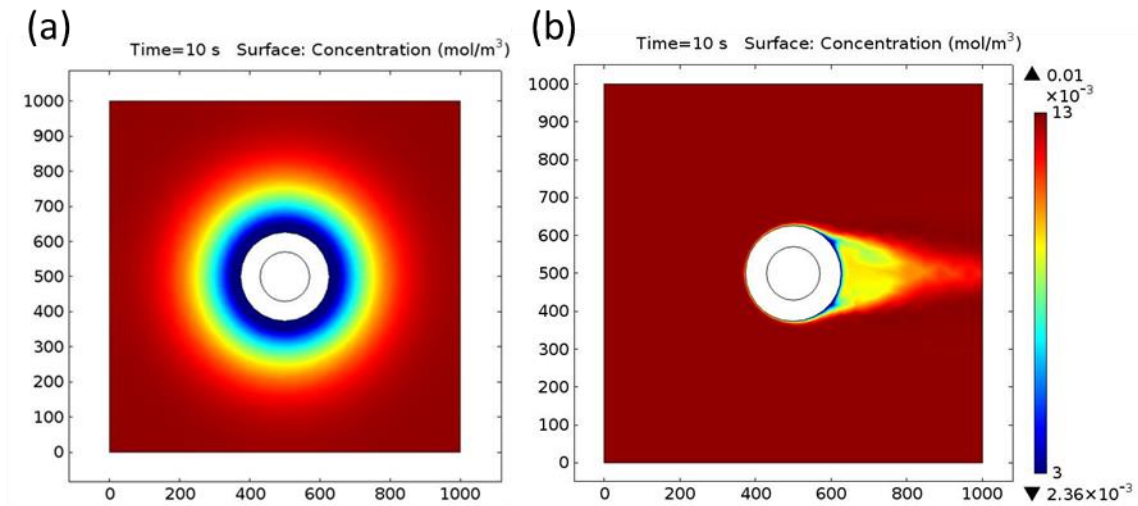
Figure 2-13. Effect of convection on the depletion layer. Relatively thick depletion layer is formed without any convection (a); however, very thin depletion layer is produced at convection of 10 cm/s.

Even with the convection, the diffusion layer around the fiber coating is of uniform thickness in the early stages of extraction, for example at 0.1 s extraction as shown in. However, as the system evolves at 10 seconds, the fluid is brought to rest at the forward stagnation point from which the boundary layer develops (Figure 2-13. b). The boundary layer, then, spans over a

distance from the coating under the influence of a favorable pressure gradient resulting from the convective flow of the analyte solution. Due to the non-uniform thickness of the boundary layer, non-symmetrical concentration distribution along the surface of the fiber coating is expected. However, in the previous exact solution of SPME, a uniform boundary layer thickness was considered for simplicity.[58] Therefore, the present numerical simulation provides more realistic results.

As shown in Figure 2-14, there is a zone of reduced analyte concentration which is called the diffusion bounday layer; in this region, the analyte is assumed to migrate only by diffusion.[2]
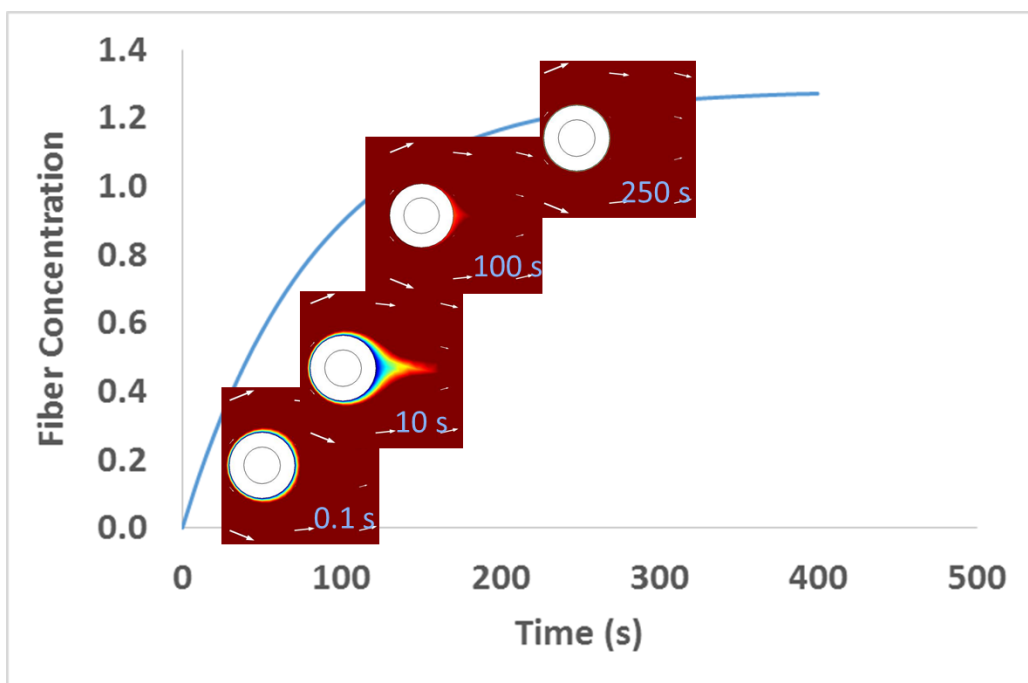
Figure 2-14. The development of the diffusion boundary layer during the SPME extraction. A layer of concentration gradient is formed around the fiber coating within 0.1 seconds of extraction. Here, the aqueous solution is passing the coating from right to left side in the images.

A time-dependent analysis was conducted to investigate the kinetics of SPME direct extraction from the analyte solution. Figure 2-15 depicts the extracted amount as a function of time at various flow rates. It can be seen that the uptake rate can be accelerated by increasing the fluids flow rate. The symbols correspond to the well-mixed case. As the flow rate increases, the Peclet number Pe increases[72], the analytes are efficiently transported to the coating surface, and we again approximate well-mixed conditions. Figure 2-15 provides another verification of the mathematical model as the numerically computed results approach analytical predictions at limiting cases.
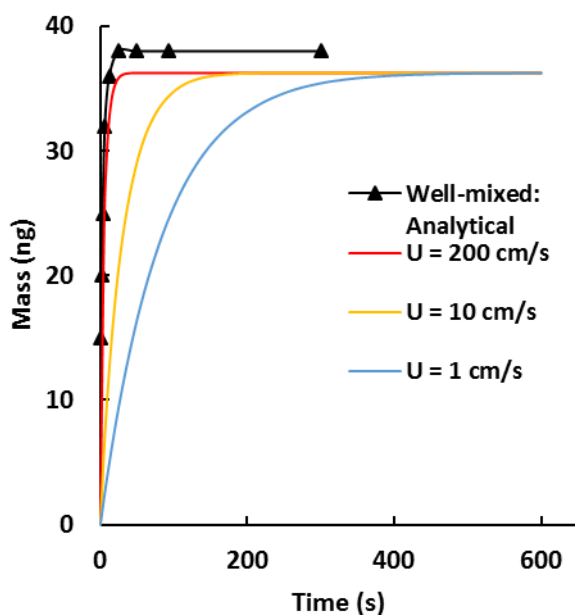
Figure 2-15. The extracted amount in coating as a function of time at various flow rates. The symbols and lines correspond, respectively, to analytical (well-mixed case) and finite element results. $C_A = 1$ ppm, $D = 1.08 \times 10^{-9}$ m^2 s^{-1}.

2.6   Analyte concentration profiles in and outside of the coating

In order to provide more insight into the extraction, the concentration profile developed in the sample domain at different extraction times with the presence of convection are shown in Figure 2-16. At the beginning of the extraction, the analyte concentration in the sample at the interface of the fiber coating and sample matrix drops dramatically due to the fast   analyte from the bulk (Figure 2-16b). As the extraction time increases, the concentration gradient in the sample matrix keeps changing and reaches equilibrium after about an hour Figure 2-16(d)). At extraction time of 4000s, the extraction equilibrium was already reached and there is no gradient of concentration in the sample matrix as shown in Figure 2-14d.
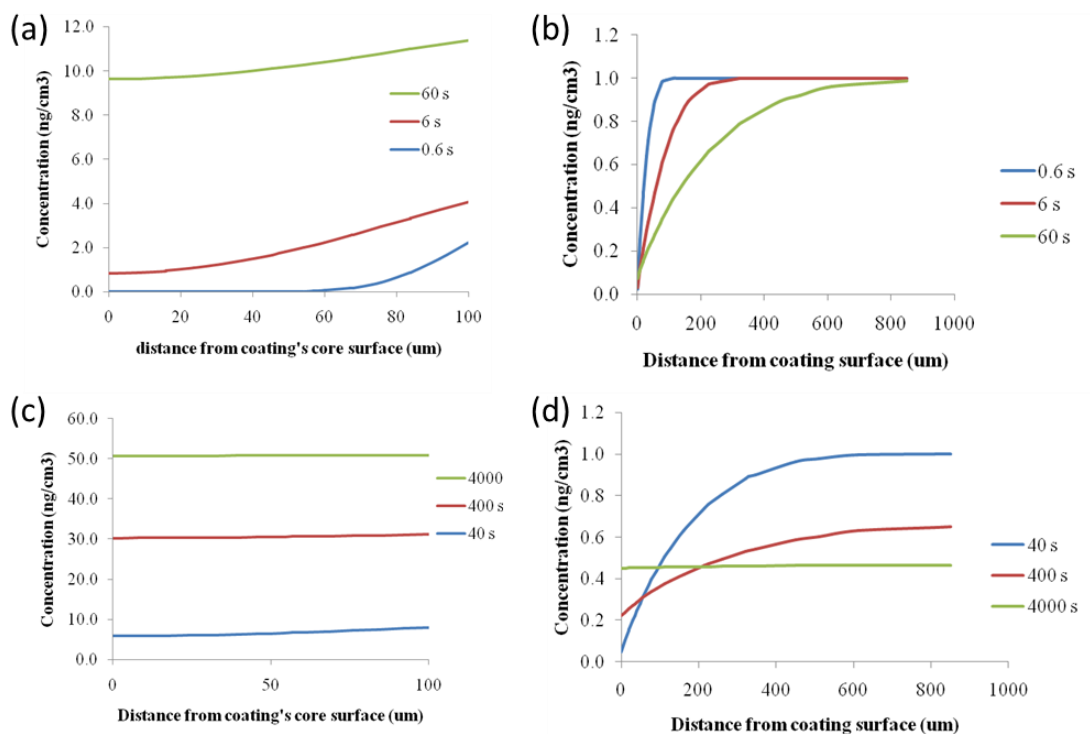
Figure 2-16. Concentration distribution profile of the analyte produced in the coated fiber (a) and in solution (b) along the distance from the coating surface to the bulk of the aqueous solutions at extraction times before 60s. Concentration profile in the coated fiber (c) and in solution (d) at longer extraction times. The SPME coating thickness was 100 µm.

Similarly, the concentration profile in the coating is shown in Figure 2-16a and Figure 2-16c. As opposed to the solution side, however, there is not a significant concentration gradient in the fiber coating even at the beginning of the extraction (~4-5 s after extraction starts). Once equilibrium has been reached, the concentrations of analyte in both the sample matrix and fiber coating remain constant. These results indicate that the diffusion of the analyte in the fiber coating is not the controlling step to determine the kinetics of SPME direct extraction in static aqueous

samples. The extraction is controlled by the diffusion in the boundary layer at this particular analyte-coating system, which agrees with the experimental results reported by Louch *et. al.*[15]

2.7   Effect of analyte concentration

As shown in Figure 2-17 the extracted amount of benzene is linearly proportional to the concentration of the analyte in solution. In addition, the equilibrium time is unaffected by the initial concentration of analytes present in solution. This feature provides an advantage of using SPME since there is no need to construct extraction time profile for a range of analyte concentrations. It can be seen from the Figure 2-17 that the computational simulation predicts the concentration variations quite well.
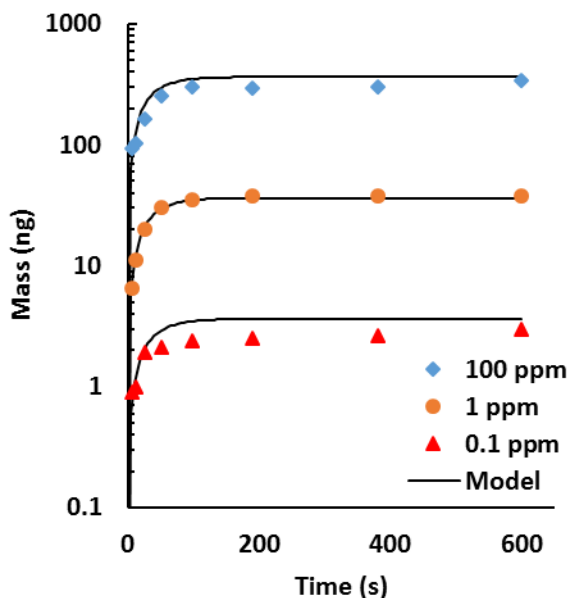
Figure 2-17. Effect of analyte concentration on extraction kinetics of 100% stirred benzene solution in water.

2.8   Effect of partition coefficient

The partition coefficient (K_{es}) is an important parameter that controls the mass of analyte extracted by the fiber coating. Extraction time profile of three different analytes benzene, toluene and p-xylene with different K_{es} such as 125, 294, and 831 respectively, have been analyzed in this study. The value of K_{es} depends on the physicochemical properties of both the analyte and the coating. As shown in Figure 2-18, the equilibration time increases from about 600 s for benzene to about 1,200 s for toluene and 3,600 s for p-xylene when K_{es} increases from 125 to 294 and to 831, respectively. The ratio of changes are similar to those reported in a previous experimental study. The trend of increasing equilibration time with increasing K_{es} can be rationalized by the fact that a larger amount of analyte needs to be transported to the fiber although the flux into the coating is approximately constant for all the analytes with similar diffusion constants values. During the extraction, the concentration of the analyte in the thin layer of the sample, i.e., close to the water/coating interface, is lower compared to the bulk concentration due to the local depletion of the analyte by the fiber coating. The higher the partition coefficient, the greater the amount of analyte that is extracted by the fiber coating, resulting in substantially slower equilibration rates because the analytes need more time to be transported to the vicinity of the fiber. These results show that the present mathematical model can be used by an experimentalist to estimate the time required to reach an equilibrium of extraction for different fiber materials while using different K_{es} values.
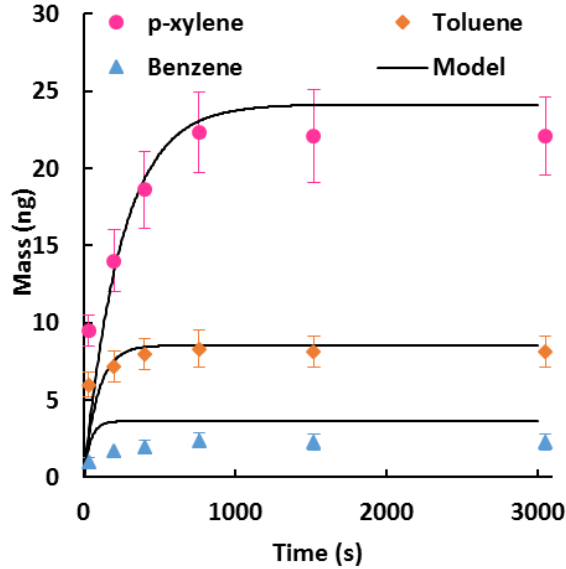
Figure 2-18. Effect of partition coefficient (K_{es}) on the extraction profile of 0.1 ppm benzene extracted by a 56 µm coating at 2500 rpm.

2.9   Effect of coating thickness

It has been shown experimentally that, by doubling the coating volume the extracted amount of benzene, and their corresponding equilibration time, are also doubled under the same stirring conditions. In the current numerical model, the same pattern was Figure 2-19. More specifically, the extracted amount of benzene and equilibration time for 100 µm coating were 70 ng and 800 seconds, whereas for the 56 µm coating the values were about 35 ng and 400 s, respectively. The increase in the equilibration time and amount obtained from both, the experimental results and the present numerical model, supports the well-established assumption that the transport of analyte is controlled by the diffusion through the boundary layer. For the 15 µm coating, the mass extracted is further reduced to about 7 ng and the equilibration time to about 100 s. With this mathematical model, where there is no assumption of two extreme conditions of being unstirred and perfect

49

agitation as considered in the previous analytical model[15], the experimental data can be predicted. Additionally, with the present mathematical model, it is possible to determine the optimum coating thickness for a particular analysis in order to achieve the desired sensitivity and equilibration times since the sensitivity of thicker fiber coating is higher due to its larger extraction phase volume. Therefore, the present model can be used to predict optimum coating thickness for a particular analysis.

Moreover, the simulated results for varying coating thicknesses provided very good fitting with the experimental data, as shown in Figure 2-19.
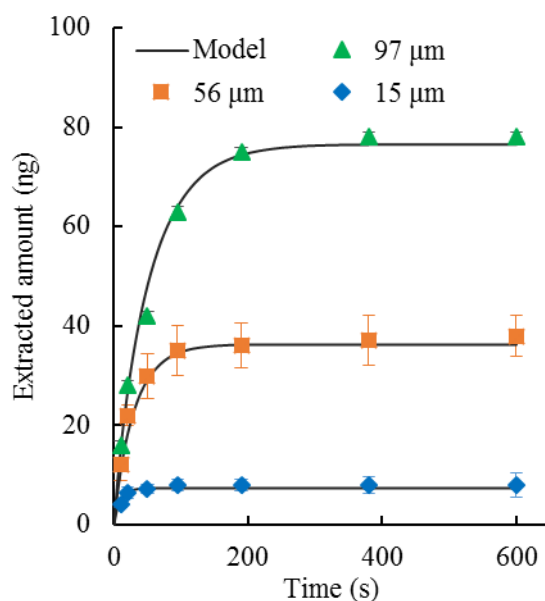
Figure 2-19. Effect of coating thickness on the extraction of benzene at the stirring speed of 2500 rpm. Three different coating thickness, 97, 56 and 15 µm were compared by keeping the same fiber core diameter at 55 µm. Here, $D_A{}^s$: 1.08×10–9 m^2/s, $D_A{}^e$: 2.8×10–10 m^2/s, $C_A{}^s$:0.0128 mol/m^3, K_{es}: 125. The error bars represent standard deviations (n=3).

2.10   Summary

In this chapter, a mechanistic-based mathematical model that describes the uptake kinetics in SPME of analytes from a standard solution. The proposed mathematical model provided excellent prediction of the experimental data available in the literature. The simulation results obtained for the present analysis have shown that the present model is a reliable and relatively inexpensive practical method of characterizing the performance of SPME. This model can be used for sample matrices containing one type of analyte binding component.

Chapter 3   **Effect of binding matrix components on equilibration**

3.1   Preamble

This chapter has been published as a part of the paper: Md. Nazmul Alam, Luis Ricardez-Sandoval, and Janusz Pawliszyn; *Numerical Modeling of Solid-Phase Microextraction: Binding Matrix Effect on Equilibrium Time*, **Anal. Chem., 2015,** 87 (19), pp 9846–9854. The contributions of Luis Ricardez-Sandoval, the co-author, involved modeling suggestions and manuscript revision. All tables and figures were reprinted from this publication with permission from American Chemical Society.

3.2   Introduction

The presence of another binding matrix or hydrophobic phase, such as serum protein or humic acids, besides the SPME fiber, may strongly influence the extraction efficiency and complicates the calibration procedure. Binding matrices may interact by adsorbing to the fiber surface, thus, possibly blocking the exchange of analyte across the fiber boundary. This may also lead to an overestimation of the concentration in the fiber coating as the matrix-bound analyte adsorbed to the fiber coating is measured along with the analyte in the fiber coating. Therefore, it would be valuable to have a model that can be used to analyse measured concentrations in the fiber coating in a very complex sample matrix as a function of time.

Equilibrium extraction is the most frequently used method. When a sample volume is very small, exhaustive extraction might occur in SPME and can be used for calibration. To shorten long equilibrium extraction times, and/or address the displacement effects that occur when porous coatings are used, extraction can be interrupted before equilibrium, and calibration is still feasible

if the agitation and the extraction time are kept constant. The last approach, the diffusion-based calibration method, is very important for field sampling. This method eliminates the use of conventional calibration curves. Fast on-site analysis and long-term monitoring are thus possible.

Quantification of freely dissolved analytes with SPME under nonequilibrium conditions can be erroneous due to the influence of matrix components in the kinetic regime of extraction.[74] Some studies reported an increased analyte uptake rate in the presence of matrix during the kinetic phase of extraction.[75] The plausible explanation for this enhanced kinetics is known as the "diffusion layer effect".[74] Conversely, other studies reported unaltered uptake kinetics in the presence of matrix.[76] Although the majority of the reports agree with the fact that the matrix can affect the uptake kinetics only if the extraction is limited by the diffusion in the boundary layer, a lack of understanding remains regarding the effect of physical parameters on transport kinetics in a complex matrix.

The mechanistic model presented in this study is able to provide insight into how physical parameters affect the extraction kinetics of an analyte from a binding matrix component-containing sample. A set of general guiding principles that were adapted from an asymptotic analysis[77] were used as a predictive tool to achieve desired uptake kinetics or to explain the experimental extraction time profile for a complex matrix. The mechanistic model was validated with previously published experimental data obtained from different sources.

3.3   Experimental
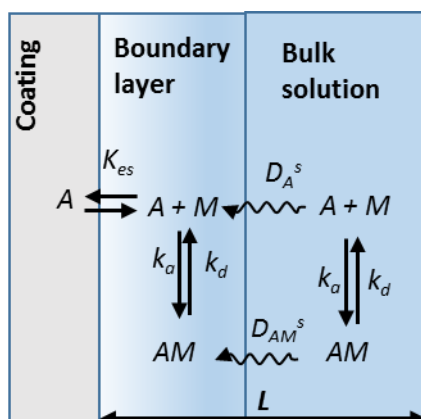
Figure 3-1. Schematic representation of the SPME/sample configuration. An analyte (*A*) binds with a matrix (*M*) with forward and reverse rate constants (k_a) and (k_d), respectively. Both the free or bound analytes can diffuse to the boundary layer with diffusivities D_A^s and D_{AM}^s, respectively. On the coating, only the analyte can be absorbed with a distribution constant of K_{es}.

3. 3. 1. Equations for Binding Matrix Component.

When a binding matrix component is present (e.g., humic organic matter in a water sample), association and dissociation between the freely dissolved analytes and the binding matrix in the sample domain can be expressed as follows:

$$\mathrm{A + M} \underset{k_d}{\overset{k_a}{\rightleftharpoons}} \mathrm{A\,M} \qquad\qquad \text{3-1}$$
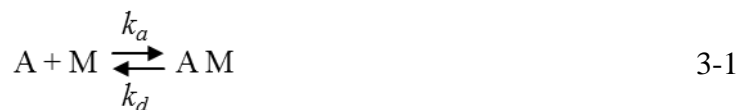
where *A* is the freely dissolved analyte, *M* represents the binding matrix component, and *AM* is the bound species. The present study assumes that the fiber coating absorbs only analytes in a matrix-containing sample and follows the same physics as described in the previous section for mass

54

transport equations. In the solution domain, simple binding kinetics between analyte and matrix were used to model the influence of the matrix on extraction of analyte (i.e., second-order forward and first-order backward).[73] The modeled experimental systems involved addition of bovine serum albumin or humic acids to water samples, as previously reported in the literature.[78],[79] The model parameters used in this study are shown in Table 3-1. Transport of the species in the sample is schematically shown in Figure 3-1.

Table 3-1. Parameters used for pyrene and chlorpromazine extraction by PDMS and polyacrylate coating respectively.

Symbols	Pyrene[78]	chlorpromazine[79]	Units	Definition
K_D	$1.17E^{-7}$	$5.5E^{-5}$	M	Equilibrium dissociation constant
k_a	$8.58E^6$	$7.3E^4$	$M^{-1}s^{-1}$	Forward rate constant
k_d	1	3.96	s^{-1}	Reverse rate constant
C_A	1.0	100.0	µM	Concentration of analyte
C_M	0.47, 1.4, 23.34	600.0	µM	Concentration of matrix (HSA)
K_{es}	$1.95E^4$	$7.3E^2$		Fiber distribution constant
$D_A{}^s$	$4.37\ E^{-6}$	$4.3E^{-5}$	cm^2s^{-1}	Diffusivity of analyte in sample
$D_A{}^e$	$D_A{}^s/6$	$6.50E^{-11}$	cm^2s^{-1}	Diffusivity of analyte in fiber
D_{AM}	$5.9\ E^{-7}$	$1.0E^{-7}$	cm^2s^{-1}	Diffusivity of Analyte-matrix in solution

The rates of association (k_a) and dissociation (k_d), commonly expressed as the dissociation constant (K_D), determine the strength of the affinity interaction in eq. 3-2, which regulates analyte release from the bound matrix into the sample medium:

$$K_D = \frac{k_d}{k_a} = \frac{C_A . C_M}{C_{AM}}$$

3-2

where C_A C_M, and C_{AM} are the molar concentrations of free analyte in the sample, free matrix component (e.g., humic acid), and bound matrix component, respectively. Mass transport within the sample can be described by the use of mass balances for free analyte and analyte-bound matrix component. The concentration of free analyte (C_A) at the diffusion boundary layer changes with respect to diffusion from the sample as well as association or dissociation with the bound matrix:

$$\frac{\partial C_A}{\partial t} = \nabla \cdot (D_A \nabla C_A) - k_a C_A (C_{M,T} - C_{AM}) + k_d C_{AM} \qquad \text{3-3}$$

where $C_{M,T}$ is the concentration of total matrix added.

The concentration of complex (C_{AM}) relies only on equilibrium binding:

$$\frac{\partial C_{AM}}{\partial t} = k_a C_A (C_{M,T} - C_{AM}) + k_d C_{AM} \qquad \text{3-4}$$

where the concentration of free binding matrix (C_M) is described as the difference between the concentration of total matrix added ($C_{M,T}$) and the concentration of complex (C_{AB}), i.e.,

$$C_M = C_{M,T} - C_{AM} \qquad \text{3-5}$$

Computational Model. COMSOL Multiphysics 4.4, a finite element method (FEM) based software package, was used in this study to analyze mass transfer processes in SPME. In order to obtain an accurate representation of the SPME system, the time-dependent partial differential equations for each of these physical processes must be solved simultaneously. The procedure used to solve this problem is divided into two steps: (1) determination of the fluid velocity profile at steady state, with the assumption of incompressible flow, and (2) use of this steady-state velocity profile as the initial condition to solve for the coupled transient mass transport and absorption equations. The extracted amount at each time point was calculated by multiplying the average

concentration in the fiber by its volume. The normalization of extracted amount was carried out by dividing the extracted amount at each time point by the equilibrium quantity.

3.4 Results and discussions

3. 4. 1. Matrix Effect on Equilibrium Time.

The matrix effect on SPME equilibrium time is still not well understood. Here, the proposed mathematical model is employed to explain the mechanism of the kinetics of extraction in the presence of a binding matrix component in sample.[80,81] The assumption was made that no significant physical adsorption or partition of matrix components occurs on the surface of the coating. In order to test whether the model can reproduce experimental data for shorter or unaltered equilibrium time, two different experimental setups were considered. First, the model was validated with experimental data reported by Hermens and coworkers[78] on the effect of bovine serum albumin (BSA) on uptake kinetics of pyrene from an aqueous sample by use of a PDMS fiber coating. Since pyrene is unstable in water sample, the authors choose to preload the analyte onto the extractant and observed the desorption kinetics to predict the extradition time profile. The experimental and simulated data are shown in Figure 3-2a. The model predicted the experimental data very well, even at different concentration levels of albumin. In this experimental setup, the equilibrium time was shorter for increased concentrations of albumin. Another validation of the model is shown in Figure 3-2b, with the experimental data obtained from Broeders et al.[79] The proposed model has been shown to predict experimental data when the time to reach equilibrium was not perturbed, while the extracted amount at equilibrium was less in the presence of matrix (albumin) than that of the standard chlorpromazine (analyte) sample. Details on the rate of

extraction influenced by the presence of a binding matrix component are discussed in detail in the following section.
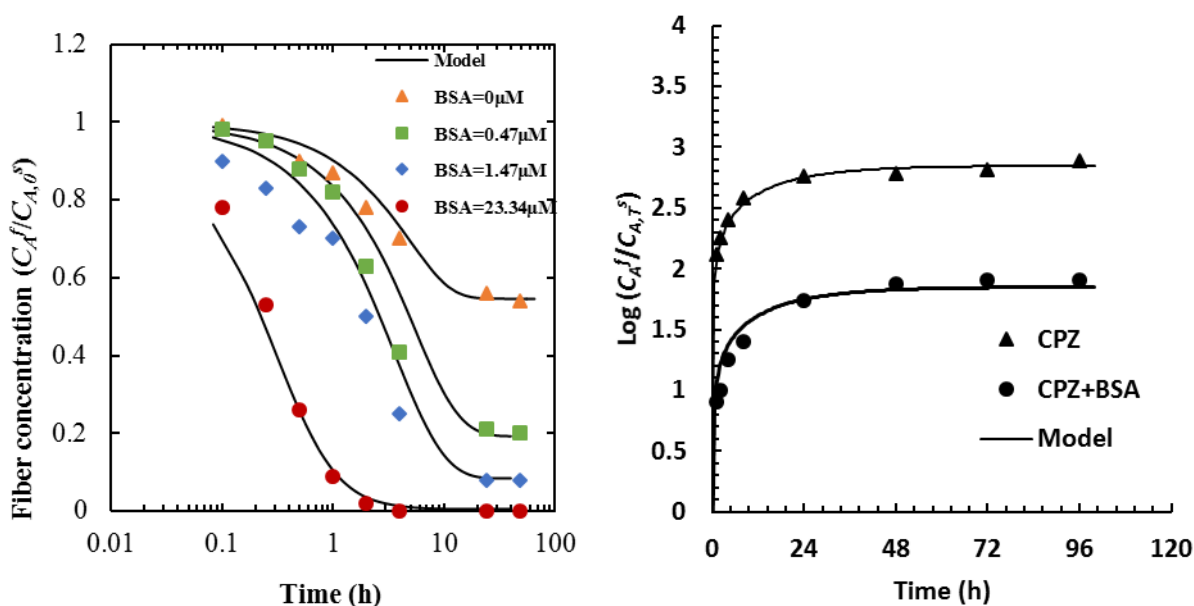
Figure 3-2. Influence of matrix (albumin) on the equilibrium time. Both the equilibrium time and concentrations of extracted analyte were influenced by the presence of albumin in pyrene extraction in PDMS fiber (a). Only the extraction amount was influenced by the presence of albumin in chlorpromazine extraction by polyacrylate coating (b). The experimental and model data are shown in Table 3-1.

3. 4. 2. Mechanisms of Matrix Effects on Equilibrium Time.

A literature review indicates that possible binding matrix effect on SPME kinetics fall into three different categories. The most common is reduced equilibrium time, which is particularly problematic when the goal is to measure the freely dissolved concentration under non-equilibrium conditions. In other words, calibration of SPME under non-equilibrium conditions would be

possible only if the binding matrix containing the sample to be analyzed and the calibration sample (without binding matrix) had identical uptake dynamics. The reduction of equilibration time was typically observed where the amount of analyte extracted by the coating was negligible (usually less than 5%) compared to the initial amount present in the sample, that is, the depletion was negligible.[74] The second class of binding matrix effect observed was with sampling systems where a significant quantity of analyte was depleted from the sample solution. While the rate of extraction becomes slower in the binding matrix-containing sample, the extracted amount is almost the same compared to the standard sample.[82] The third class of binding matrix effect pertains to an initial fast extraction followed by a slower rate, which increases the equilibration time with significantly lower extracted amount at equilibrium.[83] With the help of an asymptotic analysis,[77] these three possible scenarios can be described by the present model and are explained next.

To explain the effects of a binding matrix component on uptake kinetics, the physical process of transport under the condition of diffusion-limited extraction is described by considering the following three dimensionless parameters. A represents the amount of freely dissolved analyte (C_A) at the beginning of the experiment relative to the total amount of binding matrix ($C_{M,T}$):

$$\alpha = \frac{C_{A,0}}{C_{M,T}}$$

This term is influenced by K_D of the analyte−matrix pair, since the system is assumed to be initially at equilibrium; therefore, α represents a measure of free analyte in the sample matrix.

The second parameter, β, relates the time scale of analyte diffusion to the time scale of unbinding of the analyte−matrix complex:

$$\beta = \frac{L^2 k_d}{D_A^s}$$

This term is dependent on size of the sample container (L), dissociation rate of the complex (k_d), and diffusivity of the analyte through the sample (D_A^s).

The third parameter, γ, is the concentration of bound matrix component in the sample relative to the unbound portion at the beginning of the experiment:

$$\gamma = \frac{k_a C_{A,0}}{k_d} = \frac{C_{A,0}}{K_D}$$

For $\gamma \gg 1$, most of the binding matrix component is in the bound state initially. Conversely, if $\gamma \ll 1$, only a small fraction of the binding matrix component has bound analytes. This term is governed by K_D and the amount of free analyte at the beginning of an experiment.

3. 4. 3. Scenario 1: Shorter Equilibrium Time and Diffusion Controlled Kinetics.

At first, the diffusion-controlled kinetics of SPME was established by increasing the diffusivity of the analyte in the solution and observing the concomitant changes in extraction time profiles (Chapter-2, Figure 2-3). An increase in analyte diffusivity in the solution, from 1×10^{-9} to 5×10^{-6} m^2/s, yielded a substantially faster uptake rate, which supports the diffusion-controlled kinetics hypothesis. All the kinetic studies presented in the following sections were carried out under the condition of diffusion controlled kinetics.

Effect of K_D on uptake kinetics

In order to study the effect of different parameters on extraction, an experimental system using chlorpromazine binding to BSA was considered,[79] where the equilibrium dissociation constant

(K_D) was calculated as 5.4×10^{-4} M. K_D is a measure of binding strength between the analyte and the binding matrix; generally, the higher the hydrophobicity (higher log P), the lower the K_D value for the analyte−binding matrix complex. Please note that a PDMS coating was assumed instead of using a polyacrylamide coating, as the present scenario aims to study extraction under the diffusion-controlled regime. The mathematical model was used to investigate the effect of K_D on extraction kinetics, since the kinetics are not sensitive to changes in individual values of k_a and k_d (Figure 3-3).
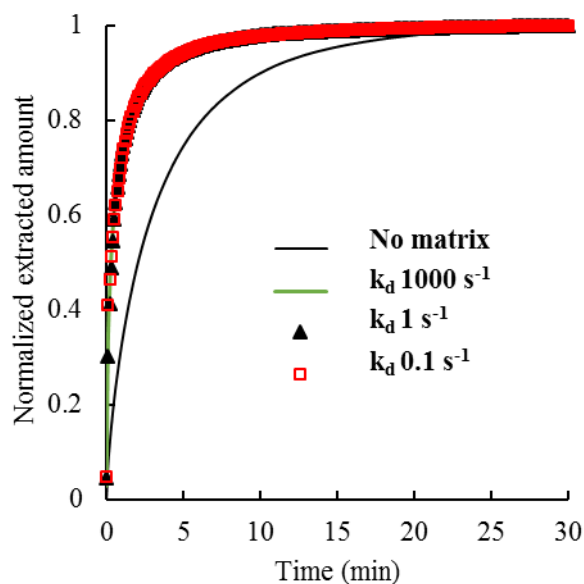
Figure 3-3. Model simulation results obtained for chlorpromazine binding to bovine serum albumin (BSA) of K_D of 5.4×10^{-4} M with different k_a and k_d values. The k_a values were calculated based on the equation $K_D = k_d / k_a$. The influence of the different physically relevant k_d values on the equilibration time was negligible. For all these experiments, $\beta \gg 1$ and $\gamma \ll 1$. The convection was set zero (static conditions). All other model parameters are presented in Table 3-1.

The effect of K_D was studied by varying k_d while keeping k_a constant, since the rate of association tends to be more consistent between binding pairs than the rate of dissociation. Figure 3-4a shows that the kinetics of extraction is influenced by the strength of the analyte−matrix pair (K_D). Interestingly, K_D values of 10^{-5} and 10^{-6} provided the most significant enhancement in this study. The asymptotic analysis provided that under the conditions of diffusion-controlled kinetics, that is, fast decomplexation ($\beta \gg 1$) and with a small proportion of bound matrix component ($\gamma \ll 1$), extraction occurs on a single time scale (t_s)[77], according to

$$t_s = \frac{L^2(1 + C_{M,T}/K_D)}{D_A^s} \qquad\qquad 3\text{-}6$$

This term demonstrates that equilibrium time is dependent on hydrophobicity of the analyte at constant values of $C_{M,T}$, L, and $D^s{}_A$. Increasing hydrophobicity under these conditions will lead to a decrease in equilibration time. The model predicts that a weak interaction (10^{-3} M) does not appreciably affect the equilibration time (equilibrium reached at 20 min), whereas a strong interaction (10^{-6} M) significantly reduced the time needed to reach equilibrium to only 5 min. A weak binding matrix component does not appreciably perturb the kinetics under these conditions, although the conditions $\beta \gg 1$ and $\gamma \ll 1$ pertained in all cases. It is worthwhile to mention that with the increase in K_D, increasing amount of analyte remains bound to the matrix and therefore the quantity of free analyte becomes less. With the decrease in the free concentration the initial uptake rate actually decreases. This can be seen if the Figure 3-4a is zoomed out and displayed without normalization of the extracted amount. This data treatment shows that the uptake rate for analyte solution without binding matrix component is the highest (Figure 3-4b). The rate also decreases as the free concentration decreases with binding strength between the analyte and matrix increases. Although the initial uptake rate for sample solution without matrix is the highest, it takes the longest time to reach equilibrium (shown in Figure 3-4a).
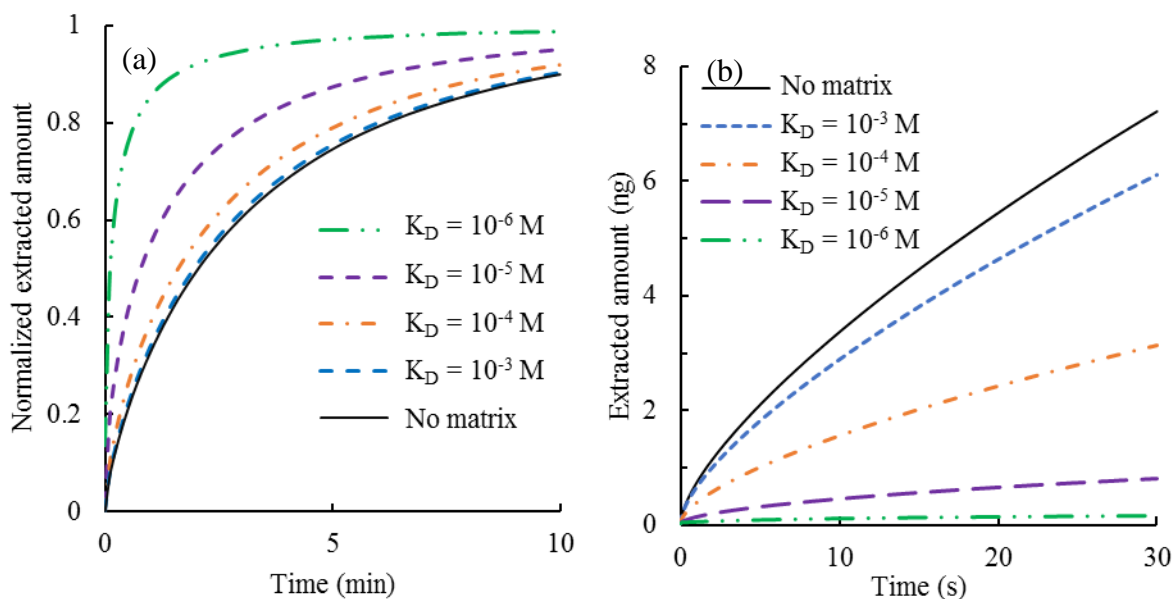
Figure 3-4. Model simulation of extraction kinetics influenced by varying the strength of the binding matrix from weak (K_D = 10^{-3} M) to strong (K_D = 10^{-6} M), for a chlorpromazine to BSA ratio of 1: 2.5, (a). Extracted amount at the initial stage of extraction, (b). For these studies, k_a was kept constant at 1×10^6 M^{-1} s^{-1} and k_d varied to obtain different K_D values. For all values of k_a and k_d, $\beta >> 1$ and $\gamma << 1$. Analyte depletion was assumed negligible (less than 5%) by setting radius of the sampling container (L) at 10 mm which is equivalent to 15 mL of the sample. Moreover, the convection was set zero to assume only diffusion controlled transport of analyte.

We assume that with the decease of free analyte concentration in solution, due to progressively stronger binding affinity toward the binding matrix, the fiber coating requires lesser amount of analyte to reach equilibrium. For instance, when K_D is equal to 10^{-5} or 10^{-6}, the binding matrix buffers the system, leading to very low free analyte concentration and consequently reducing the equilibration time. Moreover, the concentration gradient in solution domain extends a shorter distance for the high K_D values, whereas a thicker gradient is obvious for solution free of binding

matrix, as the complex located close to the coating provides the required amount of analyte to reach conditions close to equilibrium value (Figure 3-5).
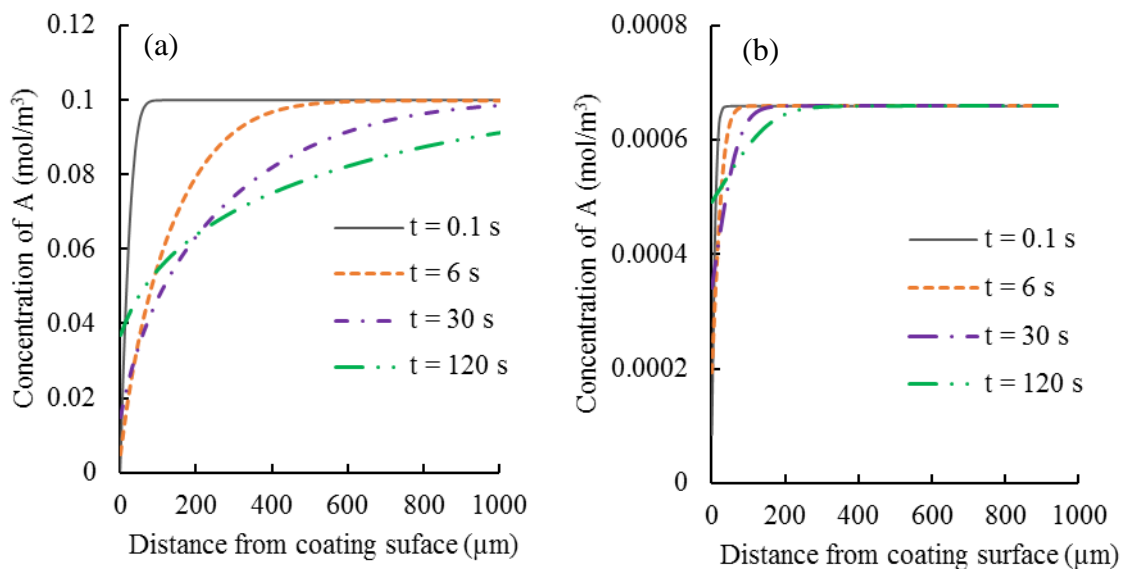
Figure 3-5. Concentration profiles of the analyte as a function of distance from the coating surface at different extraction times. Model simulation without adding matrix into analyte of concentration 100 uM (a). Model simulation with the presence of 250 uM matrix component of strong ($K_D = 10^{-6}$ M) binding affinity. The convection was set zero (static conditions). All other parameters were kept constant, as shown in Table 3-1.

Therefore, equilibration time becomes shorter for samples containing binding matrix compared to extraction from matrix free solution, when the concentration is equal to the free concentration in solution containing the binding matrix component.

Effect of Analyte to Binding Matrix Component Ratio on Equilibrium Time

The mathematical model was used to examine the effect of the ratio of initial analyte to binding matrix component (for example, BSA), containing both weak and strong binding, on the

reduction of equilibration time. In this case, the analyte concentration was held constant while the BSA concentration was varied. As shown in Figure 3-6a, for the weak binding complex system ($K_D = 5.4 \times 10^{-4}$ M), the simulation results show that an increase in analyte to BSA ratio from 1:25 to 1:1000 provides a 25% reduction of equilibration time. For the strong binding complex system ($K_D = 5.4 \times 10^{-5}$ M), shown in Figure 3-6b, a similar range of reduction is achieved with an increase in ratio from only 1:2.5 to 1:100.
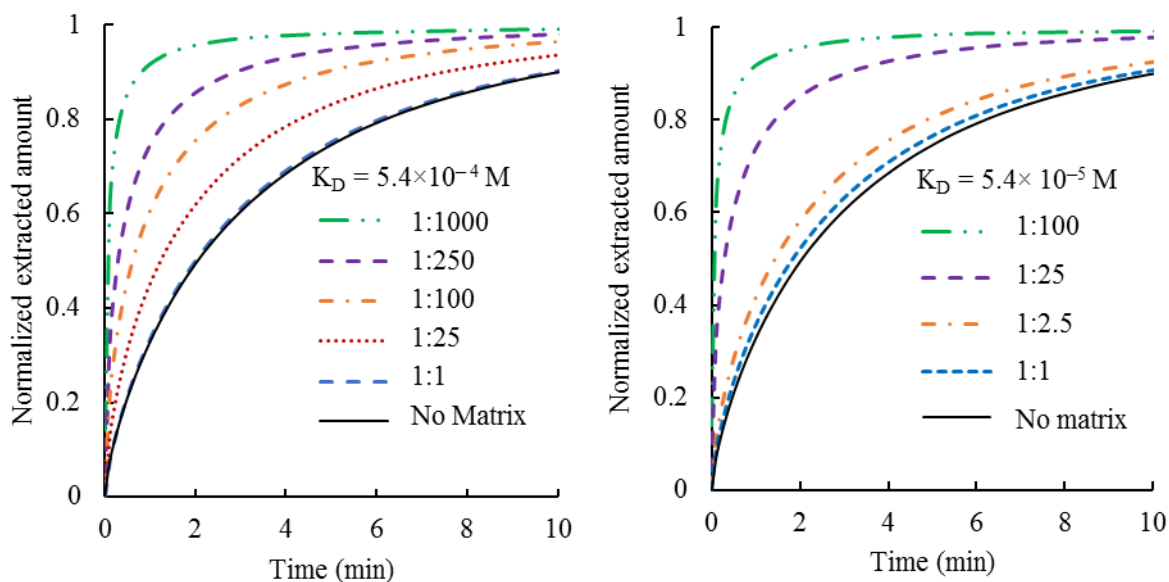
Figure 3-6. Effect of analyte-to-matrix ratio on the extraction kinetics. Weak binding complex, (a) and strong binding complex (b). The extent of kinetic enhancement is positively influenced by the strength of the binding partners.

This phenomenon can be analyzed with the time scale according to eq. 3-6. If $C_{M,T}/K_D \ll 1$, then the equilibration time is independent of both matrix concentration and K_D. Therefore, the concentration of binding matrix component must be greater than K_D for shorter equilibrium time to obtain. In other words, at a lower ratio of analyte to binding matrix component, the equilibrium

66

time is barely affected by the matrix, but the effect becomes pronounced as the ratio increases. This also supports the findings from a study of different K_D values, presented in the previous section, that the shorter equilibration time is due to the extraction of less free analytes to attain equilibrium. Ramos et al.[84] reported that the binding matrix (humic acids) did not interfere with determination of the freely dissolved concentration of hydrophobic organics under nonequilibrium SPME with a PDMS coating. Oomen et al.[85] indicated that this observed result might be due to the use of a very low concentration of matrix in the experiment, which produced a lower concentration of bound matrix than that of free analytes. The present mechanistic model with the asymptotic analysis quantitatively explained the required conditions for influencing equilibrium time.

3. 4. 4. Scenario 2: Retarded Uptake Rate and Diffusion Controlled Kinetics

A decrease in uptake rate or longer equilibrium time has been observed in cases where the uptake is still controlled by the diffusion of analyte in solution. However, in such cases, the freely dissolved analyte is locally depleted in the diffusion boundary layer due to the higher amount of extraction by the fiber; that is, local depletion is significant. In that case, analytes need to diffuse from longer distances for the system to reach equilibrium. Poerschmann et al.[82] reported a retardation in the uptake rate after addition of humic or fulvic acid to a water sample with organotin compounds; that is, the time to reach equilibrium was increased. Similarly, a retardation of uptake kinetics is observed when smaller sample volumes and lower concentrations of analyte are used compared to the capacity of the SPME coating. For instance, Reyes-Garces et al.[83] reported slow uptake rates for some moderately hydrophobic compounds (for example, metoprolol) in blood plasma samples. This category of binding matrix effect can be explained by the asymptotic analysis and the proposed mathematical model. This type of longer equilibrium is observed when the

kinetics are controlled by diffusion ($\beta \gg 1$) and when a large proportion of the binding matrix component is bound ($\gamma \gg 1$). A two-stage extraction time profile is obtained with the initial time scale of $(L^2/D_A{}^s)[1 + (C_{M,T}/C_A)]$. At this stage, the extraction kinetics depends on the total binding matrix concentration ($C_{M,T}$) and the initial free analyte concentration (C_A). Dependence of the initial uptake kinetics on the concentration of free analyte is shown in Figure 3-7. Here the initial uptake rate increases with decreasing binding matrix component to analyte ratio, whereas the equilibration times remain the same.
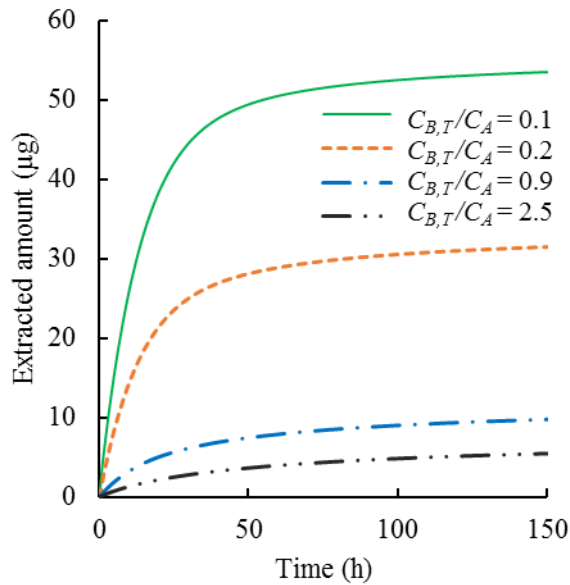
Figure 3-7. Model simulation of the extraction time profile at different ratio of binding matrix component (BSA) to analyte (chlorpromazine). The concentration of the binding matrix component ($C_{M,T}$) was kept constant at 100 µM and the free analyte concentration (C_A) was varied from 40 µM to 900 µM. The binding strength (K_D) was kept constant at $1E^{-5}$. The convection was set zero (static conditions). All other model parameters are shown in Table 3-1.

As the free analyte concentration is depleted until its concentration is equal to K_D, the second stage of extraction starts with a time scale of $(L^2/D_A{}^s)[1 + (C_{M,T}/K_D)]$ for the remaining analyte molecules present in the sample. The latter time scale is identical to the shorter equilibration time with the binding matrix discussed above in scenario 1. For the extraction time profile of sample containing binding matrix, an initial fast extraction is followed by slow diffusion-controlled conditions, compared to the one stage and faster equilibration for the solution free of binding matrix (Figure 3-8). The equilibration time is governed by the second time scale, which depends on the binding strength (K_D values) between the analyte and binding matrix component. With the increase of

binding strength, the equilibrium times are clearly shown to be decreased. Furthermore, the mathematical model was employed to study the concentration profiles in solution domain at different times of extraction under static conditions (Figure 3-9).
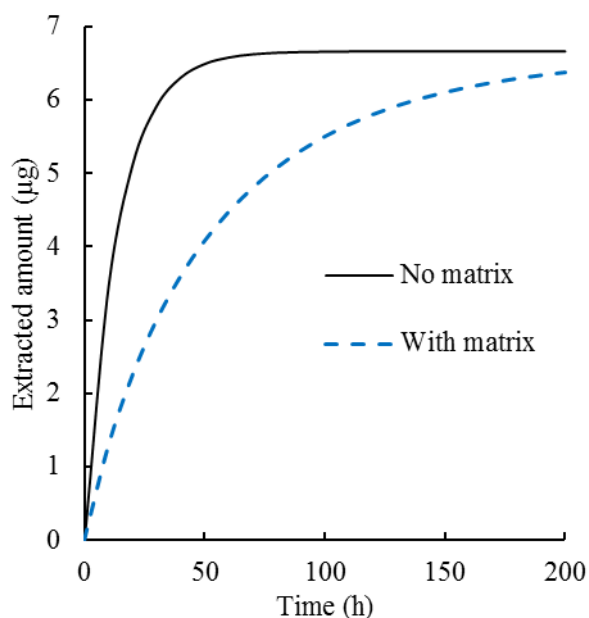
Figure 3-8. Retardation of uptake kinetics in the presence of matrix. Extraction time profiles in pure water without the addition of matrix (solid line, black) and with the addition of matrix (dashed line, blue). Parameters are shown in Table 3-1.

It is seen that the gradients are steeper for matrix-free standard analyte solution compared to the sample containing binding matrix. The concentration gradients extend throughout the vial for both sample containing binding matrix and matrix-free solution, unlike scenario 1, where the gradients are thinner for sample containing binding matrix compared to the matrix-free case (Figure 3-9). Therefore, the mathematical model presented here can be used to predict uptake profiles in cases where the rate is retarded by the local depletion of analyte but where the kinetics are still diffusion controlled.
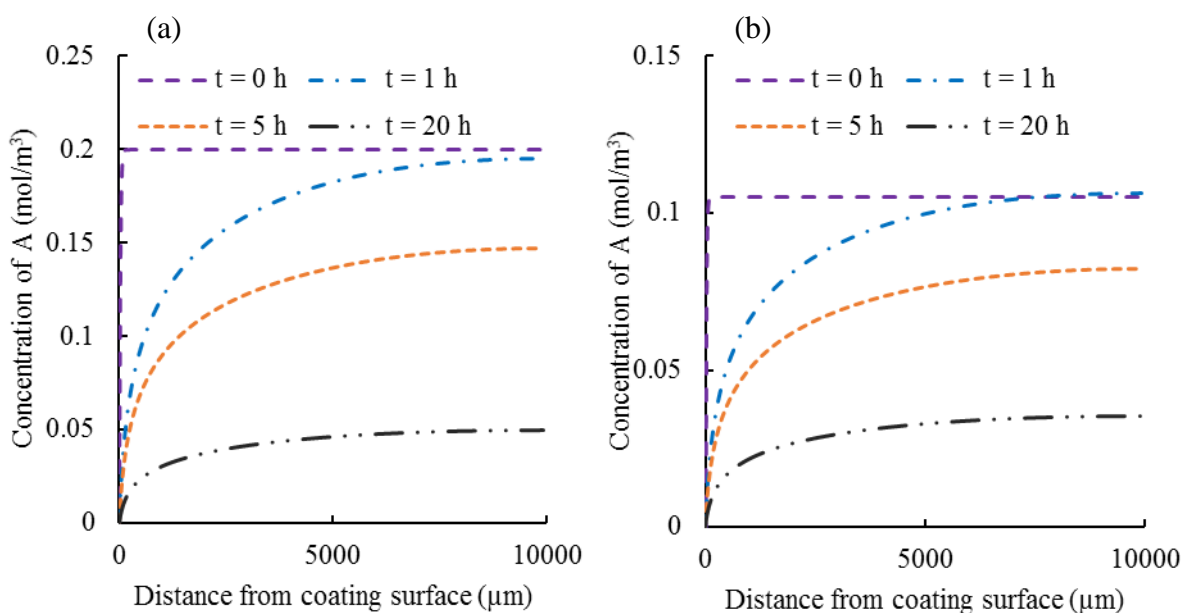
Figure 3-9. Concentration gradients of the analyte as a function of distance from the coating surface at different extraction times. Model simulation without adding binding matrix component into analyte concentration of 110 uM (a). Model simulation with the presence of 100 uM matrix component of binding affinity, $K_D = 10^{-5}$ M. The convection was set zero (static conditions).

3. 4. 5. Scenario 3: Retarded Uptake Rate and Analyte Dissociation-Controlled Kinetics.

In the third case, the matrix substantially reduces both the uptake rate and the extraction amount at equilibrium. This type of profile was recently reported by Reyes-Garces et al.[83] for extraction of a very hydrophobic analyte, stanozolol (K_D with human serum albumin, HSA, $= 5 \times 10^{-9}$ M) from a blood plasma sample. From the mathematical analysis and computational simulation, the condition for this scenario is that the dissociation of bound analyte from the binding matrix is slow compared to diffusion in solution; that is, $\beta \ll 1$ or $(1/k_d) \gg (L^2/D_A^s)$. Any free analyte produced by dissociation of the analyte−matrix pair is negligible compared to the existing

freely dissolved analytes in the sample solution. As shown in Figure 3-10, nearly all the freely

dissolved analyte is extracted by the coating over the diffusion time scale, L2/DAs.
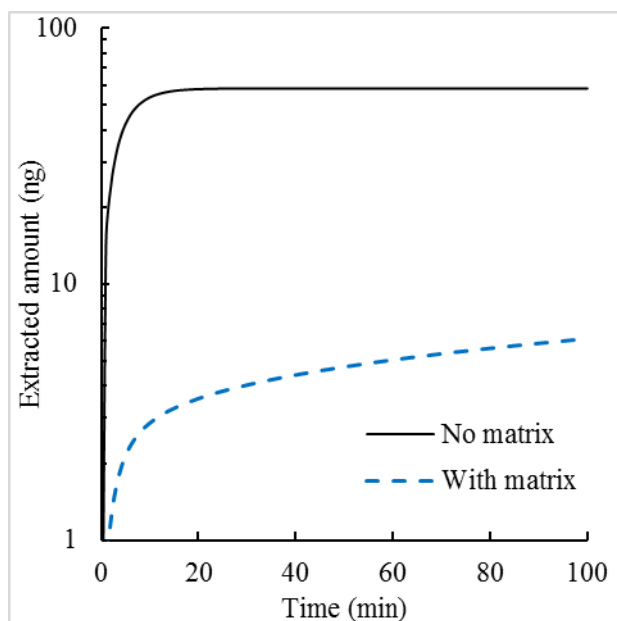
Figure 3-10. Retardation of uptake kinetics, which is controlled by dissociation of
analyte from the bound matrix. Extraction time profile in the absence of matrix (solid
line, black) and in the presence of matrix (dashed line, blue).

The initial fast diffusive uptake is followed by slow dissociation of bound analytes over the

time scale of $1/k_d$. The uptake rate in the latter stage increases with faster dissociation of analyte

from the binding matrix (see FigureS9a). Since analyte diffusivity through environmental or

biological samples does not change significantly, either k_d or L needs to be modified for our

computational sample system to observe this type of slow kinetics. It is more feasible to modify

the diameter of the sample container than the binding kinetics. If the diameter is kept constant at

10 mm, as in the previous simulation experiments, a k_d of $<10^{-4}$ s^{-1} is required for $\beta \approx 1$.
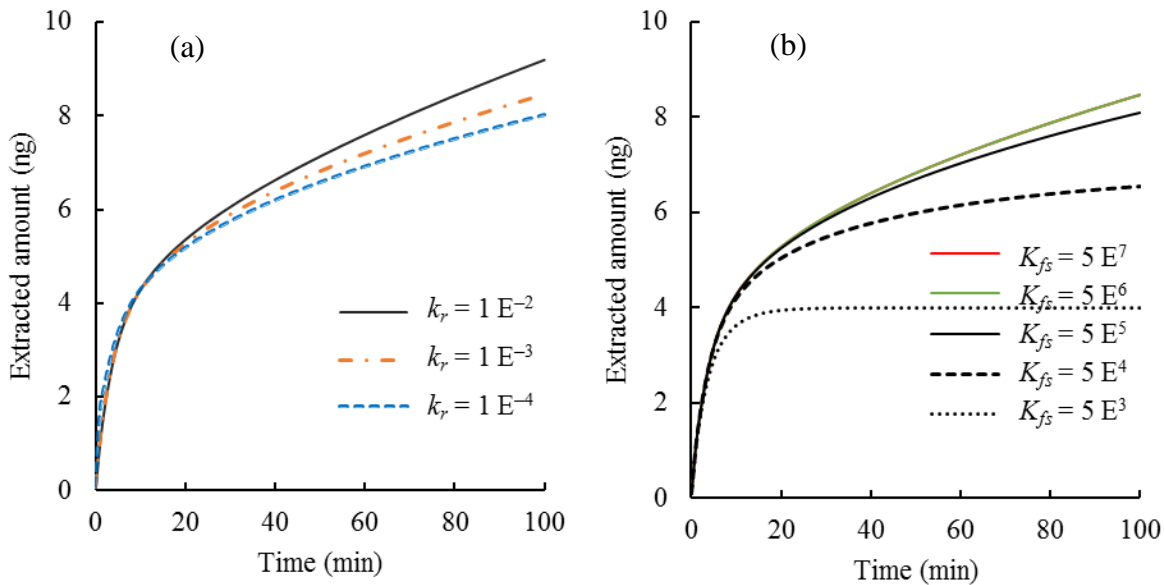
Figure 3-11. Retardation of uptake kinetics for the scenario three. Effect of unbinding constant (k_d) on the uptake kinetics of an analyte (for example, stanozolol) with the presence of a binding matrix component, (a). Extraction time profile is affected by the value of K_{es} at $k_d = 1\mathrm{E}^{-3}$, (a). Effect of K_{es} on the second stage of kinetics for the scenario three, (b). Here, $K_D = 5\mathrm{E}^{-9}$ M and $C_A = 5.1$ μM, $C_{M,T} = 100$ μM and $L = 1$ mm. The convection was set zero (static conditions).

This translates to a bound matrix with a half-life of ~3 h. However, if the vial diameter is sufficiently decreased, it is possible to achieve $\beta \ll 1$ for physically relevant k_d values. More precisely, in order to observe the unbinding-controlled dynamics, the diameter L would need to be below the order of $(D_A{}^s/k_d)^{1/2}$. It was also found that the slower uptake rate is dependent on the extraction capacity of the coating (K_{es}) when the value of k_d is kept constant (Figure 3-11b). The information provided by the above analysis can be used to design an experimental setup with desired extraction time profiles. In scenario 1, the rate of analyte extraction decreases smoothly over a single time scale. In scenarios 2 and 3, there are two distinct time scales: an initially fast

73

uptake rate, followed by a more gradual uptake rate. The two time scales in scenario 2 are related, as they are both proportional to $L^2/D_A{}^s$, whereas the two time scales in scenario 3 are independently controlled by $L^2/D_A{}^s$ and k_d, as long as $\alpha \gg \beta\gamma/(\gamma + 1)$ and $L \ll (D_A{}^s/k_d)^{1/2}$. Another key difference between scenarios 2 and 3 is that all of the bound analyte molecules remain in the bound state throughout the fast mode for scenario 3, while approximately half the bound analyte molecules undergo unbinding in the initial fast stage for scenario 2. Thus, the complex sample system can influence not only the time scales of extraction but also the amounts of analyte extracted in each stage.

3.5   Summary

In this chapter, a mechanistic-based mathematical model that describes the uptake kinetics in SPME of analytes from either a binding matrix-free standard solution or a matrix-containing solution. The proposed mathematical model provided excellent prediction of the experimental data available in the literature. The majority of discussion was limited to static conditions, but the conclusions are analogous to cases involving convection. In the case when convection (e.g., stirring) is present, mass transfer is controlled by diffusion in the boundary layer formed close to the coating surface, not in the whole vial, as demonstrated in the static case where the boundary layer is equivalent to the size of the vial. It should be emphasized that agitation level will determine the mass transfer rates and the equilibrium value, but in this contribution we focused on binding matrix effects exclusively, as they are poorly understood. It was not clear under what experimental conditions the uptake rate is altered with the presence of a binding matrix in sample solution. Now, with the help of this mathematical model and computational simulation, one can easily determine

whether the presence of a binding matrix can alter the equilibrium time, based on the physicochemical properties of analyte and matrix, as well as the choice of SPME coating. The modeling has demonstrated that the decrease in equilibration time is not due to increased rate of extraction but to the requirement of less extracted amount to reach equilibrium when binding matrix is present. Overall, the simulation results obtained for the present analysis have shown that the present model is a reliable and relatively inexpensive practical method of characterizing the performance of SPME. This model can be used for sample matrices containing one type of analyte binding component. However, for biomedical applications such as human blood or tissue sampling with SPME, further improvement of the model to describe multicomponent phenomena is needed. We are currently extending this study to the application of SPME extraction in tissue or blood sampling. In addition, the good agreement between experimental results and modeling indicates that determination of binding constants and associated kinetics can be obtained from experimental data by appropriate fit of calculated values.

Chapter 4   **Calibrant-loaded on extraction phase approach**

4.1   **Introduction**

The mathematical correlation, also called "calibration", between the extracted amount of target analytes on an extraction phase and their concentration in the sample matrix is quite straightforward when the two-phase system reaches equilibrium.[86] Typically, determinations of analyte concentrations at equilibrium conditions are conducted under certain conditions: with the use of very thin extraction phases (extractant) with low extraction capacity, for analytes with low to moderate partition coefficients, or with very high sample agitation conditions.[87] However, when sampling certain analytes in slow agitation samples, such as sampling of polycyclic aromatic hydrocarbons (PAHs) from aquatic environments, unfeasibly long periods may be needed to transport enough analytes to the extractant through the aqueous boundary layer, and thus, reach equilibrium.[88,89] In addition, aiming to reach equilibrium under such long exposure times in real sample matrices can result in deterioration of the extractant, owing to unwanted interactions with sample matrix components *in vivo* or *in situ*. In order to avoid long equilibration times, as well as increase measurement accuracy, an alternative pre-equilibrium calibration approach has been proposed by Chen et al.[90] The pre-equilibrium calibration method is based on the concurrent desorption of a chemical species previously loaded onto the extraction phase while extraction occurs under the same experimental conditions. The pre-loaded species should have similar physicochemical properties to the target analyte, and must not be present in the sample matrix. In this method, the loaded chemical is assumed to follow a desorption kinetics model that is identical to the extraction kinetics of the target analyte from the sample matrix. In the kinetic regime of the

extraction profile, this method of calibration has been called "kinetic calibration",[90] "on-fiber standardization" [91] or stable isotope solid phase microextraction (SI-SPME)[92]. Although the method was first utilized with poly(dimethylsiloxane) PDMS-based solid-phase microextraction (SPME), a number of different sorbents with different geometries have been studied, such as porous particle-based SPME, liquid-phase microextraction (LPME), hollow fiber-protected liquid-phase microextraction (HF-LPME), Stir bar microextraction (SBME), etc.[93] This kinetic calibration method has been extended to many applications, showing that the method compensates for variations in experimental conditions. For example, Zhan et al[94] demonstrated that the calibrant-loaded SPME approach can compensate for the effect of matrix tortuosity and protein binding. However, during pre-equilibrium extraction, small variations in experimental conditions such as sample volume, temperature, agitation, binding matrix components, and sampling time have been noted to sometimes result in significant experimental error.[95] In fact, some researchers in our own group have reported non-symmetric behaviors related to the adsorption kinetics (unpublished data).

It is difficult to experimentally test the suitability of different calibrants for a wide range of analyte properties. Recently, we developed a computational model for the mass transport processes in SPME [96] The model considers the extraction phase as having an analyte concentration that is equal to zero in the beginning of the extraction process. Here, diffusion only transport in the extraction phase is assumed, while analyte transport in the sample matrix is assumed to occur by convection and diffusion coupling with a reversible reaction to a binding matrix component present in sample. The model results suggest that the extraction kinetics are dependent on a number of parameters, including the concentration of the binding matrix and the binding affinity of the

analyte to the matrix. These findings served as the primary motivation for the present study, which focuses on the study of the desorption kinetics of a calibrant that is pre-loaded on the extraction phase prior to deployment to the sample matrix. While the study of chemical release from pre-loaded materials to different phases remains an active field of research, such as in areas that focus on research related to drug delivery[97] and performance reference material (PRC)[48] based calibration, modeling of the quantitative relationship between the release and sorption is still limited.[98,99]

In this chapter, a mathematical model and computational simulation to estimate calibrant desorption and analyte sorption kinetics is described. The resulting data can facilitate the selection of calibrants for a variety of applications. Moreover, the effects of various environmental conditions such as hydrodynamics, temperature, and the presence of a binding matrix have been characterized for CL-SPME quantification.

4.2   Computational models of calibrant-loaded SPME (CL-SPME)

4. 2. 1. Modeling analyte transport and reaction in the sample matrix

The computational model described in chapter 2 and 3 accounts for processes occurring during extraction by an SPME coating, namely the transport and reaction within the sample matrix .[96] In this chapter, the same model was employed for extraction. However, for desorption of calibrant, the calibrant is assumed to be present in the extraction phase, where transport occurs only by diffusion. As depicted in Figure 4-1, the model considered a two-dimensional segment of a sample-extractant system. The flow in the sample domain is governed by the Navier-Stokes equation, while the flow field is treated as steady.
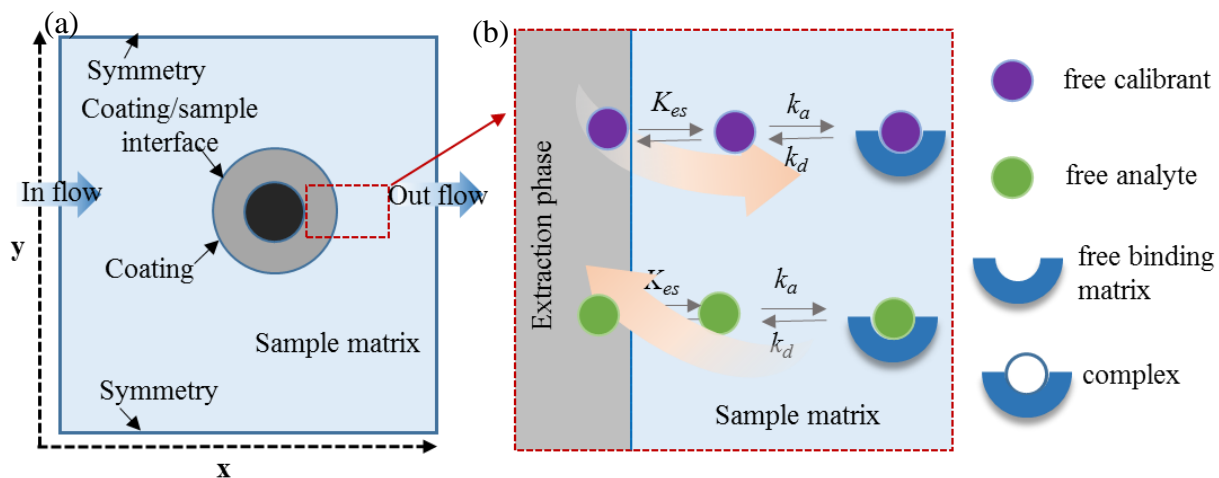
Figure 4-1. a) The geometrical configuration of the SPME-sample system used in the computational model. SPME consists of some durable structure (black) coated with a thin layer of polymer. The coating is in contact with the sample matrix. b) The interaction process in matrix-analyte-SPME system. Calibrant (purple) pre-loaded to the coating transported from the coating via diffusion to the sample matrix where it is subject to diffusion and convection in its free phase and may bind to specific binding sites of matrix components. Analytes (green) present in the sample either free or bound to the matrix transports to the coating where only free analyte is extracted. Diagram is not to scale.

Time-dependent analyte or calibrant transport occurs as follows: 1) the loaded calibrant diffuses through the coating layer and, due to a concentration jump, a mass flux is established across the interface,[100,101] where the calibrant begins being transferred to the adjacent sample medium; 2) in the sample matrix, chemicals transport via convection and diffusion, with specific binding and unbinding to the binding matrix component taking place.[102] For the interaction of calibrant or analyte with the binding matrix, a nonlinear saturable reversible binding model is considered. The

reaction shown in equation 4-1 describes a 1:1 reversible and saturable binding for a matrix component (M) with analyte or calibrant (A).

$$A + M \underset{k_d}{\overset{k_a}{\rightleftarrows}} A\,M \qquad\qquad 4\text{-}1$$

In this reaction, k_a and k_d represent the second-order association (binding) rate constant and first-order dissociation (unbinding) rate constant, respectively, for the interaction of M with A. The ratio (k_a/k_d) is defined as the association equilibrium constant (K_a) for this system. The mathematical equations for the binding of calibrant and analyte to the matrix components are the same as reported previously.[96]

4. 2. 2. Numerical methods

COMSOL Multiphysics 5.1, a finite element method (FEM) based software package, was utilized in this study to analyze the mass transfer processes in CL-SPME. In order to obtain an accurate representation of the SPME system, the time-dependent partial differential equations for each of these physical processes must be solved simultaneously. The procedure used to solve this problem is divided into two steps: (1) determination of the fluid velocity profile at steady-state, assuming incompressible flow, and (2) use of this steady-state velocity profile as the initial condition to solve for the coupled transient mass transport and sorption equations.[103,104] The rate constants a_e and a_d can be obtained through equations 1-22 and 1-23, respectively, if the initial amount (q_0) of calibrant loaded onto the coating, sampling time t, and the quantity extracted at equilibrium are known.

4.3   Results and Discussions

4. 3. 1. Desorption kinetics of loaded calibrant

Soon after the extraction phase comes into contact with the sample matrix, analytes are transported from the sample matrix and into the extraction phase, while the calibrant pre-loaded on the extraction phase releases into the sample.[90] Fractions of calibrants with different partition coefficients (K_{es}) released from the pre-loaded coating are shown in Figure 4-2. The release of chemicals with high K_{es} proceeds more slowly than that of chemicals with a low K_{es}. For the finite volume sample shown in Figure 4-2a, complete release did not occur for even the lowest K_{es} calibrant. As the calibrant is released into the finite volume sample, the calibrant concentration builds up in the external volume, allowing for local equilibrium to be established between the extraction phase and the sample. As an apparent equilibrium is established, further release of calibrant from the extraction phase comes to a halt. In addition, lower fractions are expected to be desorbed with calibrants of higher K_{es}. On the other hand, for infinite sample volumes, the release proceeds either to completeness (for low K_{es}) or linearly decreases (for high K_{es}) to reach full desorption from the extraction phase (Figure 4-2b). This is owing to the fact that the concentration of calibrant in an infinite sample medium never increases due to the existence of perfect sink conditions at any time of sampling.[105] Since the SPME-sample system is primarily controlled by the diffusion boundary layer (δ_s), the magnitude of the K_{es} is the most important driving force of desorption kinetics. Although δ_s is assumed to vary with compound diffusivity by a factor of $(D_s)^{1/3}$, aqueous diffusivity usually does not vary in most cases.[106,107] Even in cases where a difference in diffusivity between compounds is present, the primary driver of release kinetics is

the difference in partition coefficients. More discussion on the effect of diffusivities is included in the Chapter 5.
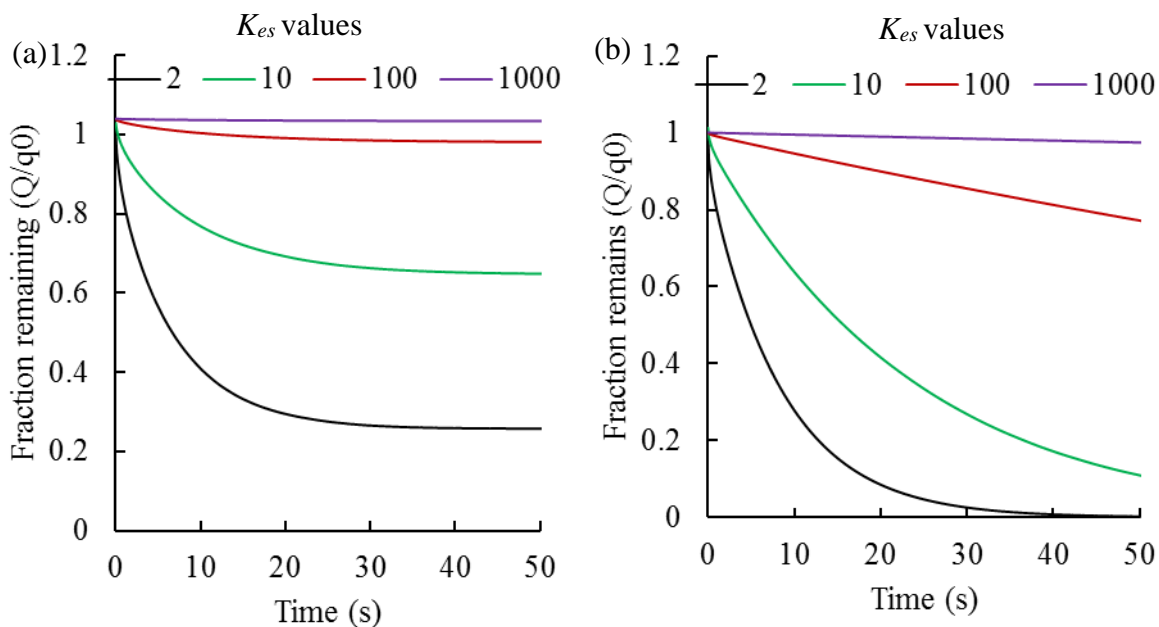
Figure 4-2. Fractions of calibrants remaining on the extraction phase at different partition coefficients (K_{es}) (a) finite sample volume, flow velocity $= 0$ cm s^{-1} (b) infinite sample volume with flow velocity of 0.1 cm s^{-1}. For both the cases, absence of a binding matrix component is assumed. Coating thickness was 45 um; D_s (7.33e^{-6} cm^2 s^{-1}) was considered for all the calibrants so that δ does not vary by the compound. $D_e = D_s/6$.

The simulation results suggest that the choice of calibrant for a given application should be primarily made based on the partition coefficient of the calibrant. If too much calibrant is released too quickly, it may have a toxic (for in vivo sampling) or short-term effect on the sample matrix. On the other hand, if the calibrant is released too slowly, then the remaining quantity may not differentiate with the initial load. From a practical point of view, it is often impossible to evaluate

the full sorption/desorption time profiles of chemicals with a high log K_{es} (>5), owing to the extremely long equilibrium times of such target analytes and the very low desorption rates for calibrants in the coating.[108] If the release of calibrant from the coating is too slow to allow for a statistical evaluation of the extraction or desorption kinetics, the estimated rate constant values (a_d) will be poor, and statistically not significantly different from zero. CL-SPME is a practicable extraction technique only for compounds for which significant desorption can be measured within the experimental time period. In contrast, the mechanistic model can be employed to obtain the fraction of analytes accumulated or dissipated at any point of the sampler deployment period for any pair of analyte and calibrant. The currently proposed model allows for the prediction of a reasonable offload amount suitable for SPME calibration.

4. 3. 2. Iso-symmetry between extraction and desorption, and model validation

Although the CL-SPME approach has been employed for the equilibrium regime of extraction[109], most applications were in the kinetic regime owing to the short sampling times afforded by the technique. The main assumption of the kinetic calibration approach is that the desorption of calibrant must follow kinetics similar to the uptake kinetics of the corresponding analytes. In order to show iso-symmetry, the extracted amount and the calibrant remaining on the extraction phase are normalized by the amount at equilibrium and the loaded amount, respectively, as plotted in Figure 4-3. In Figure 4-3a, previously published experimental data was replotted along with the model simulation results for a d8-pyrene loaded PDMS fiber exposed to a flowing pyrene aqueous solution for different extraction times[110]. Very good fitting of the experimental data validates the numerical model used in this work.
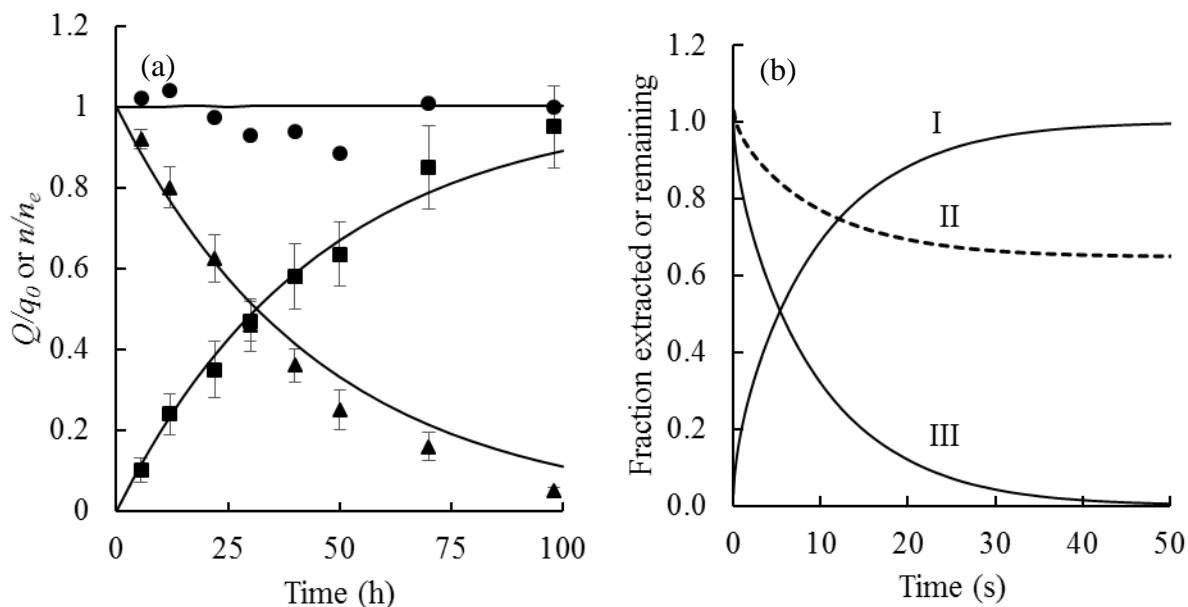
Figure 4-3. Iso-symmetry of sorption and desorption in calibrant-loaded SPME. (a) Simultaneous sorption of pyrene (■) onto the PDMS coating from the flow-through system and desorption of deuterated pyrene (▲) from the PDMS coating into the flow-through system; (●) represents the sum of Q/q0 and n/ne. (b) The iso-symmetric behavior for a finite volume sample that needs correction to account for local equilibrium; I) extraction profile of an analyte, II) desorption profile of the calibrant, and III) desorption profile of the calibrant after correction with equation 4-2). Parameters are same as shown in Figure 4-2.

The iso-symmetric behavior of sorption and desorption can be recognized by the intersection point of the two time profiles at around 0.5 of the y axis. In other words, 50 percent extraction and desorption are achieved at the same time of deployment in the sample matrix (in this example, the elapsed time is approximately 30 hours). The iso-symmetry of the processes can also be verified when the sum of Q/q_0 and n/n_e at any time is close to 1 (see eq. 1-24). With the availability of iso-

symmetric sorption and desorption time profiles for a pair of analyte and calibrant, one can easily

calculate the concentration of analyte in a sample matrix at practically any point of the time profile

with the use of eq. 1-25. Contrastingly, iso-symmetric behavior may not exist for finite volume

samples, as shown in Figure 4-3b. Therefore, the iso-symmetic profiles for sample with small

volume can be obtained by using the following equation:

$$\frac{Q - q_e}{q_0 - q_e} = \exp(-a_d t) \qquad\qquad 4\text{-}2$$

where q_e is the quantity of calibrant remaining on the extraction phase after local equilibrium

is reached. Next, the computational model was employed to study the effect of a few parameters

that might affect the desorption kinetics, and consequently, the iso-symmetry of desorption and

sorption.

4. 3. 3. Effect of K_{es} on desorption rate constant (a_d)

The influence of the partition coefficient (K_{es}) on the desorption rate constant is predicted with

the proposed model. Figure 4-4 depicts how the a_d significantly decreases with the increase of K_{es}.
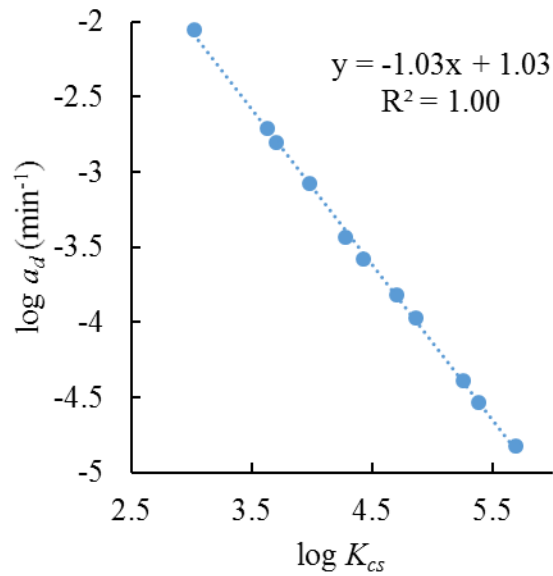
Figure 4-4. The desorption rate constant, a_d, obtained by varying the coating-sample partition coefficient (K_{es}).

For this simulation, sampling time was chosen to be equivalent to the time needed for up to five percent of the calibrant to desorb from the extractant, since equilibration times vary widely for the wide range of K_{es} values of the PAHs used in this study. The numerical simulation estimated an approximate three-fold decrease of a_d relative to a three-fold increase in K_{es}. A similar change in the coefficients was obtained by plotting the experimentally obtained a_d versus K_{es} reported by two different groups (see Figure 4-5).
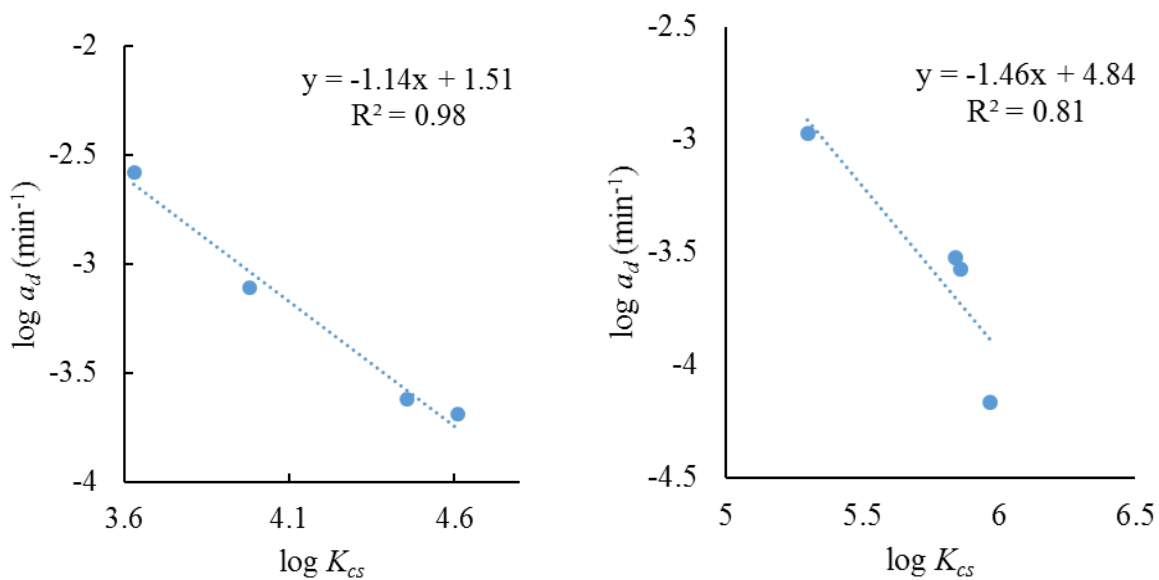
Figure 4-5. Experimental desorption rate constant (a_d) with respect to their partition coefficient (K_{es}). (a) Data obtained from Ouyang et al.[111] (b). Data obtained from Cui et al.[92]

It should be emphasized here that this trend might surprise some scientists who are familiar with other passive sampling devices where the mass transfer coefficient (k_m) is usually plotted against the partition coefficients. For such systems, Huckins et al[112] proposed that the mass transfer coefficient and the diffusion coefficient are of the form $k_m \sim D^{2/3}$. Based on this relationship, only a thirty percent variation in the mass transfer coefficients of the calibrants was obtained (see Figure 4-6). It should be noted here that the two terms km and ad are different, the former relates to only the diffusion coefficient and the later includes diffusion coefficient, partition coefficient, and geometric factor of the extractant.[113]
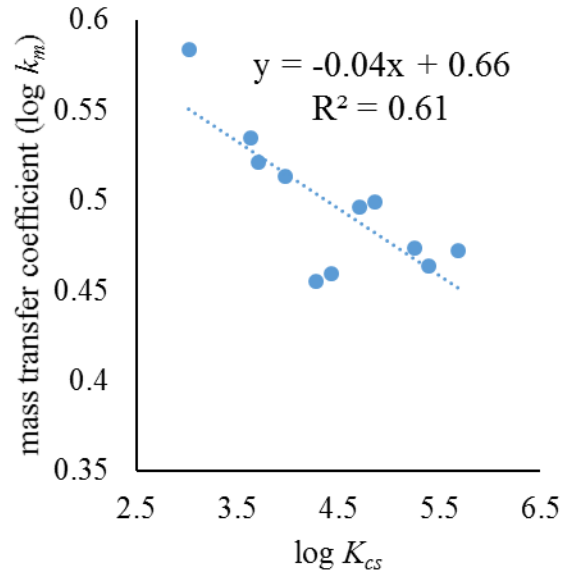
Figure 4-6. Calculation of mass transfer coefficients.

Therefore, the sharp decreasing trend of a_d with varied K_{es} cannot be explained only by considering the variation of diffusivities among the calibrants. Additionally, the a_d used in the standard-loaded calibration approach relates to the mass transfer coefficient, k_m, according to the following equation[113]:

$$a_d = \frac{Ak_m}{K_{es}V_e}$$ 4-3

where A and V_e are the area and volume of the extractant, respectively. Therefore, for a given calibrant, the a_d is a function of not only the k_m, but also the K_{es}. This implies that the steep decrease of a_d, even at the initial five percent of desorption of calibrant considered in these simulation studies, is due to the inclusion of the k_m and the partition coefficients (K_{es}) in the calculations. The simulation results support the fact that the initial mass transfer rate is influenced by both the diffusivity and K_{es} of respective calibrants. The sample fluid flow velocity affects the desorption

88

and sorption kinetics to the same extent, leaving the calibration unaffected by the change of flow velocity during a sampling period.

4. 3. 4. Effect of flow velocity

Agitation of the sample matrix decreases the boundary layer thickness, which should enhance the mass transfer kinetics for both the sorption and desorption processes. This phenomena was first investigated by exposing the calibrant-loaded extraction phase to a sample matrix at various hydrodynamic conditions. The model simulations were conducted at flow rates for which the flow was characterized as laminar for the majority of the sample domain. This was checked by observing no vortices behind the SPME coating (see Figure 4-7).
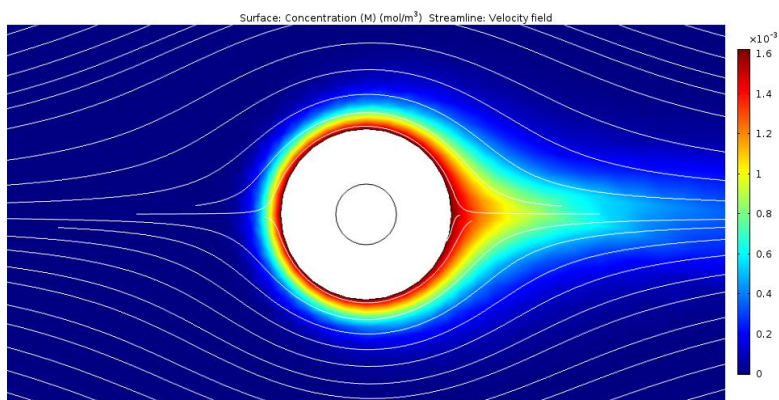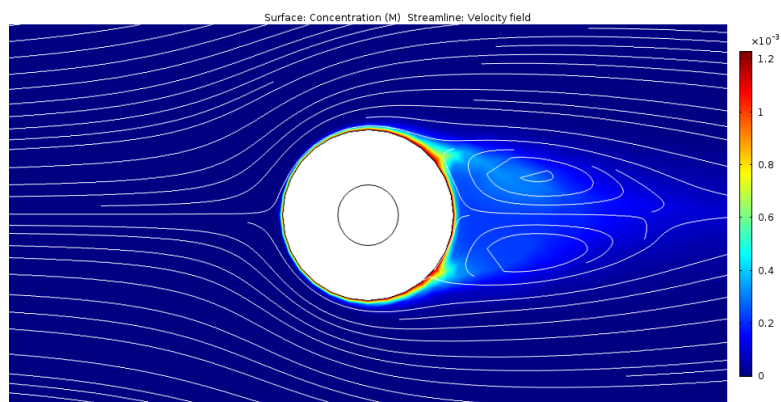
Figure 4-7. Effect of fluid flow velocity on the desorption kinetics. Surface plot shows the concentration (M) of calibrant desorbed from the extraction phase and the streamline is for the velocity field. Fluid velocity (a) 0.1 cm s^{-1}, and (b) 1 cm s^{-1}.

Figure 4-8-a shows the effect of flow velocity on the rate constant a_d under laminar flow conditions (0.001 – 0.1 cm s^{-1}). A significant increase in a_d was observed until 0.05 cm-s^{-1}, whereas the rate of increase was observed to slow between 0.05 cm s^{-1} and 0.1 cm s^{-1}. The exponential fitting of data provided a coefficient of ∼ 0.4. As shown in Figure 4-8b, as the sample flow increases, the a_d increases linearly for all of the tested velocities (up to 50 cm s^{-1}). Accordingly, an additional increase in a_d with increasing flow rate is observed when the flow creates significant flow separation at the back of the extractant with the formation of local eddies. At a high flow velocity, the Reynolds number is high, and stable vortices appear behind the SPME coating. As seen in Figure 4-7b, the vortices significantly affect mass transfer to the coating. Previous reports on other sampling devices also demonstrated similar proportional increases of mass transfer in the case of slow and fast fluid flow, showing that mass transfer is related to velocity to the power of 0.5 and 0.8-0.9 for laminar and laminar with eddies cases, respectively.[54]
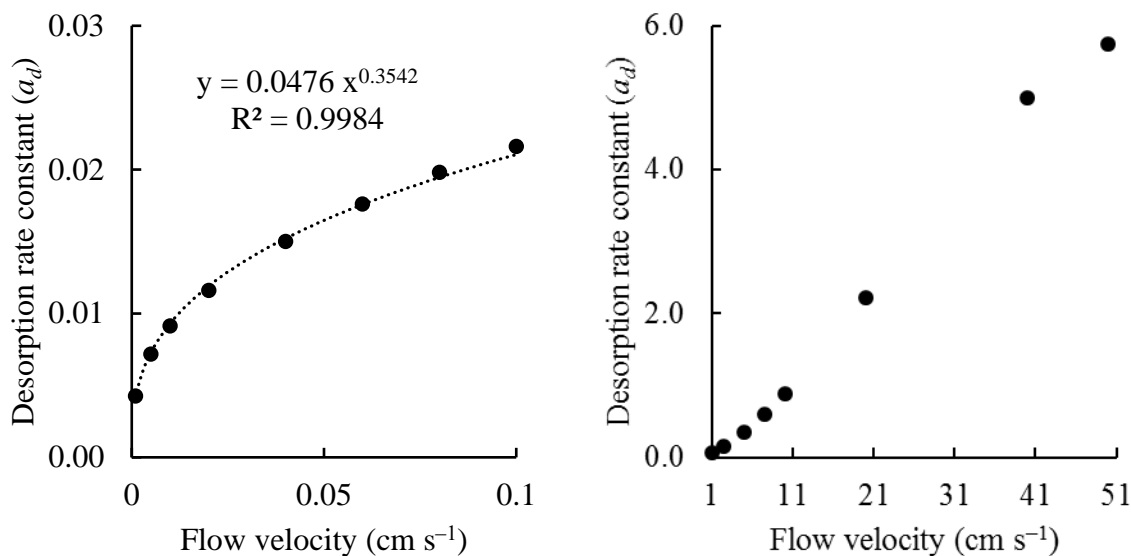
Figure 4-8. Dependence of a_d as a function of linear sample flow velocity at two flow regimes: (a) laminar flow with no eddies; (b) laminar flow with high eddies. Model simulation was carried out by using log K_{es} = 4, D_s = 1e^{-6} cm s^{-1}.

4. 3. 5. Effect of temperature

The effect of temperature on the transport of chemicals between the extractant and sample matrix is a bit complicated, since both the sample media of the transport and the properties of the chemicals can be affected by temperature. Thus, the change of a_d with temperature was simulated with the computational model and compared with the experimental data obtained from previous published work.[90] Figure 4-9 demonstrates that the higher the temperature, the greater the value of a_d. With the increase of temperature, the k_d increases owing to the mass-transfer coefficient (k_m) increase, but the increase is partially offset by the decrease of the distribution coefficient (K_{es}) (see eq. 4-3. For this study, the diffusivities and partition coefficients of the analytes were obtained from the literature.[90] The simulated data provided very good fitting with the experimental results.

91

However, the discrepancy between the experimental and model simulation results obtained for benzene is likely due to the K_{es} value (for benzene, $K_{es} \approx 60$) used in this simulation, as K_{es} values for benzene have been defined as larger than 100 in other reports.[15] For extraction, temperature also affects in the same manner and iso-symmetry is preserved. Hence, CL-SPME provides quantitative results even if there is a change in temperature during the sampling period.
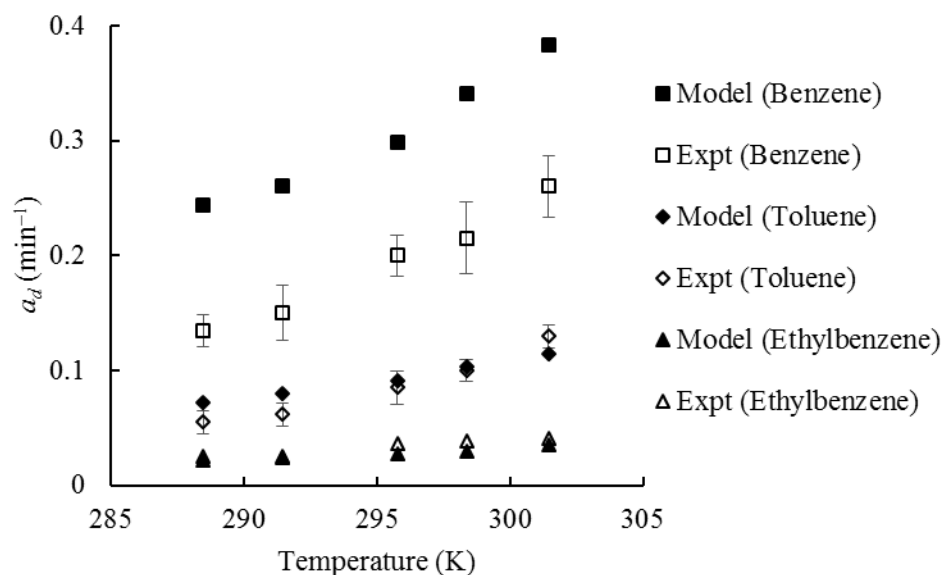
Figure 4-9. Effect of temperature on the desorption kinetics, a_d. Desorption of benzene (square), toluene (diamond), and ethylbenzene (triangle) from a 100-μm PDMS fiber into water at a rate of 0.25 cm/s at various temperatures. Model simulation data are shown in filled symbols, whereas the open symbols are used to plot the experimental data.

4. 3. 6. Effect of binding matrix on the desorption and uptake rate constants

The kinetics of both the sorption of analytes and desorption of calibrant have been experimentally reported to be affected by the presence of a binding matrix component in a sample.[94,96] At first, a computational simulation was carried out to study the effect of concentration

of a matrix component (for example, albumin) on the desorption kinetics at the finite sample volume (Figure 4-12a). In the model, the increase in the concentration of the matrix component was shown to enhance the calibrant release kinetics. For instance, one percent of albumin caused almost all of the calibrant to be released within 30 seconds, whereas most of the calibrant was shown to remain on the extraction phase if no binding matrix was present in the finite sample volume. This can be explained by the fact that as binding occurs, a greater concentration gradient is produced in the aqueous boundary layer due to the transfer of free calibrant molecules into their bound form, thus hastening faster calibrant transport from the coating–sample interface. For an infinite sample volume, the a_d was similarly affected by the presence of the binding matrix, although the a_d was much different for matrix-free samples (Figure 4-10a).
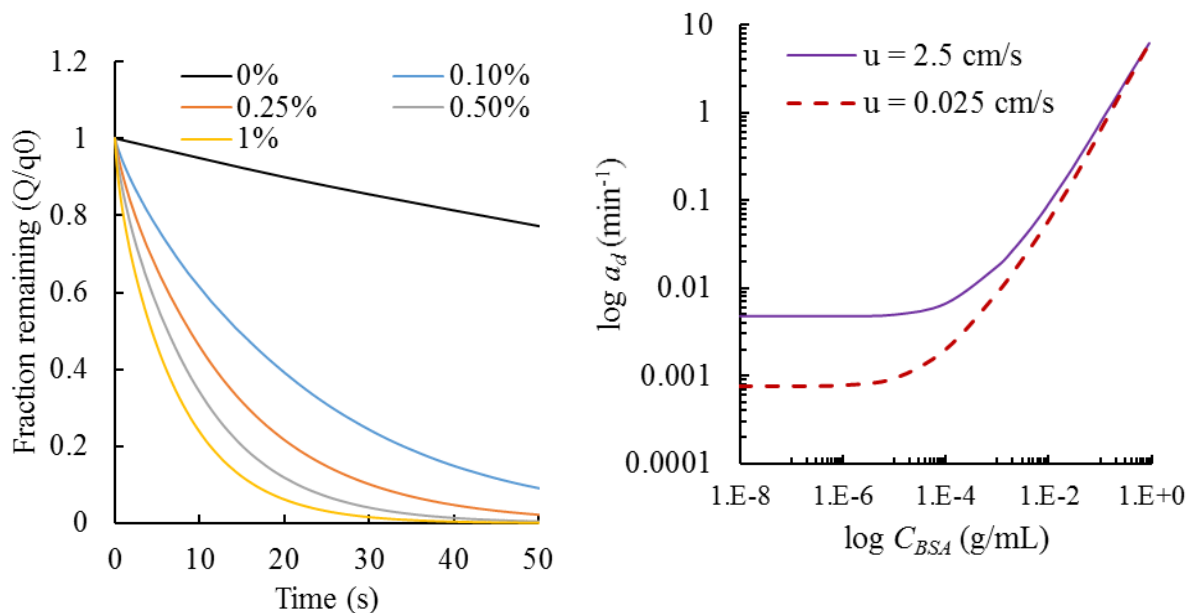
Figure 4-10. (a) Effect of matrix concentration on desorption kinetics in infinite volume case. $K_{es} = 100$, $K_a = 1 \times 10^5$ liter/kg, $k_d = 1$ [1/s] (labile). (b) The variation of a_d of pyrene with a wide range of BSA concentrations at two different fluid flow velocities

This implies that desorption kinetics might be independent of sample volume or agitation (especially for high matrix concentrations) due to the reduced boundary layer thickness. This was further verified by running simulations at two different flow velocities, the results of which are shown in Figure 4-10b. The obtained results imply that the desorption rate is controlled progressively by the diffusion of calibrant in the extraction phase. Consequently, the extraction–desorption hysteresis observed in the finite volume sample without the presence of a binding matrix was weakened in the matrix-containing sample.

Apart from the concentration of the binding matrix, a_d also depends on the binding affinity of analyte or calibrant with the binding matrix (how tight the binding is at equilibrium). As shown in Figure 4-11a, the extent of the enhancement observed for the desorption kinetics is lower for K_a

94

values of 1×10^3 liter/kg in comparison to the results shown in Figure 4-12a for K_a values of 1×10^5 liter/kg.
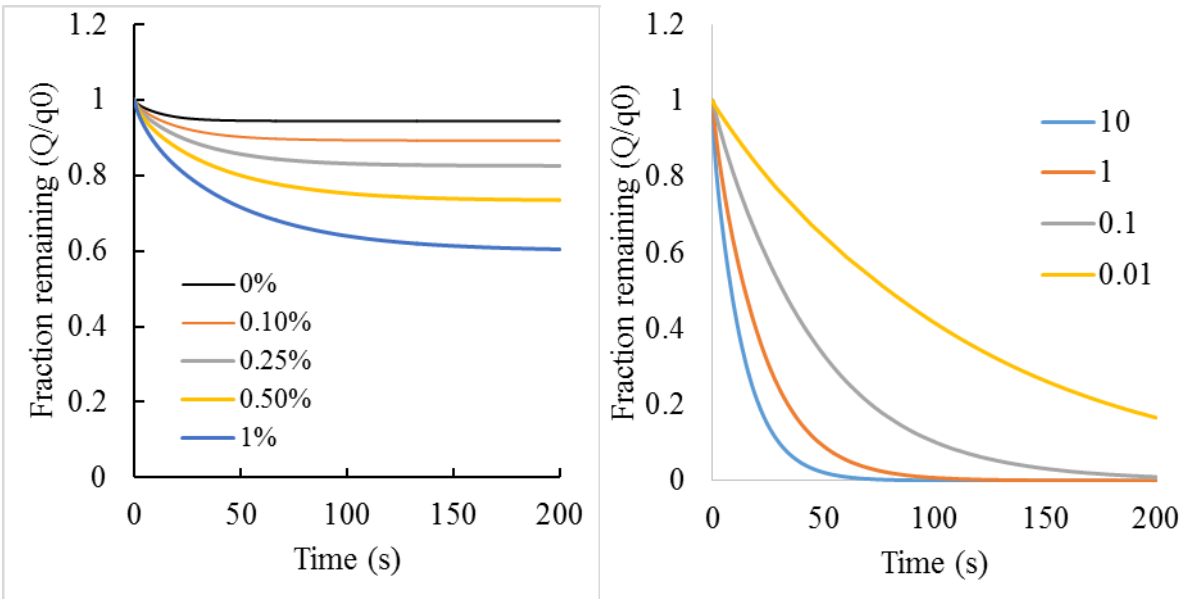
Figure 4-11. Effect of matrix concentration on desorption kinetics in finite volume case. (b) $K_a = 1\mathrm{e}^3$ liter/kg, $k_d =1$ 1/s (labile). (b) effect of kd at infinite sample volume.

The developed computational model was compared with experimental data obtained from Jiang et al.[114] As shown in Figure 4-12b, the experimental results of the enhanced desorption kinetics with increasing concentration of bovine serum albumin (BSA) were accurately predicted with the mathematical model. Although the a_d remains unchanged at very low concentrations of BSA (from 10 ppb to 10^4 ppb), the a_d values linearly increase with the decrease in its free concentration, owing to the higher concentrations of the binding matrix (BSA).
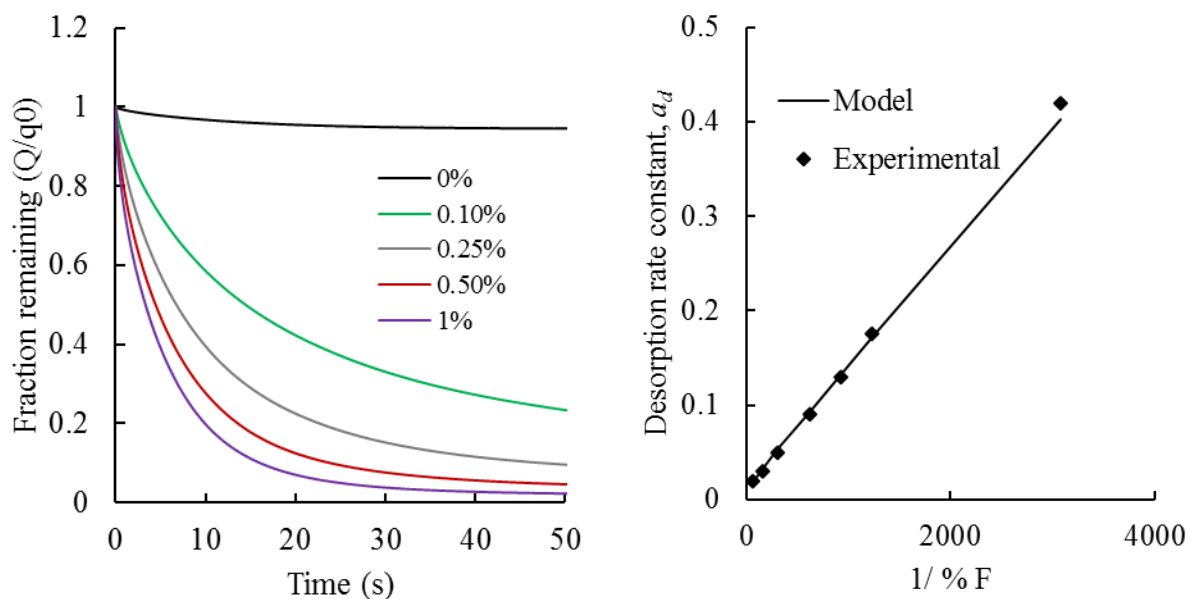
Figure 4-12. (a) Effect of matrix concentration on desorption kinetics in finite volume case. K_{es} = 100, K_a = 1×10^5 liter/kg, k_d =1 (1/s) (labile). (b) The dependence of desorption rate constant, a_d, on the free concentration of pyrene present in sample with increasing concentration of a binding matrix (BSA). The free concentration of analyte decreases with the addition of BSA in the sample.

The slopes of the dependency of a_d on the concentration of matrix components (similar to Figure 4-12b) for a number of calibrants with different K_{es} and K_a values were predicted from the model and compared with reported experimental data, as shown in Table 4-1. As can be seen, the computational model predicted very well the variation of a_d for different calibrants considered in the experiment, comprised of a wide range of different physicochemical properties.

Table 4-1. Slopes obtained from variations in a_d with respect to changes in free analyte concentrations in the presence of BSA.

Compound	K_{es}	K_a (M^{-1})	D_s x 10^6	Computational model	Expt. Data[114]
acenaphthene	4211	4074	9.20	15.20	32.0 ± 12.0
phenanthrene	8212	11220	8.80	6.07	7.49 ± 2.12
fluoranthene	27020	42658	8.06	1.39	3.29 ± 0.570
pyrene	29395	61660	7.33	1.27	1.32 ± 0.142

The a_d is also influenced by the binding kinetics or lability of the calibrant-matrix pair. The dissociation rate constant (k_d) was varied by keeping the same thermodynamic association constant (K_a) to predict the effect on the calibrant desorption kinetics from the extraction phase (Figure 4-13). Although the k_d values were close to one or more, which can be considered as labile, and have similar desorption kinetics, the lower k_d inhibits the release of calibrant from the extraction phase. Similar dependency of k_d was found in infinite volume cases (Figure 4-11b).
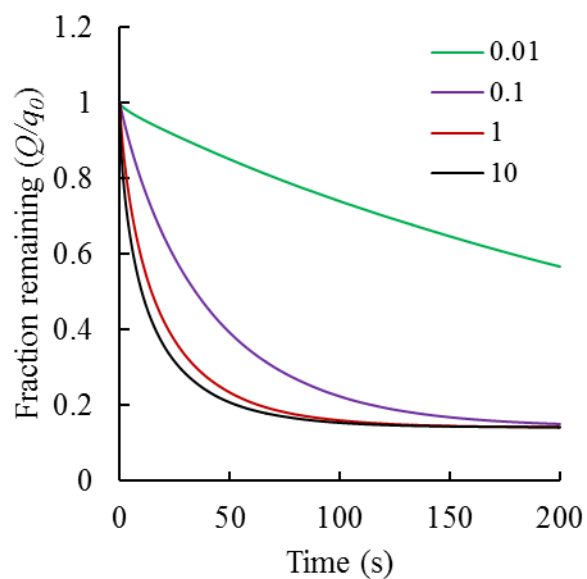
Figure 4-13. Effect of k_d (s^{-1}) on the desorption kinetics. For all simulations, the K_a and C_M were kept constant at 1×10^5 and 0.1 %, respectively.

As discussed early, the extraction rate constant of the target analytes must vary to the same extent as the rate of the calibrant desorption in order to utilize CL-SPME for quantification of sample concentrations. Therefore, the model was used to investigate the change of a_e as a function of binding matrix concentration under all other constant experimental conditions. As expected from the theory of mass transfer, the extraction kinetics are mirrored with the corresponding desorption kinetics, as shown in Figure 4-14.
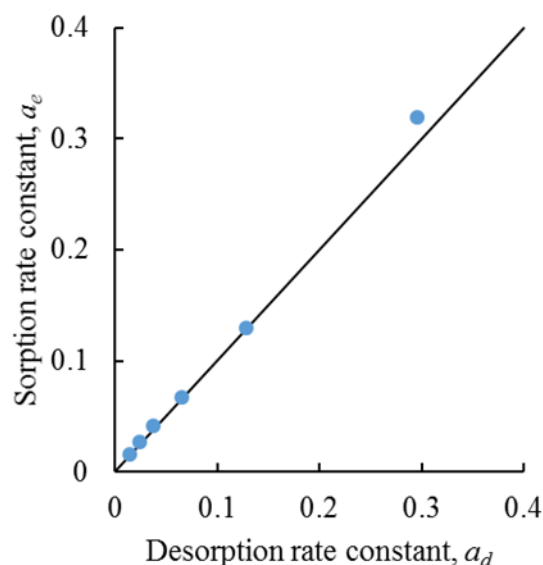
Figure 4-14. The variation of rate constants for sorption and desorption.

The observed symmetry, regardless of matrix effects, confirms that any accelerated desorption kinetics of the calibrant are exactly compensated by a commensurate acceleration in extraction kinetics, thus validating the principle underlying the use of the pre-equilibrium CL-SPME approach.

4. 3. 7. Measurement of total and free concentration

Once iso-symmetry is verified, calibration can be performed either by using the equation 1-25), where K_{es} needs to be known, or an external calibration curve. If the K_{es} is obtained from a matrix matched system, then the concentration is total; otherwise, the free concentration is obtained with the K_{es} measured from a binding-matrix free analyte solution. In order to verify that both the free and total concentrations can be obtained from the calibrant-loaded approach, an in-silico experiment using the developed computational model was carried out and the results are shown in the Figure 4-15, Table 4-2 and Table 4-3.
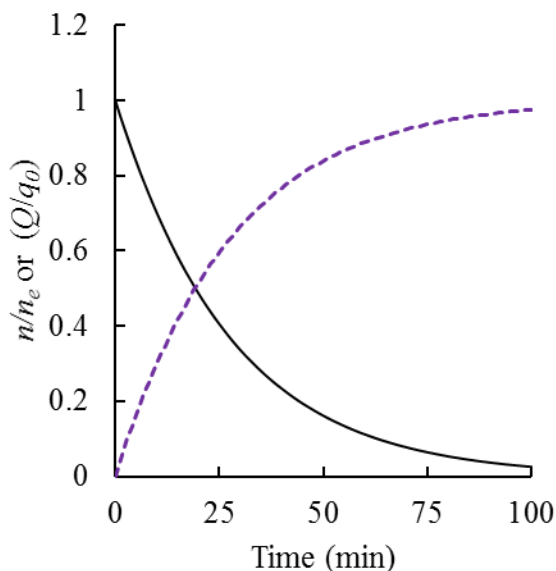
Figure 4-15. Computational simulation results shows iso-symmetry of fraction remaining (Q/q_0) of calibrant and normalized extraction amount (n/n_e) of analyte. C_A^0 = 50 ng ml^{-1}, C_M = 0.001 g ml^{-1}, K_{es} = 10,000, K_a = 1×10^5, V_e =1.8×10^{-4} ml, fluid velocity = 0.1 cm s^{-1}. Physical properties of the analyte and its calibrant is assumed same.

Table 4-2. Standard loaded calibration with the equation (eq. 1-25) to get **free** concentration with the use of K_{es} (10,000) obtained from a binding-matrix free sample solution.

True concentration		In-silico results using matrix-free K_{es}					
Cs (ng/mL) (True, total)	Cs (ng/mL) (True, Free)	Sampling time (min)	extracted amount, ng	Q/q0	Cs (ng/mL) (insilco)	Conc. Obtained	Bias
50	0.495	5	0.1461	0.8374	0.499	Free	-0.84%
		10	0.2692	0.7000	0.498	Free	-0.67%
		20	0.4604	0.4864	0.498	Free	-0.59%
		80	0.8480	0.0535	0.498	Free	-0.53%

Table 4-3. Standard loaded calibration with the equation (eq. 1-25) to get **total** concentration with the use of K_{es} (99.53) obtained from a binding-matrix containing sample solution

True concentration		In-silico results using matrix-matched K_{es}					
Cs (ng/mL) (True, total)	Cs (ng/mL) (True, Free)	Sampling time (min)	extracted amount, ng	Q/q0	Cs (ng/mL) (insilco)	Conc. Obtained	Bias
50	0.49507	5	0.1461	0.837	50.2	Total	-0.32%
		10	0.2692	0.700	50.1	Total	-0.15%
		20	0.4604	0.486	50.0	Total	-0.07%
		80	0.8480	0.053	50.0	Total	-0.01%

In cases where the K_{es} value is not available (for example, very hydrophobic chemicals that need very long equilibrium times), concentration of analytes can be obtained by using external calibration. Here, the sampling time used for constructing the calibration curve must be the same as that of the sample analysis. Although this approach is similar to the traditional external calibration method, the loaded standard serves as an internal standard to correct for variations in sample preparation, matrix effects, and detection processes.[109] Also, this approach is suitable for very small volumes of sample, where addition of an internal standard in the sample is either troublesome or can change the sample characteristics. Consequently, if a matrix-matched external calibration curve is made with the use of a calibrant-loaded extraction phase, then the **total** concentration can be obtained.

4. 3. 8. One-calibrant approach

In cases where stable isotope-labeled analogues of the target analytes are not available, it is possible to preload only one chemical that meets the criteria of a calibrant, and extrapolate the

release kinetics on the basis of the physicochemical properties (e.g., K_{es} and D_s) of the analyte/calibrant couple, as shown by equation 4-4:[111]

$$a_e = a_d \frac{D_s^A K_{es}^C}{D_s^C K_{es}^A}$$ 4-4

where the superscripts A and C refer to the analyte and calibrant, respectively, and a_e is the extrapolated extraction rate constant. As shown in Table 4-4, the predicted a_d values were correlated very well with experimental a_d figures. In addition, the use of only pyrene as a calibrant for the four chemicals provided theoretically precise quantification compared to the experimental values, whose deviation might be due to the associated experimental errors.

Table 4-4. Validation of the model with experimental data for the one-calibrant approach of SPME, where pyrene was considered as the calibrant.

Analytes			Model			Experimental		
	K_{cs}	D_w	a_d	a_e	a_c/a_d	a_d	a_c	a_c/a_d
Acenaphthene	4266	7.66E-06	3.7E-05	3.8E-05	103%	4.4E-05	3.8E-05	86%
Anthracene	9550	6.84E-06	1.5E-05	1.5E-05	104%	1.3E-05	1.5E-05	118%
Fluoranthene	28626	6.59E-06	4.9E-06	4.9E-06	100%	4.0E-06	4.8E-06	121%
Pyrene	40738	6.59E-06	3.4E-06	3.4E-06	100%	3.4E-06	3.4E-06	100%

When employing the one-calibrant approach, one must answer the question of whether the calibrant has to be from the same class as the analytes under study. What if the K_{es} of the target analytes vary widely? In order to predict the suitability of the one-calibrant approach for a range of different target analytes, the mathematical model was utilized for varied target analytes so that a correlation could be assumed. In such cases, analytes with large molecular sizes or strong hydrophobicity may present a challenge due to the slow desorption of calibrants from the coating.

Therefore, an upper limit (e.g., in K_{es}) needs to be established for the one-calibrant approach in CL-SPME applications. The mathematical model was further employed to study the limits of one-CL-SPME for the analysis of chemicals with a wide range of K_{es}, as shown in Table 4-5.

Table 4-5. . Determination of the limits of analyte K_{es} that can be calibrated with one-calibrant loaded SPME (one-CL-SPME

	Kfs	Dwx10^-6(cm2/s)[Vrana et al-2006 @ 18 C]	ad	ac (Chrysene)	ac/ad	ac (Napthalene)	ac/ad	ac (Fluoranthene)	ac/ad
Naphthalene	3.02	7.5	1.4E-04	1.7E-04	120%	1.4E-04	100%	1.6E-04	113%
Acenaphthene	3.63	6.34	3.2E-05	3.6E-05	112%	3.0E-05	93%	3.4E-05	105%
Fluorene	3.71	6.04	2.6E-05	2.8E-05	110%	2.4E-05	92%	2.7E-05	103%
Anthracene	3.98	5.88	1.4E-05	1.5E-05	109%	1.2E-05	90%	1.4E-05	102%
Benzo[ghi]perylene	4.28	4.81	5.9E-06	6.1E-06	102%	5.0E-06	85%	5.7E-06	96%
Indeno[1,2,3-cd]pyrene	4.43	4.88	4.3E-06	4.4E-06	102%	3.6E-06	85%	4.1E-06	96%
Fluoranthene	4.71	5.55	2.4E-06	2.6E-06	106%	2.2E-06	89%	2.4E-06	100%
Pyrene	4.86	5.6	1.8E-06	1.9E-06	106%	1.5E-06	88%	1.7E-06	100%
Benz[a]anthracene	5.26	5.13	6.7E-07	6.8E-07	102%	5.6E-07	85%	6.4E-07	96%
Benzo[a]pyrene	5.39	4.96	4.7E-07	4.9E-07	103%	4.0E-07	86%	4.6E-07	97%
Chrysene	5.69	5.1	2.5E-07	2.5E-07	100%	2.1E-07	83%	2.4E-07	94%

The observed results demonstrated that in cases where the calibrant was chosen from the middle of the range of K_{es} values of target analytes, the variation of a_d fell within the range of experimental error (assuming 20% error). Therefore, the one-calibrant approach based on equation 4-4) can be said to be a suitable option for cases where the isotopically-labeled calibrant is not available or not feasible to use.

4.4   Conclusions

A comprehensive study on the calibrant-loaded extraction phase approach for quantitative chemical studies has been demonstrated with both experimental data and a computational model. The model simulation data not only aids in a better understanding of the inherent mechanisms and conditions of CL-EP approach of quantification, but also predicts the essential parameters used for quantification. In this chapter, the iso-symmetric behaviors of sorption and desorption have been shown to be preserved for all variations of sample conditions, such as presence of a binding matrix, flow velocity, etc., in cases where both the calibrant and analyte interact identically with the coating. Nevertheless, for finite volume sample where the extracted amount is significant, a modified equation is proposed to obtain iso-symmetry. Further, the model can be used to predict desorption rate constants, which are needed for CL-EP quantification, of a wide range of target analytes with the use of only one calibrant for the correction of mass transfer properties, which is advantageous in cases where isotopically-labelled calibrants are unavailable or their use not feasible. The results demonstrated that this CL-EP approach might solve the complexity due to the in-vivo or in-situ sample environment compared with the simplified in-vitro release measurements carried out in buffer solutions. In particular, for a hydrophobic calibrant, where the calibrant release in the buffer is small or negligible, interactions with binding matrix components in real complex samples can alter the desorption profiles greatly. However, despite this complexity, the calibrant-loaded approach performs the necessary corrections while providing both free and total concentrations. In addition, the model can be used in predicting time weighted average (TWA) concentrations for SPME-based passive sampling. Moreover, use of the proposed model can aid

104

in reducing both time and costs associated with experiments where long equilibration times are needed.

Chapter 5 **Rapid sampling with solid-phase microextraction: Computational modelling**

of extraction for solid coatings

5.1 Introduction

The most common application of the SPME as a technique for sampling and sample preparation is based on attainment of equilibrium between the extracted analyte in the fiber coating and analyte dissolved in the sample.[86] The equilibrium method of quantification has been recognized as reliable and easy-to-use approach with SPME fibers such as poly(dimethylsiloxane) (PDMS) where extraction is known to occur via absorption. With the use of solid coating for SPME such as Carboxen/PDMS (CAR/PDMS) and PDMS/divinylbenzene (PDMS/DVB), high extraction capacity or analytical sensitivity can be obtained.[86] The main principle of analyte extraction by these solid coatings are assumed to follow adsorption on the surface. For these solid coatings, however, equilibrium-based calibration is often not a practical approach because of long equilibrium times and the competition between analytes for the same adsorption sites which leads to displacement of analyte molecules due to their difference in affinity towards the sorbents.[115] Diffusion-based rapid sampling technique was introduced to circumvent these problems.[26] The requirements for this calibration are: (i) the coating is a zero sink or perfect sorbent, which is ensured by using coatings of very high sorption capacity, (ii) the extraction is controlled by diffusion through a boundary layer formed closed to the coating surface, which can be assured by a steady fluid flow condition so that the boundary thickness (δ_s) remains unchanged and the extraction process can be calibrated based on diffusion, (iii) linear mass uptake to both sampling time and analyte concentration. Therefore, sampling time should be optimized to analyte

concentrations and sample velocities. The main advantage of the diffusion-based rapid quantification method is that no calibration curves or internal standards are needed and analyte competition for the same adsorption site can be avoided. Koziel et al.,[26] developed the first model for the diffusion-based calibration by empirically calculating the thickness of the boundary layer. However, the method introduces large errors in the calculations since the boundary layer thickness is not uniform around the fiber and depends on the physical dimensions of the fiber coating, sample flow conditions, and analyte physicochemical properties. Chen et al.[34] proposed a physical model (obtained from heat transfer in a circular cylinder in cross-flow) to describe the rapid SPME extraction in aqueous samples, as shown in eq. 5-1.

$$n = k_m A C_A t$$

<div align="right">5-1</div>

where n is the amount of analyte extracted, t is the sampling time, A is surface area of the coating, C_A is bulk analyte concentration and k_m is average mass-transfer coefficient. In this approach, the mass transfer coefficients were calculated from simple empirical correlations that do not consider the geometry of the fiber. In addition, parameters that affect the zero sink effect such as sorbent affinity (equilibrium constant, K) and capacity (maximum extracted amount) were not considered in previous models. Empirical equations developed in the previous models for the rapid sampling do not provide either accurate predictions of analyte concentration or lack of any physical meaning. Moreover, previous models cannot predict analyte displacement during SPME extractions, which occurs even at short sampling times for high analyte concentration as it has been reported when PDMS/DVB coatings were used.[116]

Numerical modelling and computational simulation is often used as a tool to explain the behavior of processes at low costs. In the Chapter-2 and 3, mathematical models for the complex processes occurring in SPME were discussed.[96] While most of the analysis in the previous chapters were carried out under diffusion only conditions, the rapid sampling SPME method requires the fiber to be placed in a flowing stream of analyte (dynamic sampling). It is therefore of utmost importance to quantitatively predict the effects of a convective flow, geometry of the fiber, and affinity of the analyte on the magnitude of the transport controlled extraction by the coating.[102,117,118] The aim of this study is to present a computational model for rapid sampling with a SPME fiber placed in a flow through system as depicted in Figure 5-1. The predictions obtained with the proposed model have been compared with the predictions reported by the model proposed by Chen et al.[4] and with experimental data reported in the literature.

5.2   Mathematical model

5. 2. 1. Fluid flow model

In the chapter, we have used the same model described in the chapter-2 for fluid flow in the sample matrix. As depicted in Figure 5-1, the model considered a two dimensional segment of a sample-extractant system. The flow in the sample domain is governed by the Navier-Stokes equations, while the flow field is treated as steady.
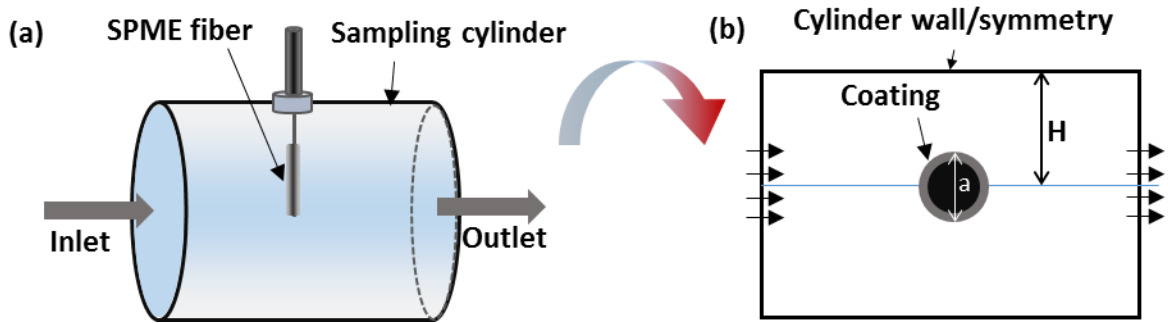
Figure 5-1. Schematic of experimental setup for rapid sampling in flow-through system. (a) The sampling cylinder is used to mimic the environmental sampling (e.g., river water). Here, the sampling solution is flowed from one side to the other using a pump. (b) Schematic of a 2-D cross-section of the sampling cylinder and SPME coating fiber (not to scale). The fiber is located in the middle of the cylinder. Here, H is the distance between the fiber center and the cylinder wall, a is the fiber's diameter.

5. 2. 2. Analyte transport in sample solution

The analyte is transported by diffusion and convection in the bulk solution. According to Fick's law, the following mass balances can be formulated to describe the time-dependent mass transport model for the present system:

$$\frac{\partial C_A}{\partial t} + \vec{u} \cdot \nabla C_A = \nabla \cdot (D_A \nabla C_A) \qquad \text{5-2}$$

where C_A denote the concentrations (mol m^{-3}) of the analyte A in the bulk solution phase; D_A is the diffusivity coefficient (m^2 s^{-1}) in the solution phase; $\vec{u}$ denotes the velocity field (m s^{-1}) and that is obtained from the solution of the momentum transport model governed by the Navier-Stokes equations.

5. 2. 3. Adsorption on the surface extractants

Previous studies have shown that Langmuir adsorption isotherm describes equilibrium analyte extraction by solid coatings.[119, 120] The Langmuir isotherm model uses the active sites concept in the adsorption expression to describe the effect of the adsorption rate as a function of the coverage of the coating. Therefore, this model has been used in this study to develop the theoretical description of the adsorption process. Adsorption is treated as a one-step reversible reaction where an analyte molecule *A* in solution (of bulk concentration C) reacts with the active site *S* for adsorption on the surface to yield an adsorbed complex *AS* immobilized onto the active sites of the coating, i.e.

$$A + S \; \underset{k_{des}}{\overset{k_{ads}}{\rightleftharpoons}} \; A\,S \qquad\qquad 5\text{-}3$$

The constants k_{ads} and k_{des} represent the rate constants of adsorption and desorption of the analyte onto the active sites, respectively. The maximum attainable surface concentration of the immobilized complex is Γ_{max} (mol cm^{-2}); the surface concentration at time *t* is $\Gamma(t)$. Therefore, the free active site concentration at any time instance *t* is Γ_{max} - $\Gamma(t)$. Accordingly, the kinetics of the process is described as follows: the mass balance for adsorbed analyte (*AS*) at the coating surface, including surface diffusion and the reaction for its formation, can be described by the following equation,

$$\frac{\mathrm{d}\Gamma(t)}{\mathrm{d}t} = D_A^e \nabla^2 C_A^e + k_{ads} C_A(t)\big(\Gamma_{max} - \Gamma(t)\big) - k_{des}\Gamma(t) \qquad 5\text{-}4$$

where $D_A{}^e$ and $C_A{}^e$ are the diffusion coefficient and the concentration of the analyte A at the extractant surface, respectively, C_A is the free analyte concentration in sample solution at time t.

The ratio of the adsorption and desorption constants k_{ads}/k_{des} determines the equilibrium constant K (Equation 5-5). As the adsorption progresses, $\Gamma_{max} - \Gamma(t)$ decreases while $\Gamma(t)$ increases until the equilibrium is reached. We can ignore the surface diffusion term in eq. 5-4. At equilibrium, $d\Gamma(t)/dt = 0$ in eq. 5-4 and $C_A{}^{eq} = C_A{}^0$ (i.e. the initial concentration of A), leading to an analytical expression for the adsorbed centration of the analyte equilibrium Γ_{eq}, eq 5-5.

$$K = \frac{k_{ads}}{k_{des}} = \frac{\Gamma_{eq}}{C_A^0 (\Gamma_{max} - \Gamma_{eq})} \qquad 5\text{-}5$$

Equation 5-5 can also be expressed as follows:

$$\frac{\Gamma_{eq}}{\Gamma_{max}} = \frac{K C_A^0}{1 + K C_A^0} \qquad 5\text{-}6$$

Or,

$$\Gamma_{eq} = \frac{\Gamma_{max} C_A^0}{1/K + C_A^0} \qquad 5\text{-}7$$

Considering the surface area (cm^2) of coating, Γ (nmol cm^{-2} or ng cm^{-2}) can be modified as

$$n_{eq} = \frac{n_{max} C_A^0}{1/K + C_A^0} \qquad 5\text{-}8$$

where n represents the amount of analyte (nmol or ng).

Since eq. 5-4 includes the sample bulk concentration C_A of analyte, it must be solved in combination with the mass transport equation in the sample. The coupling between the concentration distribution in the bulk sample (2D, eq. 5-2) and the concentration distribution at the

surface (1-D, eq. 5-4) is obtained by imposing a boundary condition for eq. 5-2. Boundary condition at the reaction surface is given in the term of mass flux,

$$-\vec{n} \cdot (C_A v - D_A \nabla C_A) = k_{ads} C_A(t)(\Gamma_{max} - \Gamma(t)) - k_{des}\Gamma(t) \qquad \text{5-9}$$

where $\vec{n}$ is the unit normal vector to the surface. Other boundary conditions for eq.5-2 are as follows

At time $t = 0$, $C_A = 0$ and $C_A{}^s = 0$ everywhere on the coating surface.

For all $t > 0$,

At the cylinder's inlet, the analyte concentration was fixed at $C_A = C_A{}^0$

Insulation is applied to at the walls of the cylinder, i.e.:

$$-\hat{n} \cdot (C_A v - D_A \nabla C_A) = 0 \qquad \text{5-10}$$

There is no diffusive mass flux at the outlet of the cylinder (analyte is removed by convection only):

$$-\hat{n} \cdot (-D_A \nabla C_A) = 0 \qquad \text{5-11}$$

5. 2. 4. Numerical methods

COMSOL Multiphysics 5.1 was used to implement and solve the convection-diffusion-reaction equations described above with a geometry representing a flow-through SPME sampling containing a fiber vertically oriented to the flow (Figure 5-1b). A few assumptions were made to simplify the analysis for the fluid velocity and analyte concentration profiles in the system. First,

the 3-D flow through geometry (Figure 5-1a) was reduced to the 2-D cross section along the length of the channel shown in Figure 5-1b. This is an acceptable approximation when the fiber is situated in at the center of the cylinder and the cylinder's walls are away from the fiber. Since typical analytical samples have the bulk analyte concentrations in the sub-micromolar regime, the effect of mass transport on the fluid velocity is negligible; hence the simulations can be spitted into two stages: (1) solution for fluid flow and (2) the result is used in solving the coupled transient mass transport and surface reaction equations. In addition, the range of flow velocities studied were assumed to fall within the laminar flow regime.

5.3   Results and discussions

5. 3. 1. Basics of diffusion based rapid calibration

After insertion of the extraction phase into a sample, a rapid increase in mass uptake is followed by a slow mass transfer kinetics to the extraction phase until attainment of an equilibrium between the extraction and sample phases. The analytical expression of time scale of extraction can be described by the following equation [120]

$$t_{eq} \approx t_{95\%} = \frac{\delta_s K L}{D_A \Gamma_{max}} \qquad\qquad 5\text{-}12$$

where δ_s is the aqueous boundary layer thickness, L is the thickness of the extraction phase, and D_A is the diffusion coefficient of the analyte in the sample matrix. At a particular sample agitation (constant δ_s) and coating thickness, the extraction kinetics depends only on the equilibrium constant (K) and diffusivity (D_A) of the chemicals under study (eq. 5-12). After the extraction reaches equilibrium between the extraction phase and the sample, the calibration process is rather

simple and discussed in detail elsewhere.[86] In this work, calibration based on the kinetic regime of the sorption profile has been illustrated with the mathematical model. Figure 5-2 shows the kinetic part of typical sorption time profiles obtained from the mechanistic mathematical model for constant concentrations of a few polycylic aromatic hydrocarbon (PAHs) in a continuous fluid flow condition (Figure 5-1). As shown in Figure 5-2a, the extent of equilibration depends on the K for the analytes; higher the K (or log$P$ or hydrophobicity) longer the equilibration time, whereas the extracted amount for all four analytes were very similar up to about twenty five minutes of extraction. Since the diffusion coefficients of the selected PAHs in water are very close to each other, the extracted amount is similar at the diffusion controlled initial stages when the coating is considered to be a zero sink. During this initial stage, the effect of equilibrium constants (or, partition coefficients for liquid coatings, K_{es} or, log P) has little effect on the kinetics. This initial independence of analyte log P on extraction rate provides an interesting features of SPME by providing the possibility of calibration with only one calibrant. The minor variation of the analytes diffusivity will provide uptake rate within the expected experimental error (approximately 20%). For analytes with significantly different diffusion coefficients, calibration can be obtained based on the "Diffusion based calibration" developed by Koziel et al.[26] In this approach the uptake is only affected by diffusion coefficient of analytes. Figure 5-2b shows excellent prediction of the model simulation results to the experimental data obtained by Chen et al. [34] The major limitation of the diffusion based calibration is that the fluid velocity must be constant during the sampling period, which might be an issue especially for in-vivo sampling. Therefore, parameters that affect the adsorption process, including sample flow velocity, extractant maximum adsorption capacity, analyte concentration were investigated with the developed model.
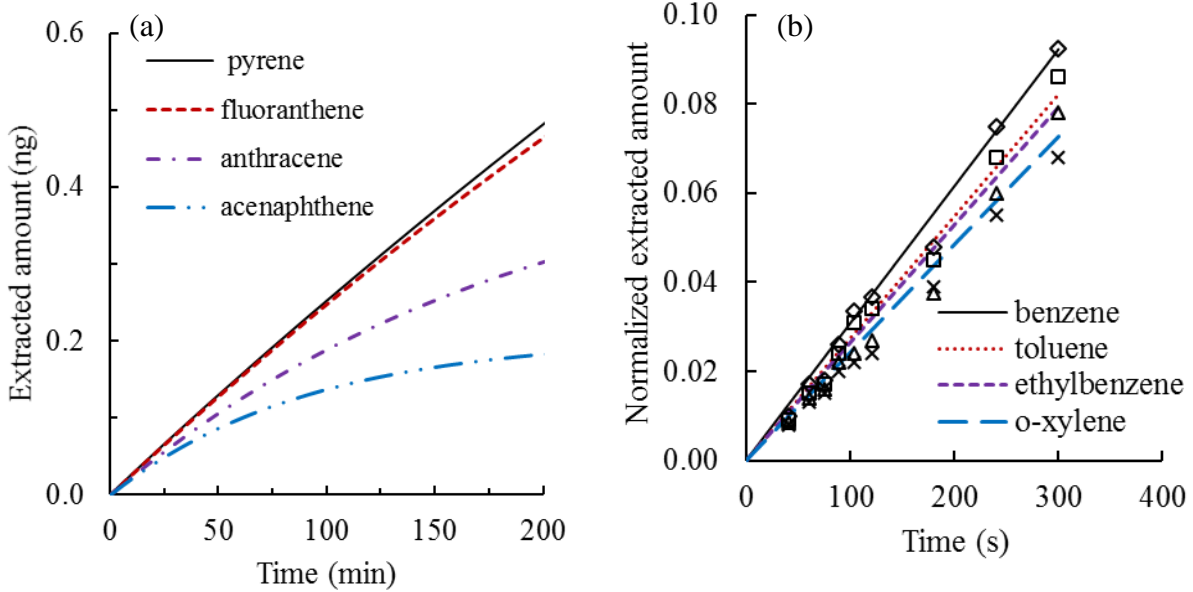
Figure 5-2. (a). Typical kinetic portion of the adsorption time profiles for the PAHs obtained from the developed model simulation. D values are: 7.66×10^{-6}, 6.84×10^{-6}, 6.59×10^{-6}, 6.59×10^{-6} cm^2 s^{-1} ; K are 1×10^6 M^{-1}, 2×10^6 M^{-1}, 7×10^6 M^{-1}, 10×10^6 M^{-1} for acenaphthene, anthracene, fluoranthene, and pyrene, respectively. Γ_{max} was set at 8×10^{-5} mol m^{-2}. (b). Comparison of simulated extraction time profiles with experimental ones obtained from Chen et al.[34] The lines are for simulated data and symbols are for benzene: ◊; toluene: □; ethylbenzene: Δ; o-xylene: ×. Assumptions: concentration of all analytes were 20.8 ng/mL, fluid linear velocity of 0.2 cm/s using a 75-µm CAR/PDMS fiber. Γ_{max} and K values are assumed as 1×10^5 mol/m^2 and $\times 10^8$ M^{-1}.

5. 3. 2. Effect of fluid flow to the adsorption kinetics

Figure 5-3 shows the concentration profiles in the sample (2D) solution domain corresponding to the center of the fiber at various fluid flow velocities. The normally symmetrical diffusion layer obtained from diffusion only conditions (Figure 5-3a) is distorted with the convective flow (Figure 5-3b). The flow compresses the diffusion layer about the upstream edge (entrance to the fiber) of

115

the fiber whereas expansion of the diffusion layer is observed downstream of the fiber, i.e. at the outlet. The average thickness of the diffusion layer is dependent on the solution's inlet flow rate, being much more relatively thinner at faster flow rates (Figure 5-3c).
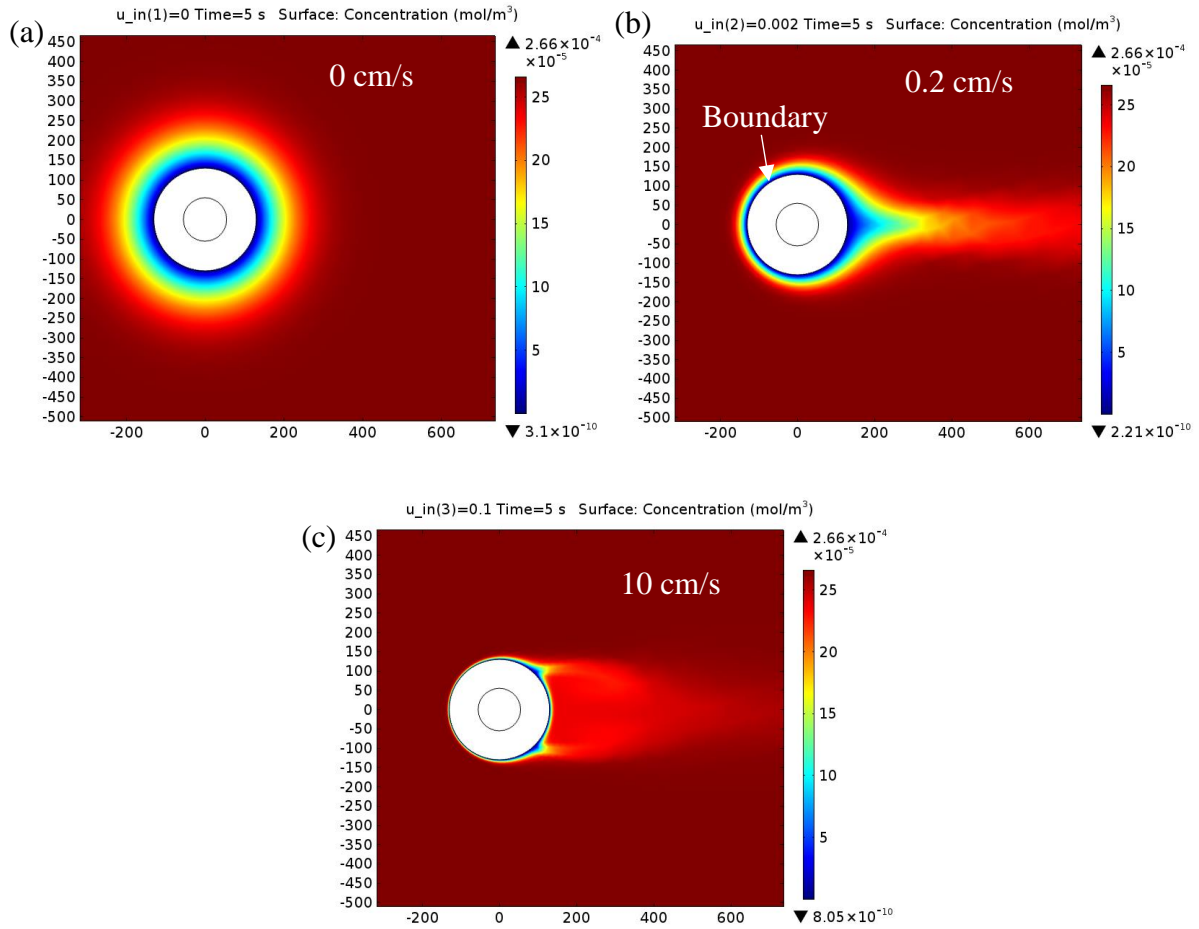
Figure 5-3. Effect of fluid flow on concentration boundary layer around the fiber, at 5 s. (a) diffusion only case with flow velocity of 0 cm/s, (b) with flow velocity of 0.2 cm/s, (c) with flow velocity of 10 cm/s.

To quantify the role of transport in isolation to the adsorption onto the coating surface, assumptions of perfect and rapid adsorption kinetics were considered by setting very high k_{ads} and low k_{des} values in the eq. 5-4. Furthermore, the concentration of surface active sites (Γ_{max}) was

considered to be very high (8×10^{-4} mol m^2). Therefore, analyte molecules are transported by the combination of convection and diffusion towards the coating surface that adsorbs analyte immediately and never saturates. The benefit in considering this simplified case is that the analyte transport can be quantified in isolation from binding or saturation considerations.[121]

In a typical flow-through SPME sampling, the ratio of sample cylinder diameter to the fiber diameter is high; hence, the downstream convection prevents rapid diffusion to the cylinder wall. Most of the analyte molecules are swept downstream before they can diffuse far to the wall and the analyte species that interact with the fiber are confined to a thin layer near the fiber coating. For such flow conditions, the flow is approximated by a linear shear flow on the fiber.[122] The mass transfer can then be characterized by a single dimensionless parameter, called the shear Peclet number, Pe_s which is defined as follows[123]:

$$Pe_s = \frac{\vec{u}a^2}{D_A H}$$

5-13

where $\vec{u}$ is the inlet velocity, a is the fiber diameter, H is the cylinder radius and D_A is the diffusion coefficient in sample. The thickness of the boundary layer, which is denoted as δ_s, can be calculated from the following equation,

$$\delta_s = \frac{a}{Pe_s^{1/3}}$$

5-14

Therefore, the Pe_s indicates whether the depletion zone is thick or thin relative to the coating diameter. The rate of mass transport through the depletion zone to the coating surface can be generalized as a dimensionless flux function, F (also called Sherwood number), which is defined as follows[121,122]:

$$F = \frac{J_D}{D_A C_A^0}$$
5-15

where J_D is the total diffusive analyte flux to the coating surface quantified through integration of the flux density at the coating surface. To evaluate the effect of fluid velocity and diffusion coefficient on the extraction of analyte from water, sample velocities ranging from 5×10^{-4} to 4×10^{-1} m s^{-1} and diffusion coefficients from $2\times10^{-9} - 2.5\times 10^{-12}$ m^2 s^{-1} were considered at 300 seconds of extraction and shown in Figure 5-4a.
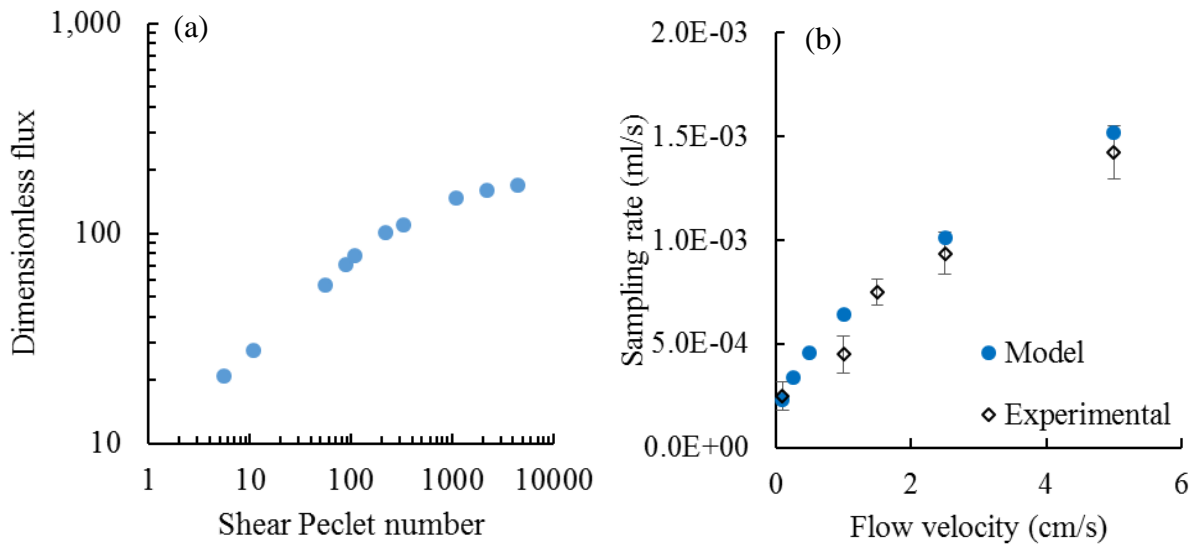
Figure 5-4. Effect of mass transport in terms of Peclet number (Pe_s) on the dimensionless flux (F). Here, the inlet velocity ($\vec{u}$)ranges from 5×10^{-4} to 4×10^{-1} m s^{-1}, diffusivity (D_A) $= 2\times10^{-9} - 2.5\times10^{-9}$ m^2/s, $H = 1.5$ cm, $C_A^0 = 20.8$ ng/mL and $K = 1\times10^{12}$ M^{-1}. (b) Comparision of exepirmantal results with the simulated data for the effect of flow velocity on sampling rate.[34]

The dimensionless flux increases with increasing the Peclet number, which is also correlated with the eq. 5-14 that increasing Pe_s reduces the boundary layer thickness which in turn enhances

the flux. At high Peclet numbers, the depletion zone becomes thinner than the coating thickness. In the lower range of Pe_s, significant effect on the flux change was observed, which is reflected by the reduction of the thickness of the boundary layer. Therefore, at a very high fluid velocity, the extraction can be converted from transport-limited to reaction (adsorption) rate limited regime. In the higher range of Pe_s, a lesser effect is observed where nonlinear relationship between the flux and Pe_s is noted. Figure 5-4b shows excellent correlation of the experimental data to the model simulation results.[34]

5. 3. 3. Effect of analyte concentration on equilibrium time

Theoretically analyte concentration should not affect the equilibration time for a well-designed SPME experiment. However, if the coating tends to saturate due to minimum adsorption capacity, the bulk analyte concentration might affect the rate of adsorption. In this section, the analyte concentration was varied from 0.01 to 100 nM while the coating maximum binding sites were fixed at 10^{-7} mol m^{-2}. Figure 5-5 shows that it takes 10 times longer time for an analyte with a lower bulk concentration (0.01-1 nM) to reach equilibrium at both of the tested flow velocities than an analyte with a higher concentration (100 nM). This phenomena is due to the limited number of adsorption sites on the solid coating which is not seen in liquid coatings. In order to conduct extraction experiments with SPME within a reasonable time, the match between the coating capacity and the sample concentration is very important, especially when the sample volume is large. However, equilibration time should be linear to the concentration at lower sample concentration, lower sample volume and a coating with higher capacity.
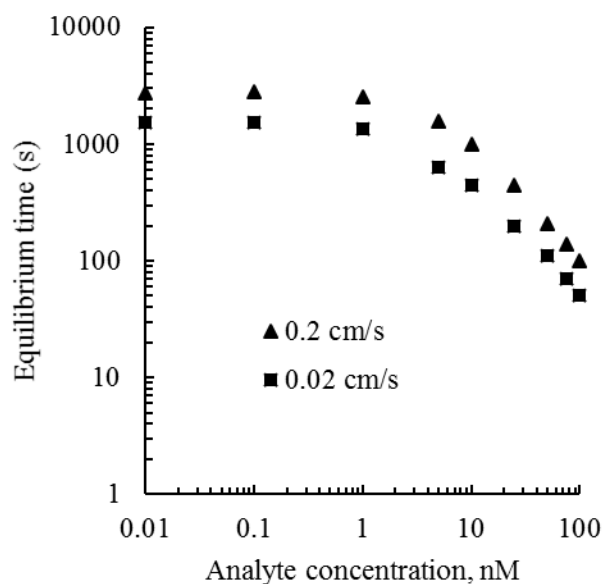
Figure 5-5. Effect of initial analyte concentration in sample on the equilibration time
at two different flow velocities.

5. 3. 4. Effect of adsorption constant (K)

In the previous section, the effect of fluid flow velocity on the rate of extraction defined by

the dimensionless flux (F) was studied under the assumption that the reaction (eq. 5-4) was

extremely fast (i.e., $K \approx \infty$). However, the equilibrium constant (K) of commercially available solid

coatings are typically in the range of 10^6 and 10^8.[91] The SPME fibers also have limited number of

active sites to extract analytes from solution. Therefore, the amount of analyte extracted by the

fiber surface is directly influenced by the analyte's K values. In other words, the range of analyte

concentration (i.e., linear dynamic range) that can be quantified with a particular SPME fiber

depends on the analyte's K values. Figure 5-6 illustrates the predicted dependence of the amount

of the analyte extracted by the fiber as a function of the initial concentration of the analyte in the

sample for two different K values.
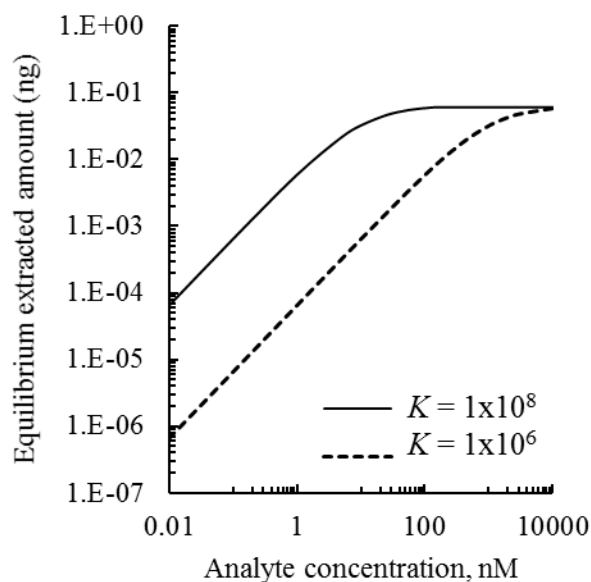
Figure 5-6. Amount of analyte extracted by the fiber vs. initial concentration of the analyte in the sample at different equilibrium constant (K_f) values. $\vec{u} = 0.2$ m/s, $\Gamma_{max} = 1 \times 10^{-7}$ mol m^{-2}, $D_A = 7.66 \times 10^{-6}$ cm^2 s^{-1},

At low analyte concentrations, the dependencies can be approximated by straight lines. At higher concentrations they cease to be linear, and finally they level off when all active sites on the extraction phase are occupied by the analyte molecules. The shapes of the isotherms, and particularly their linear ranges, depend strongly on the K value. When K is large (the curve for $K = 1 \times 10^8$), the response remains practically linear until the fiber becomes saturated with the analyte. After this point, the curve levels off rather abruptly. When K is low (the curve for $K = 1 \times 10^6$), the extracted amount changes with the initial analyte concentration C_A^0 in a broader concentration range. Hence, the model can predict the linear dynamic range of a particular SPME experimental set-up which is very useful especially when the samples contain wide range of analyte concentrations.

121

5. 3. 5. Effect of adsorbent capacity

For infinite sample volume, the equilibration time and extraction amount increases with increasing coating capacity. Therefore, extracted amount linearly increases with increasing capacity at any given analyte concentration (Figure 5-7a). The extraction isotherm (Figure 5-7b) shows that the linear dynamic range is same for both the coating capacities. This is important information for onsite or in-vivo sampling where increasing coating capacity might only increase sensitivity of measurement but not improve the linear dynamic range.
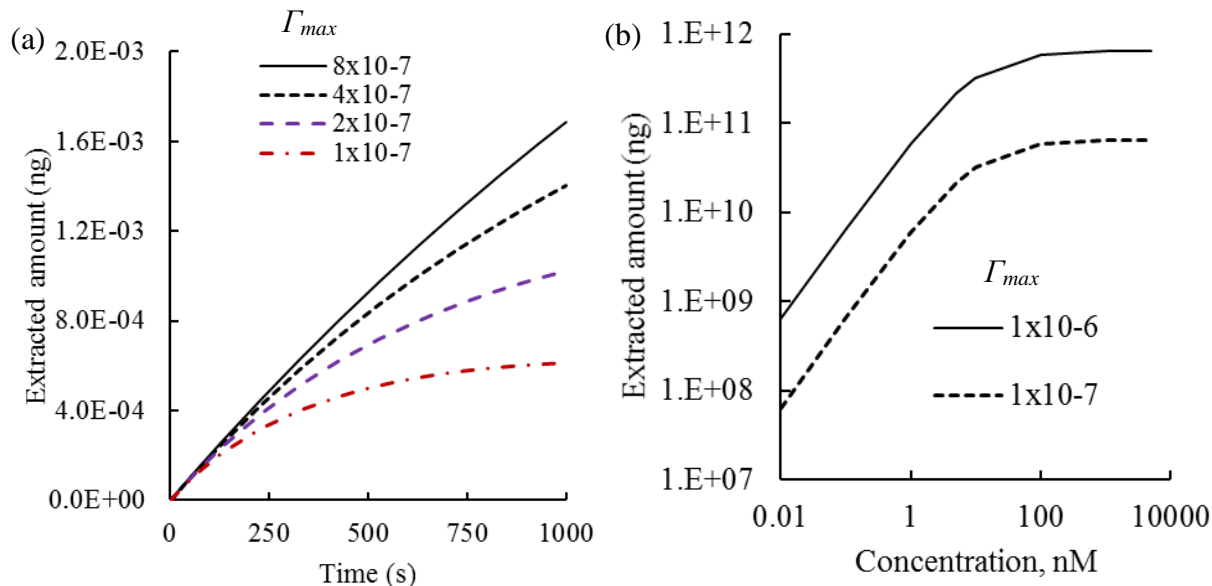
Figure 5-7. Effect of maximum capacity (Γ_{max}) of coating on the amount of analyte extracted at different extraction time (a) and initial concentration of the analyte (b) in infinite sample volume. Assumptions: $K = 1 \times 10^8 \ M^{-1}$

However, in cases where finite sample volume is used, such as in bioanalysis, a different effect of coating capacity is seen in Figure 5-8. A coating with small capacity will saturate with increasing analyte concentrations sooner than a coating with higher capacity. Hence, the linear dynamic range

122

can be improved by employing coating with higher capacity. The higher the number of active sites, the broader is the linear range of the isotherm. Therefore, during the optimization for coating capacity one has to consider the volume of the sample to be analyzed.
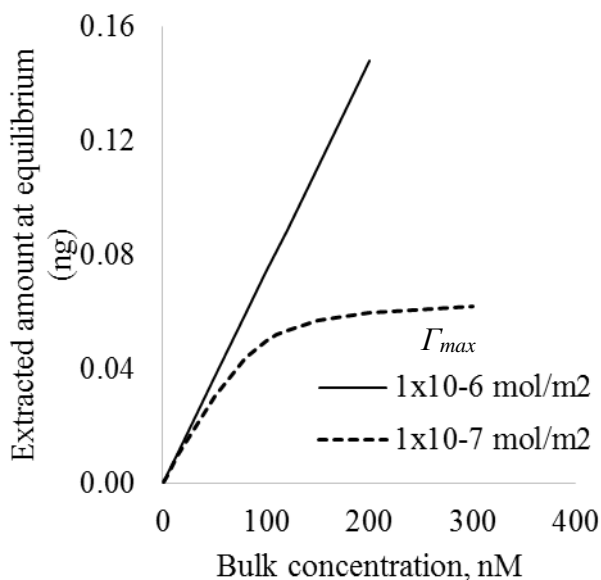
Figure 5-8. Effect of maximum capacity (Γ_{max}) of coating on the amount of analyte extracted at different initial concentration of the analyte in limited sample volume. Assumptions: $K = 1 \times 10^8$ M^{-1}

5. 3. 6. Analyte displacement

At the beginning of extraction, all chemicals with some sort of affinity to the coating start to adsorb linearly at a rate determined by the convection and diffusion properties as discussed in section 5. 3. 1. After the linear portion is passed, the extraction profiles start to be dominated by their partition coefficients (K values). The uptake quantity and equilibration time is higher for chemicals having higher K compared to one with lower K values. Since solid coatings contain finite number of adsorption sites (or capacity) where analyte molecules are reversibly bound,

123

chemicals with lower K are often displaced by other chemicals with higher K present in the sample. This phenomena is explained by assuming a sample with two model analytes, A and B. Figure 5-9a shows the extraction time profiles of A with variation of K values of B (K_B). Uptake is not influenced when the K_B is the same as K_A. However, the co-presence of B of high K_B tend to decrease the adsorbed A with time and reaches a steady state. The extent of decrease in adsorbed A from the coating is directly correlated to the uptake of B from the sample. As shown in Figure 5-9b, the uptake quantity and equilibration time increases with the increase of K_B, which is directly correlated to more prominent displacement of A from the coating surface (Figure 5-9a).
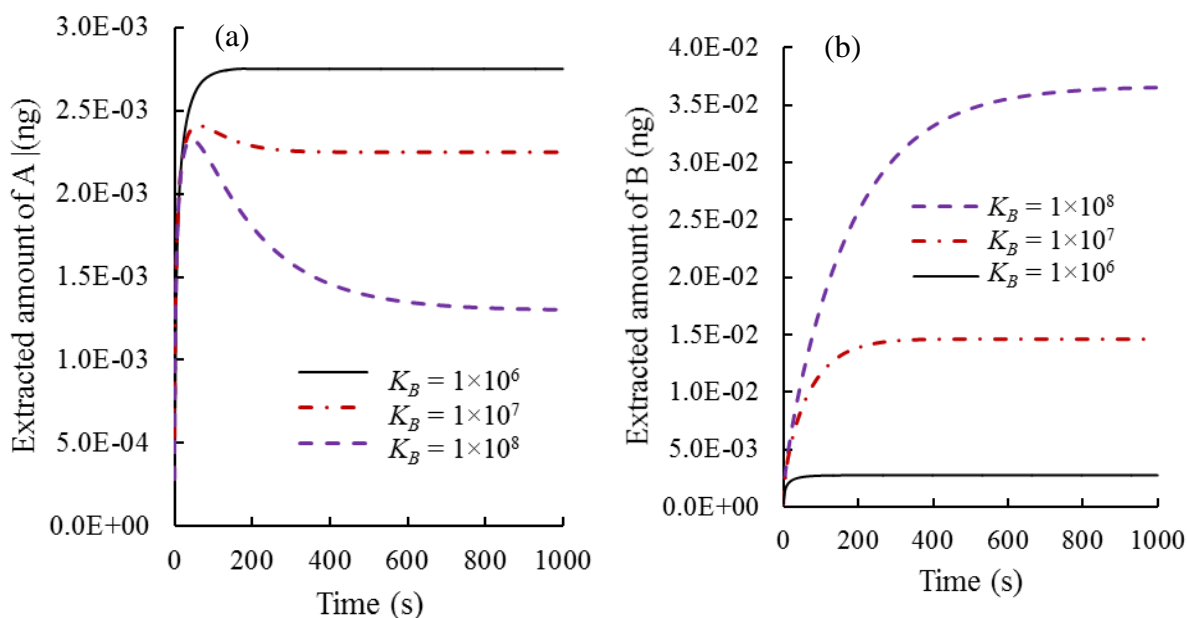
Figure 5-9. (a). Extraction time profiles show the displacement of analyte A by the analyte B with higher K values than that of analyte A. (b). Extraction profiles of analyte B with different K values. Assumption: $K_A = 1\times10^6$, limited sample volume was considered. C_A and C_B 50 nM

The presence of co-extracting compounds can affect both the amount extracted and the linear range of the method using the porous particle based solid coatings. Difficulties in performing accurate quantification of multi-analyte system with solid SPME coatings have been reported by several authors.[124] A calibration curve simulated with the computational model shown in Figure 5-10 described the fact that the linear dynamic range of analyte A decreases with the presence of high affinity B (high K_B).
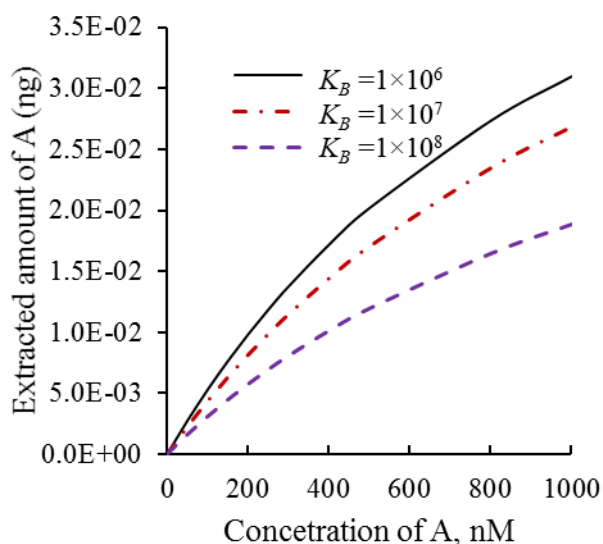
Figure 5-10. Calibration curve simulated with the computational model showing the amount of analyte A extracted by the coating vs. initial concentration of A in the sample when another model analyte B with three K_B values are present in the sample (limited volume). Assumptions: $\Gamma_{max} = 1 \times 10^{-7}$ mol/m^2, $K_A = 1 \times 10^6$ M^{-1}.

The problem of displacement that affects the linearity of calibration curve can be addressed by reducing the sample volumes, because extracted amount is proportional to the sample volume, especially for analytes with higher K values where the extraction might be exhaustive, and the decreased uptake of high K analytes results in decreased occurrence of displacements. Otherwise, extraction at the kinetic regime and employing either standard-loaded calibration,[90] or diffusion based[26] calibration will solve the displacement issue with solid coatings. It has been recently shown experimentally that careful optimization of coating chemistries allows to quantify a wide range of analytes without encountering a significant effect of coating saturation.[125]

5. 3. 7. Effect of analyte depletion from samples

The sample solution depletes because the analyte which adsorbs at the coating surface is not renewed by either semi-infinite diffusion in un-agitated sample or limited quantity of analyte in an agitated static system. The eq. 5-16 for calculating extent of depletion is applicable only for liquid coating where the total volume of the coating is responsible for absorptive extraction.

$$\text{Depletion (\%)} = \frac{V_f K_{es}}{V_s} \times 100 \% \qquad \text{5-16}$$

where, K_{es} is the partition coefficient, V_f and V_s are the volume of the extraction phase and sample, respectively. In addition, this does not include the effect of analyte concentration on equilibration or saturation of the coating. Therefore, the computational model was employed to study the analyte depletion in SPME where the measured sample concentration value at equilibrium is not C_A^0 (as in an ideal large volume case), but C_A^{eq} and eq. 5-6 can be rewritten as:

$$\frac{n_{eq}^{l.v.}}{n_{max}} = \frac{K C_A^{eq}}{1 + K C_A^{eq}} \qquad \text{5-17}$$

In addition, the final extracted amount $n_{eq}^{l.v}$ is then lower than in an ideal large volume microextraction system. This phenomenon is explained by the variation of C_A/C_A^0 with the distance from the coating surface for different times after the extraction begins (Figure 5-11a). After 10 seconds, the solute starts to be depleted because of the limited volume of the sample. The concentration depletion extends to the whole sample container after 10 seconds. At 200 seconds the equilibrium is reached: C_A^{eq} is about 50% of C_A°. However, $C_A^{eq} = C_A^\circ$ is obtained for the infinite volume system (not shown here). Consequently the concentration at equilibrium in equation 5-8, C_A^{eq}, is not equal to C_A° any longer, and this equation should be rewritten as eq.

5-17.The final extracted amount is therefore lower than the theoretical one attainable in a larger sample volume or in a system where the solution is renewed (e.g. with a flow).
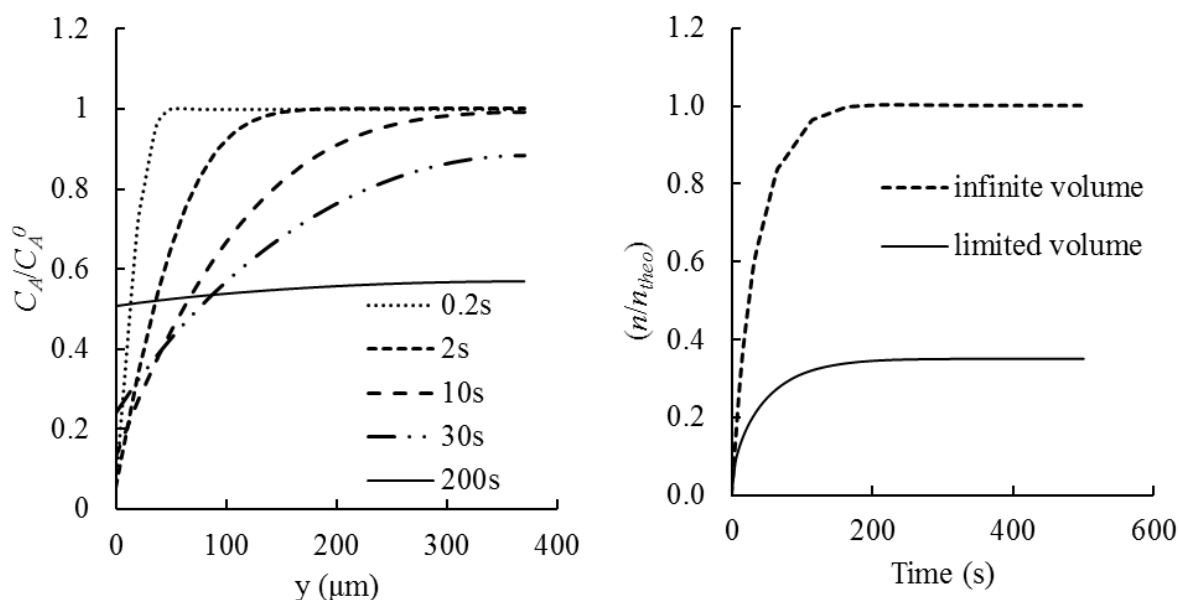
Figure 5-11. Variations of C_A/C_A^0 with distance from the coating surface (y) for different times after the beginning of extraction. (b) Extracted amount normalized by the theoretical extracted amount calculated by eq 5-8 with respect to time for limited and infinite sample volume. Infinite volume simulation was performed with flow through configuration at flow velocity of 0.2 cm s^{-1} while the limited volume was assumed by deactivating the fluid flow nodes in the simulation software. $C_A^0 = 0.1$ nM, $\Gamma_s = 1 \times 10^{-7}$ mol m^2, $K = 1 \times 10^7$ M^{-1}, $L = 75$ um, no agitation.

The extraction time profile obtained from limited and infinite sample volume is shown in Figure 5-11b. The extracted amount increases sharply at the beginning of extraction and thereafter reaches a plateau value. It is illustrated that the extracted amount in the limited volume was less than 50 percent compared to the ideal equilibrium case (whose value can be calculated from 5-8). The equilibrium extracted amount n_{eq} obtained in the limited volume system are compared with

theoretical ones, n_{theo} in Table 5-1. We can observe that n_{eq} is nearer the theoretical one at high ψ (high $C_A°$) due to the lower bulk depletion.

$$\frac{n_{eq}}{n_{max}} = \frac{\psi}{1 + \psi}$$

5-18

where the parameter $\psi (= KC_A^0)$ indicates the capacity of the system to extract maximum extracted amount of the coating. If $\psi \ll 1$, equation is converted to a linearized isotherm:

$$n_{eq} = n_{max}KC_A^0$$

5-19

Table 5-1. The variation of extracted amount at equilibrium with respect to different values of ψ. Theoretical extracted amount was calculated using eq. 5-8.

ψ	n_{eq}^{theo}	n_{eq}^{model}	difference
10	5.89×10^{-3}	3.38×10^{-3}	42.34%
1	3.24×10^{-2}	2.57×10^{-2}	20.51%
0.1	5.89×10^{-2}	5.85×10^{-2}	0.62%

Therefore, the model can be used to calculate maximum possible extracted amount without significant depleting the system. Since a high recovery is suitable in many applications, the general conditions to fulfill in order to avoid depletion can be determined with the model simulation.

5. 3. 8. Model Validation

The developed mathematical model was compared with the model previously reported by Chen et al. and the experimental data for rapid water sampling of benzene used in their report.[34] As clearly demonstrated in Figure 5-12, the computational model predicted the mass uptake with better accuracy than the previous model. In Chen's model, an accurate solution was not available

due to the difficulty of estimating $\bar{h}$, and an empirical correlation was used. On the other hand, the present computational model can capture the complex multi-phase extraction process as most of the data points fall on the straight-line. In addition, the present model describes an idealized physical mass-transfer process using a mechanistic model, which model parameters have a physical meaning.
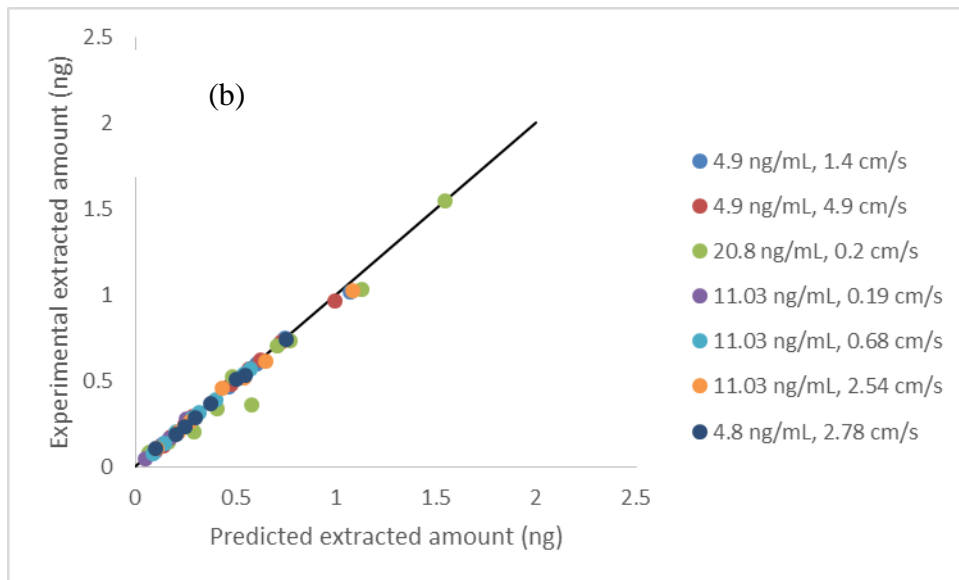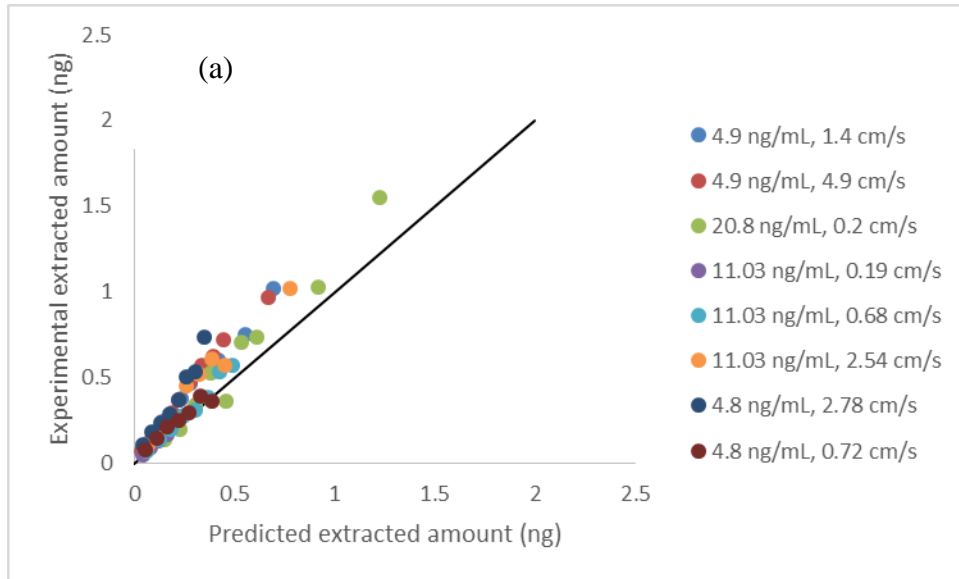
Figure 5-12. Model validation, (a) Chen's model[1], (b) Simulation data obtained from the developed computational model.

5.4   Conclusions

A novel computational model was proposed in this chapter to quantitatively describe extraction by porous particle based solid coatings and their application in pre-equilibrium based rapid and direct extraction of analyte with SPME. The amount of extracted mass predicted by the new model compares well with experimental mass uptakes. It was demonstrated that analyte flux is proportional to diffusion coefficient of analyte and fluid flow velocity at the early stage of extraction. The model demonstrated excellent prediction of the effect of mass transfer caused by the variation of fluid flow on the extraction rate in the SPME sampling. Therefore, with the aid of the model, estimation of sampling time and calibration of the rapid sampling based on diffusion is possible within short time and low cost. In addition, optimization of flow velocity and maximum extraction capacity can be evaluated for wide range of analytes with varied equilibrium constant values (K). For the application of solid coatings, one should decide the flow velocity carefully in order to avoid the reaction-limited regime for the rapid calibration approach. The coating capacity needs to be determined for a particular sample concentration in order to avoid shortening the equilibration time near the saturation of the coating. Since high affinity coatings demonstrated lower linear dynamic rage, samples with higher concentration may need to be diluted. Optimization of sample volume, coating capacity and affinity is important to avoid analyte depletion from the small volume sample. This might be important in determining free concentration where bound matrix components should be unperturbed due to the analyte depletion. Overall, the simulation results provide detail understanding of employing porous particle based solid coating in SPME.

Chapter 6 **Aptamer-functionalized solid-phase microextraction for selective extraction**

of protein

6.1 Preamble

This chapter has been published as a part of the paper Fuyou Du, Md. Nazmul Alam, J. Pawliszyn; "Aptamer-functionalized solid phase microextraction-liquid chromatography/tandem mass spectrometry for selective enrichment and determination of thrombin" Anal. Chim. Acta. 2014 3; 845: 45-52. The contributions of Fuyou Du involved experiments and writing the manuscript and manuscript revision. All tables and figures were reprinted from this publication with permission from Elsevier.

6.2 Introduction

The development of novel coatings has allowed for improved throughput, biocompatibility and robustness of the SPME LC–MS/MS methods for various target analytes. However, based on their partition coefficients, most coatings can extract a class of analytes that leads to quantification complications; this is often due to the co-extraction of undesired species or displacement by stronger adsorbents present in complex biological matrices such as blood, plasma and serum. It has been proposed that improvements in coating selectivity can potentially circumvent the challenges of competition, displacement and non-specific binding.[126,127] Inspired by the traditional immunoassay technologies, the immobilization of antibodies on SPME fibers has been applied successfully to extract drug molecules from human serum samples.[128,129] While antibody-based coatings have shown very good selectivity for the analytes in serum samples, the limited capacity of such coatings restricts quantifications in very low dynamic ranges. For the development of

selective and biocompatible SPME coatings, aptamers are a valid alternative to antibodies or other receptors due to the numerous unprecedented advantages of aptamers such as high specificity and affinity, high reproducibility, superior stability, versatile target binding, and low cost of development.[130,131] These unique properties make aptamers perfectly suitable for biosensing, diagnostics, therapeutics, and separation sciences.[132] To date, many aptamer-based affinity approaches, including aptamer-based chromatographies,[133,134], electrochemical,[135,136] aptamer-based capillary electrophoresis, and aptamer-based microfluidics,[137] have been successfully developed for extraction,[138] separation,[139] purification, and detection of targets of interest, ranging from small molecules to proteins and cells.[140] Aptamers have also been immobilized on magnetic beads for analyte detection from biological samples.[140-142] Therefore, an aptamer-based SPME method is very promising for selective analysis of targets of interest in biofluids.[143-145] So far, most of the developed SPME methods to date have been focused on small target analytes.[5] Macromolecules, such as proteins in biofluids, are attractive targets for biomarker or drug discovery. In spite of the advances in mass spectrometry, the quantification of low-abundance proteins in plasma and serum remains a challenge due to the level of sample heterogeneity along with the technical robustness and throughput required for routine clinical assays. We envisaged that the open-bed format of SPME probe will provide efficient protein enrichment by providing no clogging and reduced sample interference. To demonstrate the applicability of SPME for enriching low-abundance proteins from human plasma, we have chosen thrombin as a model protein.

The aim of this study was to develop an aptamer based novel selective SPME probe for human alpha-thrombin in plasma samples with the aid of liquid chromatography/tandem mass

spectrometry (LC-MS/MS). At first, carboxy- functionalized microfiber structure was prepared by elecrospinning of poly(acrylonitrile-co-maleic acid) (PANCMA) co-polymer on pre-cleaned stainless steel rods. . The 29'-mer DNA aptamer selective to the heparin binding site of the thrombin was then immobilized on the polymer substrate providing the aptamer based SPME (Apt-SPME) probe. The prepared Apt-PANCMA probes were evaluated in terms of selectivity, binding capacity, extraction ability and reusability. Under the optimal conditions, the proposed Apt-SPME coupled with LC-MS/MS approach has been successfully applied to analyze thrombin in real human plasma samples.

6.3   Experimental

Chemicals and Materials: Human α-thrombin and prothrombin were purchased from Haematologic Technologies Inc. Human serum albumin, human hemoglobin, cytochrome C, trypsin, maleic anhydride (≥99.0%), acrylonitrile (≥99.0%), formic acid (98%), 1-ethyl-3-(3-dimethylaminopropyl)carbodiimide hydrochloride (EDC·HCl, ≥99.0%), N-hydroxysuccinimide (NHS, 98%), potassium persulfate (≥99.0%) and anhydrous sodium sulfite (≥98.0%) were purchased from Sigma-Aldrich (St. Louis, MO). HPLC grade acetonitrile and methanol were purchased from Fisher Scientific (Unionville, Ontario, Canada). N,N-dimethylformamide (DMF) was obtained from Caledon Labs (Ontario, Canada). An anti-thrombin DNA aptamer (Apt) with an amine terminal group (5′/5AmMC6/-AGT CCG TGG TAG GGC AGG TTG GGG TGA CT-3′) was purchased from Integrated DNA Technologies Inc. (Canada). The internal standard peptide was purchased from Anaspec Incorporation (Fremont, CA, USA), and the amino acid sequence is

SSIIHIER. Clinical human plasma from a patient was kindly given by Toronto Hospital and other human plasma samples were from Lampire Biological Laboratories (LBL), Inc. (Pipersville, PA).

All solutions were prepared with ultrapure water purified by a Barnstead/Thermodyne NANO pure water system (Dubuque, IA, USA). 1.0 mg/mL of thrombin was prepared in phosphate buffered saline (PBS) buffer solution (10 mM, pH 7.4) and NH_4HCO_3 buffer (25 mM), respectively. The two stock solutions were stored at 5 °C in a refrigerator.

Preparation of Poly(acrylonitrile-co-maleic acid): Poly(acrylonitrile-co-maleic acid) *(PANCMA) was* prepared by using a free radical *water-phase* precipitation polymerization according to the method described by Nie *et al* with minor modifications.[146] Briefly, 7.4 g maleic anhydride, 10.6 g acrylonitrile and 20 mL of deionized water at 60 °C were added into the reactor equipped with mechanical stirrer, thermometer, and nitrogen inlet tube, and then 135 mg $K_2S_2O_8$ and 75 mg Na_2SO_3 were added into the stirring solution while maintaining the reaction temperature at 60 °C under nitrogen atmosphere. The pH value of the mixture was adjusted to around 2 using dilute H_2SO_4 solution. The copolymerization was continued for 3 h and the precipitated copolymer was filtered and washed with excess de-ionized water and ethanol to remove residual monomers. The obtained PANCMA was dried for 12 h under vacuum at 60 °C.

Preparation of the PANCMA Probe via Electrospinning: Four gram of PANCMA was dissolved in 50 mL of DMF at room temperature with gentle stirring for 12 h. The obtained homogeneous solution was placed in a syringe bearing a 1.0 mm inner diameter metal needle which was connected with a high voltage power supply (UW-SYS E2047, University of Waterloo, Canada). A grounded counter electrode was connected to the stainless steel rod-collector (55

mm×1.5 mm, i.d.), which was rapidly rotated by an electrical power unit during electrospinning experiments. According to our experimental results, the optimal electrospinning voltage was 10.0 kV, the distance between the needle tip and the collector was 130 mm, the flow rate of the solution was 0.30 mL/h, which controlled by a K_d Scientific syringe pump (Holliston, MA, USA), the coating length of probe-collector was 30 mm, and the collection time was 50 min. The obtained membrane on probe was dried for at least 3 h at 60 °C in vacuum oven before it was used.

Aptamer Immobilizing on the Surface of the PANCMA: As shown in Figure 6-2, for aptamer immobilization, the PANCMA matrix was first activated with EDC/NHS dissolved in 50 mM PBS buffer (pH 8.0), and then the amine functionalized DNA aptamer was added for preparation of Apt-PANCMA. Briefly, four PANCMA probes were thoroughly washed with water and rinsed with 50 mM PBS solution containing 20 mM KCl and 600 mM NaCl (pH 8.0). After this, the pretreated probes were submerged into 2.0 mL of EDC/NHS solution (100 mM EDC and 100 mM NHS in 50 mM PBS buffer, pH 8.0) and shaken gently at room temperature to activate the -COOH group of PANCMA. After incubation for 2 h, 240 nmol aptamer was added and incubated overnight. The prepared aptamer functionalized PANCMA (Apt-PANCMA) probes were taken out and washed several times with 10 mM PBS buffer (pH 7.4), and then dipped into the same PBS solution for future use. The microstructure of the prepared Apt-SPME probe was investigated by scanning electron microscope (SEM, Zeiss ULTRA plus). The aptamer concentration in sample solution before and after immobilizing reaction was measured by NanoDrop 2000 UV-VIS spectrophotometer (Thermo Scientific).

Thrombin Capture on Apt-SPME Probes: Briefly, Apt-SPME probe was first washed with 10 mL of PBS (10 mM, pH 7.4), and then were dipped into 2.0 mL of sample solution. After

incubation for 1.0 h at room temperature under shaking (130 rpm, SK-300 SHAKER, JEIO TECH, Ontario, Canada), the probe was taken out from the sample solution, and as follow washed with 2 mL of PBS for three times and 10 mL of pure water for three times to remove any unspecific bound or weakly bound species. The target analyte specifically bound on the Apt-SPMe probe was eluted with 2 mL of eluting solution (acetonitrile/water, 80/20, v/v). The elution solution was collected and then dried at ambient temperature with N_2 gas. Finally, the probes were regenerated by successive washes with 10 mL of PBS and stored in the PBS buffer solution at 5 °C.

The obtained residual sample was dissolved in 146 uL NH_4HCO_3 buffer (25 mM), and then 30 μL of trypsin solution (1.0 mg/mL in NH_4HCO_3 buffer) was added. The obtained sample solutions were incubated for overnight at 37 °C. After that, 4 μL internal peptide SSIIHIER solution (500 nM in formic acid/acetonitrile/water (0.1/10/90, v/v/v) solution) and 20 μL acetonitrile/formic acid (80/20, v/v) was added into the digestion solution, and then filtered by 0.22 μm Supor® membrane (Pall Corporation, USA) for LC-MS/MS analysis.

Selectivity and Binding Capacity on Apt-SPME Probe: To demonstrate the selectivity on the Apt-PANCMA probe for thrombin, prothrombin, hemoglobin, human serum albumin and cytochrome C were chosen as reference proteins.

The binding capacity of thrombin on a single Apt-PANCMA probe was *evaluated* by determining the recovery amount of thrombin with the increase of the *concentration* of *standard* thrombin in PBS buffer (10 mM, pH 7.4).

Recovery Test and Determination of Thrombin in Human Plasma: To test the applicability of the proposed method to complex biological samples, we used 20-fold diluted

human plasma as sample matrix and determined the corresponding recovery of the spiked thrombin. Briefly, before extraction with Apt-PANCMA probe, different amounts of thrombin were spiked into 20-fold diluted human plasma sample, and then the diluted human plasma samples spiked with thrombin (0, 0.5, 5, 10, 20, 50, 100, 120 and 150 nM) were extracted and analyzed by the same procedure described above for thrombin capture and detection, respectively.

For analysis of real human plasma, the concentration of thrombin in human plasma was determined by using the calibration equation, which was obtained by the measurement of the intensity of the signal peptide from thrombin with the increase of the spiked thrombin ranged from 0.5 to 150 nM in 20-fold diluted human plasma.

Instrumentation and Operating Conditions: A Shimadzu (LC-10AD) high pressure liquid chromatography (HPLC) system (Kyoto, Japan) coupled to an API 4000 mass spectrometer (AB Sciex, Concord, Ontario, Canada) equipped with TurboIonSpray source was used in the qualitative and quantitative analysis of thrombin. Instrument control was performed using the Analyst 1.5 software. A CTC PAL autosampler platform from Leap Technologies (CTC Analytics, NC, U.S.) was used to inject 20 μl of samples for LC-MS/MS analysis. The LC separations were performed on a BioBasic-C8 column (100 mm × 1.0 mm i.d., particle size 5 μm) from Thermo Scientific (Waltham, MA, USA). The sample oven temperature was maintained at 5 °C, and the column was at ambient temperature. The mobile phases consisted of 0.1% (v/v) formic acid in water (solvent A) and 0.1% (v/v) formic acid in acetonitrile (solvent B), and the flow rate was 120 μL/min. According to our preliminary experiments for thrombin analysis, the optimal gradient profile was as follows (min/% of mobile phase B): 0.0/5, 0.5/5, 20.5/25, 21.0/99, 26.0/99, 27.0/5, and 47.0/5.

The MS/MS analysis in API 4000 mass spectrometer was performed in positive mode under multiple reaction monitoring (MRM) conditions at 477.76→417.188, 477.76→554.31 and 477.76→667.452 for internal peptide SSIIHIER, and 598.20→460.50, 598.20→623.70, 598.20→710.80 and 598.20→839.38 for ELLESYIDGR, respectively. According to our preliminary experiments for determination of thrombin, the ionspray voltage and source temperature were set at 5000 V and 400 °C, and collision gas, curtain gas, ion source gas 1, and ion source gas 2 were optimized at 4, 10, 20 and 0 (arbitrary units), respectively. The optimized value for declustering potential (DP), entrance potential (EP), collision-induced dissociation energies (CE), and collision cell exit potential (CXP) were 20, 10, 30, and 15 V, respectively. For other three proteins, the same MRM conditions were used, and the specific signal peptide for determination of each protein was shown in the Figure 6-1

Method Validation: After acquisition the specific ions were extracted from the spectra using the Analyst 1.5 software. Identification was based on retention time, accurate mass and product ions of the parent ions relative to external standards. The peak area of the corresponding extracted ion chromatogram (XIC) at 477.76→554.31 for internal peptide SSIIHIER and at 598.20→839.38 for ELLESYIDGR, respectively, was used to quantify the amount of thrombin based on the calibration curves. Method validation involved the determination of dynamic range, limit of detection (LOD, S/N=3), accuracy and precision according to the accepted criteria.

Calibration curve for LC-MS/MS analysis was built using serial digestion solution of different thrombin concentration. 200 nM thrombin in NH_4HCO_3 buffer (25 mM) was diluted to the desired concentration (1, 5, 10, 20, 50, 80, and 100 nM) with NH_4HCO_3 buffer, and 30 μL of trypsin solution (1.0 mg/mL in NH_4HCO_3 buffer) was added in the corresponding sample solution (final

volume: 960 μL), respectively. The prepared sample solutions were incubated for overnight at 37 °C. After that, 20 μL of 500 nM internal peptide SSIIHIER and 20 μL acetonitrile/formic acid (80/20, v/v) was added into the obtained digestion solution, respectively, and then the all samples were filtered by 0.22 μm Supor® membrane and analyzed by LC-MS/MS system (Figure 6-1). For the analysis of the other four proteins, the similar procedure was used.
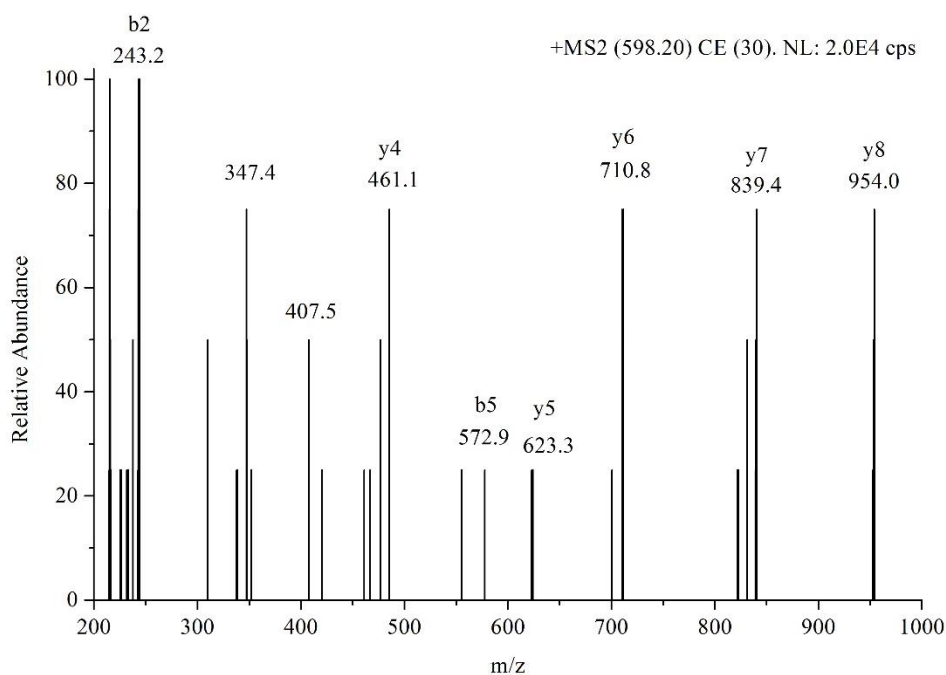
Figure 6-1. MS/MS spectra of [M+2H]$^{2+}$ of ELLESYIDGR (m/z 598.20) from the digestion of synthetic thrombin (50 nM). The product ion spectrum of the peptide fragment presented indicating predominant y and b ions.

Additionally, the accuracy of the proposed method was estimated by determining the recovery of thrombin at different concentration levels. Precision was confirmed by evaluating relative standard deviations (RSDs) of the retention time and the peak area of extract ion chromatogram (EIC). The limits of detection were calculated using a signal-to-noise ratio of 3 (S/N=3, the ratio

141

between the EIC peak intensity and the noise). All data presented in this work were obtained by averaging three replicates at least unless otherwise noted.

6.4   Results and Discussion.

6. 4. 1. Preparation and Characterization of Apt-PANCMA probe

Efficient extraction of targeted protein analytes with the immobilize affinity ligand is highly dependent on the physicochemical properties of the solid support. The strategy of immobilizing the aptamer on a steel rod coated with a functional polymer is presented in Figure 6-2
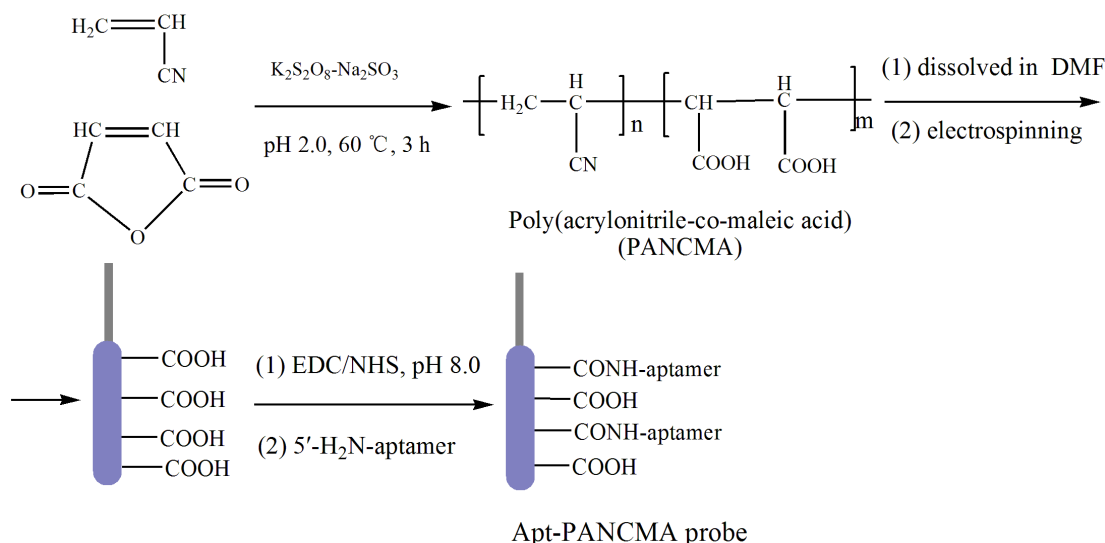
Figure 6-2. Schematic representation of the processes for preparation of aptamer functionalized SPME probe (Apt-SPME) probe

We chose a polymeric support based on a combination of polyacrylonitrile (PAN) and maleic acid (MA). PAN provides porosity and physical strength, while the presence of MA was proven to improve hydrophilicity and chemical functionality.[146] Electrospinning technique was employed to create micro/nanofibers of the polymer as an inexpensive and simple method of obtaining high

surface area substrate.[147] Using this method the polymer mat is attached to a stainless rod without the need of a binder. The fibrous structures, possessing reactive carboxyl groups were used to immobilize DNA aptamers. In order to obtain maximum carboxyl groups without sacrificing the mechanical strength of the support, the ratio of acrylonitrile to maleic acid was increased from 2:1 to 8:1. The results showed that the prepared PANCMA was partly dissolved in water when the ratio was 2:1. With the ratio higher than 4:1, the polymer was chemically and mechanically stable, therefore, the optimal ratio of 4:1 was chosen for preparing the PANCMA support. Under the optimal electrospinning experimental conditions discussed in experimental section, the thickness of the obtained electrospun PANCMA fiber coating on the stainless steel rod was estimated to be approximately 60-65 μm. The thrombin-specific DNA aptamer modified with 5´-amine functional group was covalently conjugated to the electrospun PANCMA support through the reactive carboxyl moieties via EDC/NHS protocol. The aptamer coupling efficiency was approximately 84.6% evaluated by comparing the immobilized aptamer amount on the SPME probe with the original quantity of aptamer added in the coupling reaction solution. Figure 6-3 (A) shows a uniform surface in terms of thickness throughout the Apt-PANCMA probe. Moreover, the surface morphology of the electrospun PANCMA fiber was not changed before and after reaction with the aptamer. Additionally, the SEM images (Figure 6-3 A and B) show that the diameters of the prepared fibers were about 1.0 μm possessing highly porous surface, which should significantly increase the surface area availability on the probes. The spaces among the fibers are in the range of 200–5000 nm and this should facilitate faster protein mass transfer leading to efficient analyte binding.

(A)   (B)
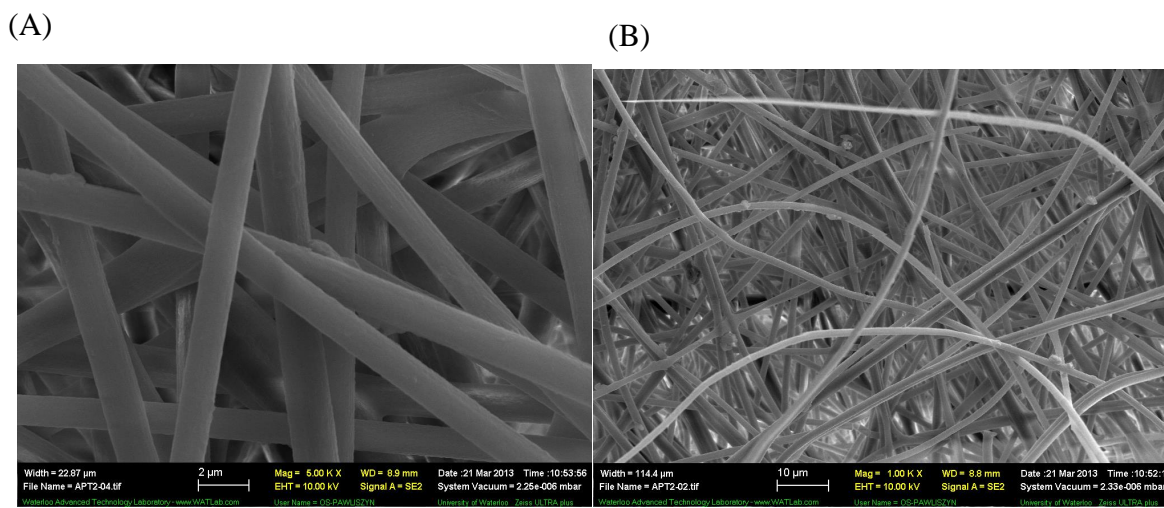
Figure 6-3. Photographic image (A, 10×) and SEM images of Apt-SPME probe (B, 1000×; C, 5000×magnification).

6. 4. 2. *Specificity of Apt-SPME probes for thrombin*

First of all, the specific capture ability of the Apt-SPME probe was evaluated by investigating the recovery of human α-thrombin, with the addition of prothrombin, hemoglobin, cytochrome C and human serum albumin (HSA) in PBS buffer. The obtained results shown in Figure 6-4 indicated that the recovery of thrombin was significantly higher than that of the other proteins, which suggested that the prepared Apt-SPME probe was able to capture thrombin with high selectivity, due to the specific interaction of thrombin with its aptamer on the Apt-SPME probe.
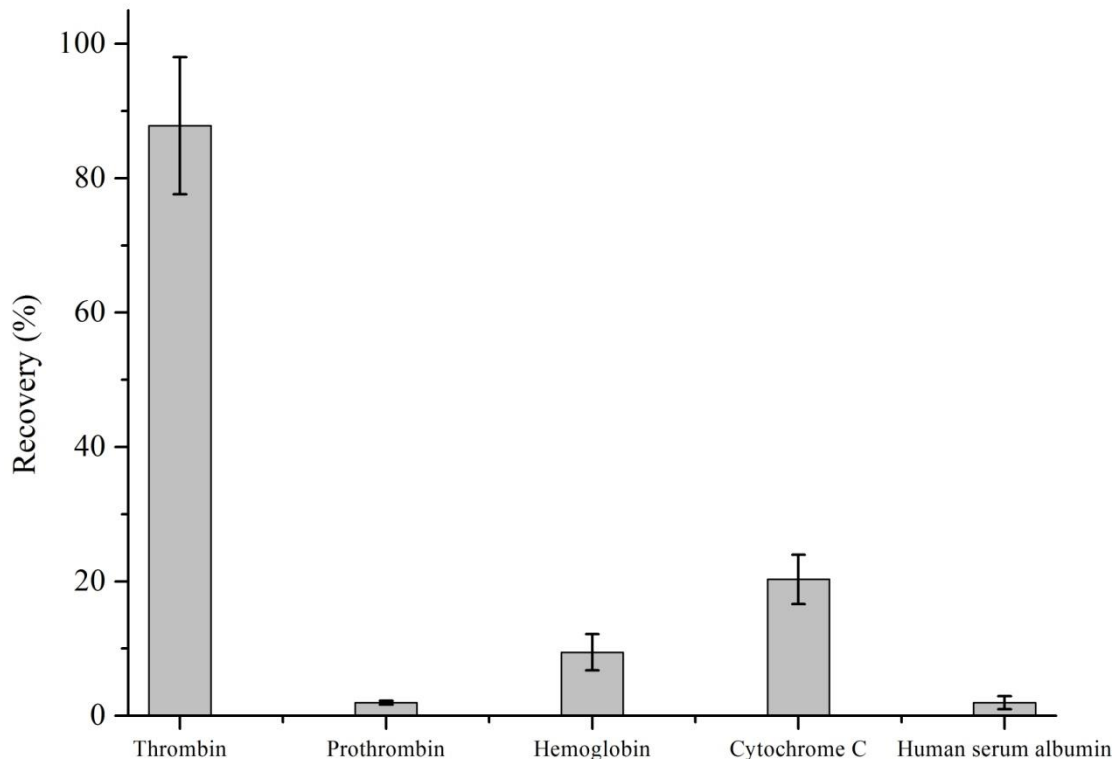
Figure 6-4. Specificity of Apt-PANCMA probes for thrombin from the most potential interfering proteins spiked in PBS buffer (pH 7.4). The concentrations of alpha-thrombin, prothrombin, hemoglobin and human serum albumin were 5 nM. The concentration of cytochrome-C was 10 nM. Total volume of the sample solution was 2 mL. Percent recovery was calculated from the calibration curves obtained by injecting different concentrations of standard proteins to the LC-MS/MS as shown in Figure 6-9

In order to test the selectivity of the Apt-SPME probe for thrombin compared to its parent protein, prothrombin, a separate study was carried out. As shown in Figure 6-5, percent recovery of prothrombin was less than two percent even with higher concentration of prothrombin spiked.
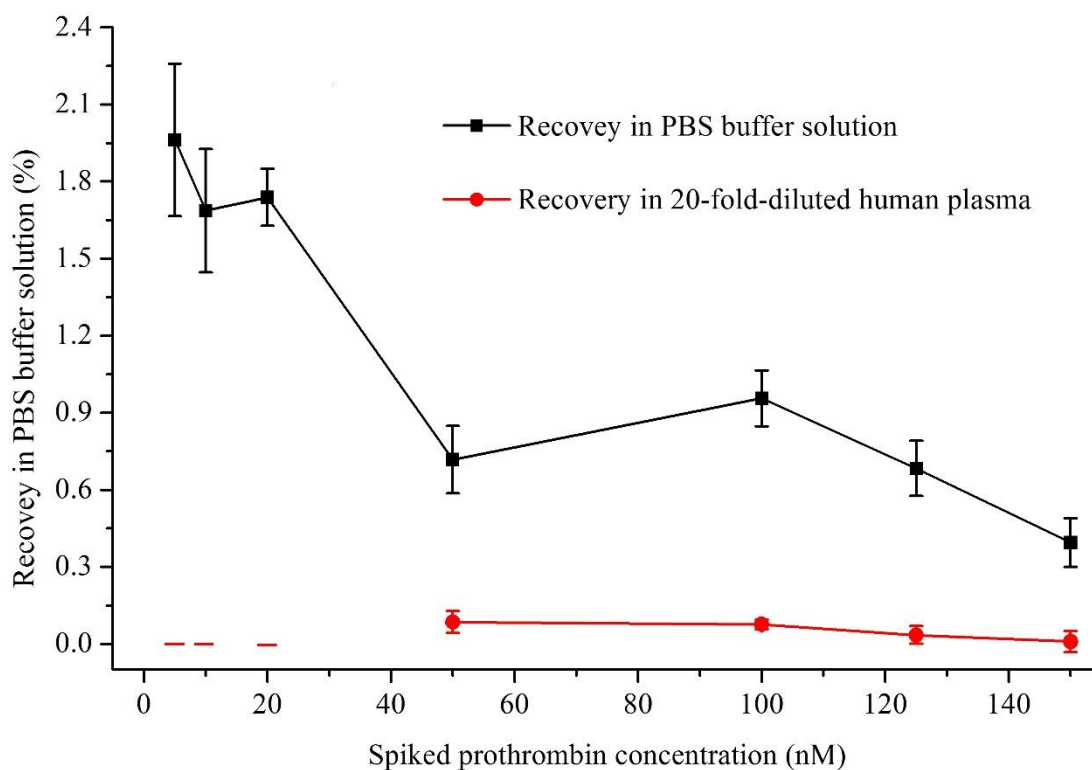
Figure 6-5. Recovery of prothrombin with the increase of prothrombin concentration in PBS buffer (pH 7.4) and 20-fold-diluted human plasma. The recovery of prothrombin was not estimated when the concentration of spiked prothrombin in 20-fold-diluted human plasma was 5, 10, or 20 nM, because the intensity of signal peptide (m/z 839.38) from the digestion solution of the extracted prothrombin was quite low at the corresponding three levels. Here the concentration of prothrombin was calculated by the curve equation ($Y=1.124\times10^{-2}X-4.720\times10^{-3}$, $R^2=0.9999$) described in Figure 6-9

These results suggested that the immobilized aptamer is functional for selective extraction of thrombin.{Wang, 2016 #1462} In order to see if the polymeric substrate extracts the target thrombin, the electrospun PANCMA substrate (without aptamer functionalized probe) was employed as a negative control to extract thrombin according to the same procedure. The results showed that the thrombin recovery on the control PANCMA was 14.9%, which is significantly

lower than 87.8% obtained by using Apt-SPME probes, resulting from the high specific binding affinity of the 29-mer aptamer instead of the unspecific adsorption affinity of the matrix. Moreover, the lower non-specific extraction can be due to the presence of surface carboxyl group that leads to the ionic interaction with the protein positive charges.[148]

6. 4. 3. Optimization of extraction, desorption and detection conditions

The extraction time is a fundamental parameter governing the efficiency of the extraction, and may be shortened by intensive stirring for the direct extraction mode. In this work, the effect of extraction time was investigated by varying it from 10 to 120 min under moderate shaking (130 rpm). Figure 6-6 shows that the extraction recovery of thrombin in PBS buffer was increased with the increase in extraction time from 10 to 60 min, and then was not obviously affected by the extraction time more than 60 min. Therefore, 60 min of extraction time was selected for the following experiments in order to effectively extract thrombin from samples.
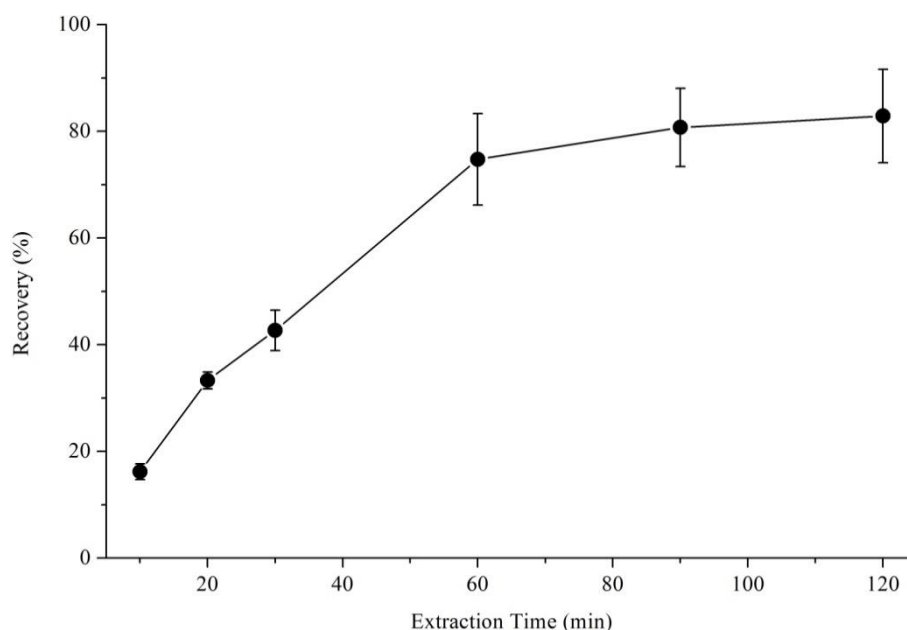
Figure 6-6. Effect of extraction time on the recovery of thrombin from PBS buffer (pH 7.4). The concentration of thrombin was 5 nM and the volume of solution was 2 mL. Percent recovery was calculated from the calibration curves obtained by injecting different concentrations of standard proteins to the LC-MS/MS as shown in Figure 6-9.

To avoid the carry-over effect and to enhance sensitivity, rapid and effective desorption is necessary. Several desorption solvents (70% (v/v) methanol, 70% (v/v) acetonitrile, and 80% (v/v) acetonitrile) were tested to achieve a complete desorption of thrombin from Apt-SPME probes, and the results showed that 2.0 mL of 80% (v/v) acetonitrile was found to be optimum for eluting thrombin from the probes.

In order to identify and determine thrombin in real samples, Apt-PANCMA probe combined with LC-MS/MS has been used in this work. Thrombin was identified by the corresponding extracted ion chromatogram (XIC), retention time and mass spectrum of ELLESYIDGR, which is

the strongest signal peptide from digestion of thrombin in accordance with the results of Zhang et al.[149]

The calibration curve for LC-MS/MS analysis was constructed by measuring the relative XIC intensity of the signal peptide ELLESYIDGR at m/z 598.20→710.80 from thrombin and the internal standard peptide SSIIHIER at m/z 477.76→554.31. Table S1 shows that the calibration curve were linear over the concentration range of 1.0-100 nM with a good correlation coefficient (R^2=0.9993). The linear regression equation is $Y=1.497 \times 10^{-2}X – 5.880 \times 10^{-3}$, where Y stands for the logarithm of intensity ratio of the peak area of the selected signal peptide at m/z 839.38 versus that of the internal peptide at m/z 554.31, X stands for the logarithm of concentration of thrombin in nM. The detection limit of the developed LC-MS/MS method was 0.24 nM, which were evaluated on the basis of a signal-to-noise ratio of 3.

The reproducibility of the retention time and peak area were estimated by six repetitive determinations of the digestion solution from 5.0 nM of thrombin. The variation coefficients of retention time and XIC peak area of the selected signal peptide were not larger than 1.0% and 5.7%, respectively. The results indicated that the repeatability of the LC-MS/MS method for determination of thrombin was satisfactory.

6. 4. 4. *Evaluation of thrombin binding capacity, reproducibility, and stability of Apt-SPME probes*

In order to compare the specific extraction properties of the Apt-SPME probe, a binding assay was performed with thrombin spiked in either standard solution (PBS) or in diluted plasma as shown in Figure 6-7.
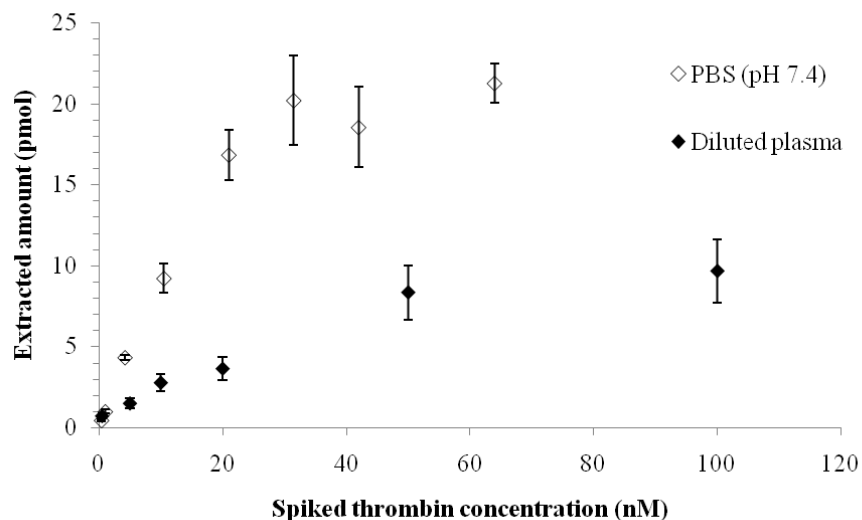
Figure 6-7. Extraction efficiency of Apt-SPME probe for thrombin in standard solutions (PBS, pH 7.4) and in spiked plasma samples. Thrombin was spiked in 2 mL of PBS or 20 fold diluted plasma and one Apt-SPME probe was incubated for 1 hour at room temperature.

Extraction profile in PBS indicates that thrombin can be extracted nearly quantitative yield at lower concentration (below 10 nM), however, the extraction gets lower and finally the probe reaches saturation at around 22 nM concentration. The maximum binding capacity of the prepared Apt-SPME probe for thrombin was estimated was approximately 20.7 pmol. The same experiment repeated in 20 fold diluted human plasma is shown in the filled symbols (Fig. 4). The experimental data indicate that the specific capture and detection of thrombin from blood plasma is possible by Apt-SPME probe. For all concentration ranges, however, the extracted amount of thrombin from plasma is significantly lower than that obtained from PBS sample. In addition, the extraction isotherm in plasma shows a different saturation behavior; the maximum thrombin extraction capacity was almost half compared to the amount in PBS. First of all, we thought this reduction of

recovery might be related to the inactivation of the specific aptamer probes by some other high abundant proteins. We investigated this assumption by spiking increased level of human serum albumin (HSA) up to the level of human blood (Figure 6-8).
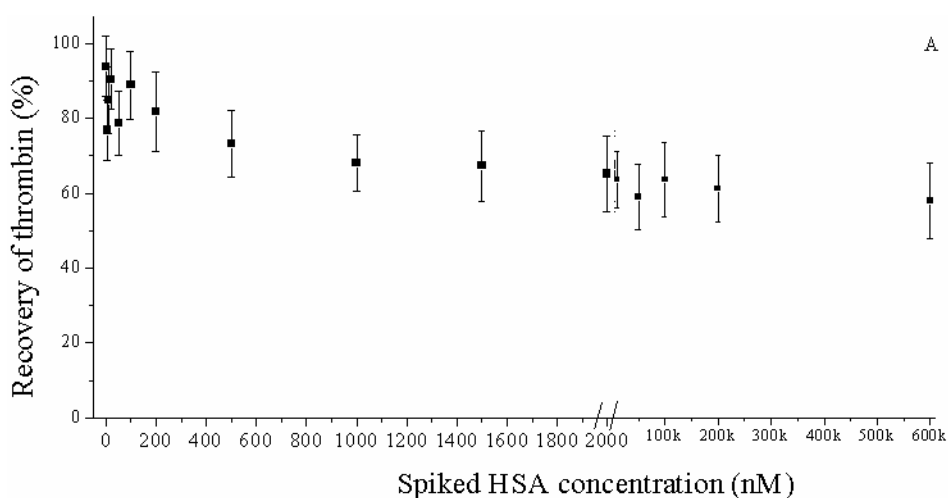

Figure 6-8. (A) Results of thrombin recovery with the increase of spiked HSA concentration from 0 to 600000 nM in PBS buffer samples (containing 5.0 nM thrombin). The thrombin concentration in the prepared samples is 5.0 nM. (B) Results of the HSA recovery and the extraction amount of HSA with the increase of spiked HSA concentrations raning from 0 to 600000 nM in PBS buffer. Here the HSA concentration was calculated by the curve equation (Y=9.991×10-2X–4.453×10-2, R2=0.9981).

The results of the HSA addition experiments show that the recovery of thrombin was more than 60 % even if the concentration levels are the same as the human blood, which indicates that the probe surface was quite functional and specific for thrombin at such a high protein concentrations. It is worth mentioning that some other research groups have also observed similar reduction of thrombin recovery from complex sample matrix. For instance, the Hu's group[150] and the Le's group[151] reported that up to 80% thrombin recovery decreases in the 10 fold diluted serum

compared to the buffer solution by using aptamer as a specific receptor of thrombin. Reduction of signal intensity in 10 fold diluted serum was also observed by Tok et al., where they have used immobilized anti-thormbin antibody as the specific probe.[152] All of these studies indicate that the reduction of thrombin recovery might be due to the decrease in functional thrombin concentration after spiking in the plasma/serum sample.[153,154] This thrombin inactivity is probably due to the presence of thrombin inhibitors in serum or plasma. It has been reported that, the most common enzymatic inactivation of thrombin occurred by forming an inactive complex with antithrombin III present in serum or plasma.[155] The results indicate that in order to extract intact thrombin with high recovery from plasma or serum by affinity ligands, it is necessary to indirectly protect inactivation of thrombin by spiking some artificial inhibitor so that the endogenous inactivation site is blocked while leaving the aptamer affinity site free for binding.

This approach of aptamer-based SPME can be miniaturized into high throughput 96-well format for quantitative proteomics.[156,157] Furthermore, selective extraction of targeted low-abundant therapeutic or disease related proteins in vivo from human blood will be possible for the detection with mass spectrometry.

Considering the effect of plasma matrix on the extraction performance, a calibration curve based on the thrombin recovery was built to determine thrombin in human plasma. Figure 6-9 (A) shows that the peak area of the signal peptide (ELLESYIDGR) at m/z 839.38 from thrombin was increased with increase of the concentration of spiked thrombin from 0.5 to 150 nM, while that of the signal peptide did not obviously change when the concentration of spiked thrombin was higher than 100 nM, resulting from the limited binding capacity of the Apt-PANCMA probe.
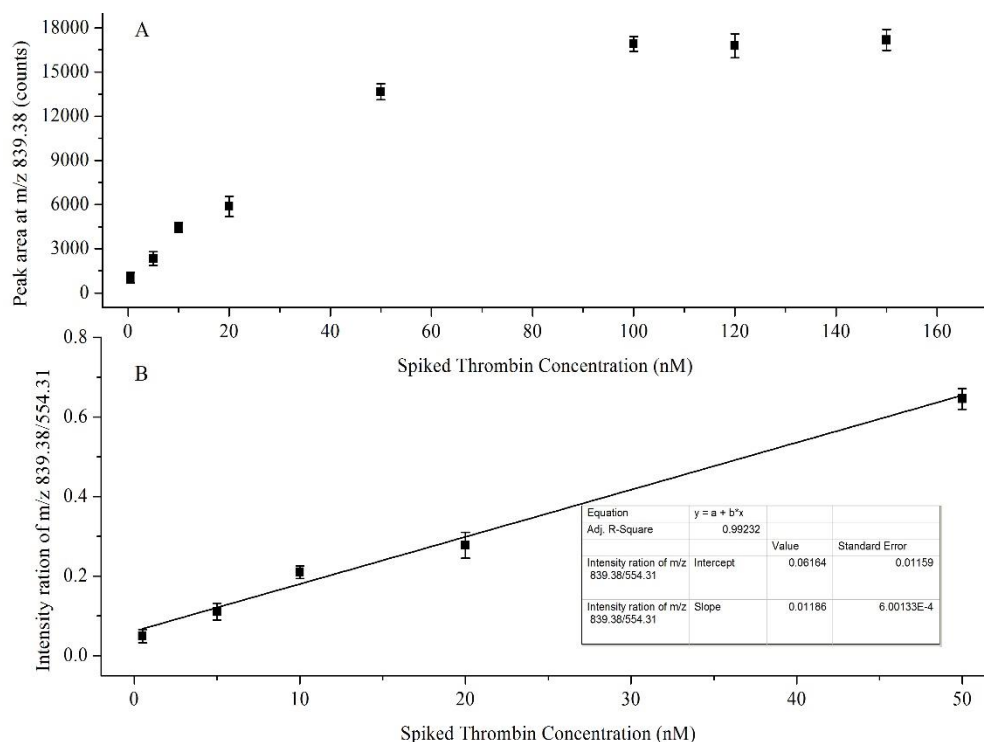
Figure 6-9. (A) Peak area of signal peptide (ELLESYIDGR) at m/z 839.38 with the increase of spiked-thrombin concentration from 0.5-50 nM. The value of the peak area is the difference between the peak area of the signal peptide from thrombin in 20-fold diluted human plasma spiked with standard thrombin and that of thrombin in the sample matrix. (B) Calibration curve and linear regression coefficient (R2) for determination of thrombin using Apt-PANCMA in combination with LC-MS/MS. The inset table shows the corresponding curve equation, where Y is the intensity ratio of peak area between the selected signal peptide at m/z 598.20→839.38 from spiked-thrombin and internal peptide SSIIHIER (10 nM) at m/z 477.76→554.306, and X is the spiked-thrombin concentration as nM.

As can be seen in Figure 6-9 B, the calibration curve were linear over the concentration range of 0.5-50 nM with a good correlation coefficient (R2=0.9923), which indicated that the obtained

calibration curve can be used to determine the concentration of thrombin in diluted human plasma, although the recoveries of thrombin from 20-fold diluted human plasma were not high. According to the above obtained results, the detection limit of the proposed Apt-PANCMA probe coupled with LC-MS/MS method was found to be 0.30 nM.

The probe-to-probe reproducibility was determined by evaluating the thrombin recovery on six different Apt-SPME probes. The obtained results showed that the thrombin recoveries at a concentration level of 5.0 nM spiked in PBS buffer ranged from 87.8% to 103.2% for all six probes with the corresponding RSDs lower than 14.6%, which indicated that the Apt-SPME probe could be produced and operated reproducibly.

To investigate of the stability of Apt-SPME probe, the same probe was used for two days every week for one month. The RSD of the thrombin recovery at the same loading amounts was 11.7%, demonstrating that the Apt-SPME probe maintained good stability, resulting from the good mechanical stability of PANCMA micorfibers on the probe and the good intrinsic stability of aptamer conjugated on the surface of PANCMA. In addition, the thrombin recovery at a concentration level of 5.0 nM spiked in PBS buffer on Apt-SPME probe maintained about 80% after 40 times reuse for the extraction of thrombin from diluted human plasma samples, which indicated that the Apt-SPME probe was stable and could be repeatedly used for more than 40 purification circles in the extraction of analytes from real samples.
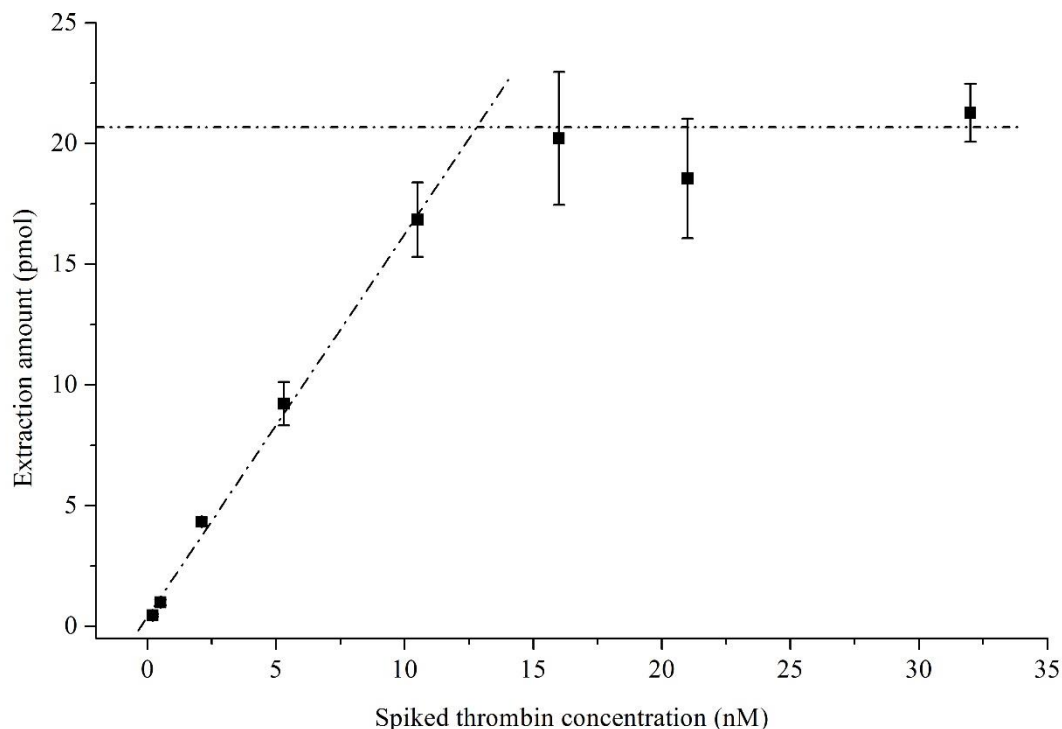
Figure 6-10. Variation extraction amount of thrombin obtained with Apt-PANCMA *probe* at different amounts spiked into 2.0 mL of PBS buffer samples.

6. 4. 5. *Application of the* Apt-PANCMA-probe-*LC-MS/MS to complex sample*

The proposed Apt-SPME-probe combining with LC-MS/MS method developed above were applied for the determination of thrombin in clinical human plasma samples. Considering the matrix effect of diluted human plasma on the determination of thrombin, the concentration of thrombin in human plasma samples was determined by the linear regression equation based on the thrombin recovery. Table 6-1 shows that thrombin concentrations were found to be different in different clinical human plasma. According to the results of Table 6-1, the thrombin concentrations were about 248 and 285 nM in undiluted plasma samples before and during bypass surgery, respectively, which was beneficial to help control bleeding during bypass surgery.[158] The above

results suggested that the proposed Apt-SPME-probe-LC-MS/MS method was valid in the determination of thrombin in human plasma samples.

Table 6-1. Results of thrombin concentration in selected human plasma samples (n=3)[a]

Sample	Detected concentration in the 20-fold diluted plasma sample (nM)
Human plasma (Before bypass surgery)	12.38±0.87
Human plasma (During bypass surgery)	14.23±0.62
Human plasma (After bypass surgery)	4.09±0.41
Human plasma from LBL Inc.	—[b]

[a]*Note*: The detected concentration was calculated by the calibration curve based on the recovery of thrombin (see Fig. 6). [b] "—" means "Not detected".

6.5   Summary

A novel selective SPME probe based on the covalent immobilization of aptamer on electrospun PANCMA micro-fiber was developed to enrich thrombin from human plasma samples. Due to high surface area and high selective recognition, the prepared Apt-SPME probe has been shown to be a suitable selective SPME coating for extracting trace thrombin from samples. Under the optimal conditions, the Apt-SPME probes were used to directly extract thrombin from diluted human plasma without any further sample preparation, and were stable enough for more than 40 replicate extraction cycles in the analysis of real samples. The employed LC-MS/MS analysis helped to improve the sensitivity and accuracy of the whole assay, enabling the identification and quantification of trace thrombin from complex clinical samples. The proposed Apt-SPME probe coupled with LC-MS/MS method was successfully applied for the determination of thrombin in human plasma samples, which demonstrated that the proposed method was a promising for selective determination of trace proteins in clinical biological samples.

Upon further optimization of the probe in terms of matrix effects and biocompatibility, this approach can be used for in vivo protein extraction from human blood. Moreover, this selective SPME can be combined directly with mass spectrometry to provide simple, high throughput diagnostic tool in biomedicine by eliminating most of the matrix interferences from body fluids without the time consuming chromatography steps.

Chapter 7   **Conclusions and Future direction**

In this thesis, computational models of mass and momentum transport, partitions and reactions involved in the SPME methods of sample preparation were developed. The mechanistic-based models describe the uptake kinetics of analytes from both a standard solution and a complex binding matrix containing sample. The proposed mathematical models can be used as a reliable and inexpensive predictive tool of SPME method development. With the help of these models, one can easily determine whether the presence of a binding matrix can alter the equilibrium time, based on the physicochemical properties of analyte and matrix, as well as the choice of SPME coatings. The modeling has demonstrated that the decrease in equilibration time is not only due to increased rate of extraction but also to the requirement of less extracted amount to reach equilibrium when binding matrix is present. In addition, determination of binding constants and associated kinetics can be obtained from experimental data by appropriate fit of calculated values.

A comprehensive study on the calibrant-loaded extraction phase approach for quantitative chemical studies has been demonstrated with both experimental data and a computational model. The results demonstrated that this CL-EP approach might solve the complexity due to the *in-vivo* or *in-situ* sample environment compared with the simplified in-vitro release measurements carried out in buffer solutions. In particular, for a hydrophobic calibrant, where the calibrant release in the buffer is small or negligible, interactions with binding matrix components in real complex samples can alter the desorption profiles greatly. However, despite this complexity, the calibrant-loaded approach performs the necessary corrections while providing both free and total concentrations. The model can be used to predict desorption rate constants, which are needed for CL-EP quantification, of a wide range of target analytes with the use of only one calibrant for the

correction of mass transfer properties, which is advantageous in cases where isotopically-labelled calibrants are unavailable or their use not feasible.

A mechanistic model was also proposed to quantitatively describe extraction by porous particle based solid coatings and their application in pre-equilibrium based rapid and direct extraction of analyte with SPME. It was demonstrated that analyte flux is proportional to diffusion coefficient of analyte and fluid flow velocity at the early stage of extraction. The model demonstrated excellent prediction of the effect of mass transfer caused by the variation of fluid flow on the extraction rate in the SPME sampling. Therefore, with the aid of the model, estimation of sampling time and calibration of the rapid sampling based on diffusion is possible within short time and low cost. In addition, optimization of flow velocity and maximum extraction capacity can be evaluated for wide range of analytes with varied equilibrium constant values (K). Overall, the simulation results provide detail understanding of employing porous particle based solid coating in SPME.

Finally, a novel selective SPME coating based on the immobilization of a DNA aptamer was developed to enrich thrombin from human plasma samples. Due to high surface area and high selective recognition, the prepared Apt-SPME probe has been shown to be a suitable selective SPME coating for extracting trace thrombin from samples. Under the optimal conditions, the Apt-SPME probes were used to directly extract thrombin from diluted human plasma without any further sample preparation, and were stable enough for more than 40 replicate extraction cycles in the analysis of real samples.

In future, *in-silico* optimization of experimental conditions for both liquid and solid coatings can be performed with the help of the computational models described in this thesis. However, for biomedical applications such as human blood or tissue sampling with SPME, further improvement of the model to describe multicomponent phenomena is needed. Upon further optimization of the selective aptamer based probe in terms of matrix effects and biocompatibility, *in vivo* protein extraction and quantification from biological sample is possible. The selective and high affinity coating might allow rapid diffusion based calibration for bed-side diagnostics. Moreover, this selective SPME can be combined directly with mass spectrometry to provide simple, high throughput diagnostic tool in biomedicine by eliminating most of the matrix interferences from body fluids without the time consuming chromatography steps.

References

(1) Gomez-Rios, G. A.; Pawliszyn, J. *Angew. Chem. Int. Ed. Engl.* **2014**, *53*, 14503-14507.

(2) Bojko, B.; Cudjoe, E.; Gomez-Rios, G. A.; Gorynski, K.; Jiang, R.; Reyes-Garces, N.; Risticevic, S.; Silva, E. A.; Togunde, O.; Vuckovic, D.; Pawliszyn, J. *Anal. Chim. Acta* **2012**, *750*, 132-151.

(3) Płotka-Wasylka, J.; Szczepańska, N.; de la Guardia, M.; Namieśnik, J. *TrAC, Trends Anal. Chem.* **2015**, *73*, 19-38.

(4) Padron, M. E.; Afonso-Olivares, C.; Sosa-Ferrera, Z.; Santana-Rodriguez, J. J. *Molecules* **2014**, *19*, 10320-10349.

(5) Souza-Silva, É. A.; Jiang, R.; Rodríguez-Lafuente, A.; Gionfriddo, E.; Pawliszyn, J. *TrAC, Trends Anal. Chem.* **2015**, *71*, 224-235.

(6) Souza-Silva, É. A.; Reyes-Garcés, N.; Gómez-Ríos, G. A.; Boyacı, E.; Bojko, B.; Pawliszyn, J. *TrAC, Trends Anal. Chem.* **2015**, *71*, 249-264.

(7) Souza-Silva, É. A.; Gionfriddo, E.; Pawliszyn, J. *TrAC, Trends Anal. Chem.* **2015**, *71*, 236-248.

(8) Wen, Y.; Chen, L.; Li, J.; Liu, D.; Chen, L. *TrAC, Trends Anal. Chem.* **2014**, *59*, 26-41.

(9) Zaitsev, V. N.; Zui, M. F. *J. Anal. Chem.* **2014**, *69*, 715-727.

(10) Leo, A.; Hansch, C.; Elkins, D. *Chem. Rev.* **1971**, *71*, 525-612.

(11) Pereira, J.; Silva, C. L.; Perestrelo, R.; Goncalves, J.; Alves, V.; Camara, J. S. *Anal. Bioanal. Chem.* **2014**, *406*, 2101-2122.

(12) Brunetti, A. E.; Merib, J.; Carasek, E.; Caramao, E. B.; Barbara, J.; Zini, C. A.; Faivovich, J. *J. Chem. Ecol.* **2015**, *41*, 360-372.

(13) Wang, S.; Oakes, K. D.; Bragg, L. M.; Pawliszyn, J.; Dixon, G.; Servos, M. R. *Chemosphere* **2011**, *85*, 1472-1480.

(14) Nicolle, J.; Desauziers, V.; Mocho, P. *J. Chromatogr. A* **2008**, *1208*, 10-15.

(15) Louch, D.; Motlagh, S.; J., P. *Anal. Chem.* **1992**, *64*, 1187-1199.

(16) Liu, C.; Shi, S.; Weschler, C.; Zhao, B.; Zhang, Y. *Aerosol Sci. Technol.* **2013**, *47*, 125-136.

(17) Pigeonneau, F.; Jaffrennou, B.; Letailleur, A.; Limouzin, K. *Int. J. Heat Mass Transfer* **2016**, *96*, 381-395.

(18) Zhang, Y.; Xiong, J.; Mo, J.; Gong, M.; Cao, J. *Indoor air* **2016**, *26*, 39-60.

(19) Kang, D. H.; Choi, D. H.; Seong, Y.-B.; Yeo, M. S.; Kim, K. W. *Building and Environment* **2013**, *68*, 193-201.

(20) Zhan, L.-t.; Zeng, X.; Li, Y.; Chen, Y. *J. Environ. Engin.* **2014**, *140*, 57-68.

(21) Hu, G.; Gao, Y.; Li, D. *Biosens. Bioelectron.* **2007**, *22*, 1403-1409.

(22) Jason Li, Y. Z., Steve To, Lidan You, and Yu Sun. **2011**.

(23) Leary, T. F.; Manafirasi, S.; Maldarelli, C. *Lab Chip* **2015**, *15*, 459-477.

(24) Harraz, A. A.; El Gheriany, I. A.; Abdel-Aziz, M. H.; Zewail, T. M.; Konsowa, A. H.; Sedahmed, G. H. *Biochem. Eng. J.* **2015**, *103*, 1-11.

(25) Carslaw, H. S.; Jaeger, J. C. *Conduction of Heat in Solids*, 2nd Edition ed.; Clarendon Press: Oxford, 1986.

(26) Koziel, J.; Jia, M.; Pawliszyn, J. *Anal. Chem.* **2000**, *72*, 5178-5186.

(27) Garcia-Penarrubia, P.; Galvez, J. J.; Galvez, J. *J Math Biol* **2014**, *69*, 553-582.

(28) Tayi, V. S.; Bowen, B. D.; Piret, J. M. *Biotechnol. Bioeng.* **2010**, *105*, 195-209.

(29) Bansal, P.; Hall, M.; Realff, M. J.; Lee, J. H.; Bommarius, A. S. *Biotechnol. Adv.* **2009**, *27*, 833-848.

(30) Mao, Y.-F.; Li, Z.; He, Y.-L.; Tao, W.-Q. *Int. J. Heat Mass Transfer* **2016**, *99*, 613-621.

(31) Liang, Y.; Xu, Y. *Atmos. Environ.* **2015**, *103*, 147-155.

(32) Sigurdson, M.; Wang, D.; Meinhart, C. D. *Lab on a chip* **2005**, *5*, 1366-1373.

(33) Hale, S. E.; Martin, T. J.; Goss, K. U.; Arp, H. P.; Werner, D. *Environ. Pollut.* **2010**, *158*, 2511-2517.

(34) Chen, Y.; Koziel, J. A.; Pawliszn, J. *Anal. Chem.* **2003**, *75*, 6485-6493.

(35) Hilpert, R. *Forsch. Geb. Ingenieurwes* **1933**, *4*, 215.

(36) Noguchi, M.; Yamasaki, A. *Building and Environment* **2016**, *100*, 197-202.

(37) Altinkaya, S. A. *Chem. Eng. J.* **2009**, *155*, 586-593.

(38) Martos, P. A.; Pawliszn, J. *Anal. Chem.* **1999**, *71*, 1513-1520.

(39) Fernandez, L. A.; Harvey, C. F.; Gschwend, P. M. *Environ. Sci. Technol.* **2009**, *43*, 8888-8894.

(40) Huckins, J. N.; Petty, J. D.; Orazio, C. E.; Lebo, J. A.; Clark, R. C.; Gibson, V. L.; Gala, W. R.; Echols, K. R. *Environ. Sci. Technol.* **1999**, *33*, 3918-3923.

(41) Chang, W. T.; Lee, C. L.; Brimblecombe, P.; Fang, M. D.; Chang, K. T.; Liu, J. T. *Mar. Pollut. Bull.* **2015**, *97*, 217-223.

(42) Shaw, M.; Mueller, J. F. *Environ. Sci. Technol.* **2009**, *43*, 1443–1448.

(43) Petersen, J.; Paschke, A.; Gunold, R.; Schüürmann, G. *Environ. Sci.: Water Res. Technol.* **2015**, *1*, 218-226.

(44) Estoppey, N.; Schopfer, A.; Omlin, J.; Esseiva, P.; Vermeirssen, E. L.; Delemont, O.; De Alencastro, L. F. *Sci. Total Environ.* **2014**, *499*, 319-326.

(45) Birch, H.; Sharma, A. K.; Vezzaro, L.; Lutzhoft, H. C.; Mikkelsen, P. S. *Environ. Sci. Technol.* **2013**, *47*, 12958-12965.

(46) Vermeirssen, E. L.; Asmin, J.; Escher, B. I.; Kwon, J. H.; Steimen, I.; Hollender, J. *J. Environ. Monit.* **2008**, *10*, 119-128.

(47) Vrana, B.; Mills, G. A.; Kotterman, M.; Leonards, P.; Booij, K.; Greenwood, R. *Environ. Pollut.* **2007**, *145*, 895-904.

(48) Tcaciuc, A. P.; Apell, J. N.; Gschwend, P. M. *Environ. Toxicol. Chem.* **2015**, *34*, 2739-2749.

163

(49) Lampert, D. J.; Thomas, C.; Reible, D. D. *Chemosphere* **2015**, *119*, 910-916.

(50) Pascoal, A. D. S. M. R.; da Silva, P. M.; Coelho Pinheiro, M. N. *International Communications in Heat and Mass Transfer* **2015**, *61*, 118-127.

(51) Perez, M.; Reynaud, S.; Lespes, G.; Potin-Gautier, M.; Mignard, E.; Chery, P.; Schaumloffel, D.; Grassl, B. *Anal. Chim. Acta* **2015**, *890*, 117-123.

(52) Deng, B.; Zhang, B.; Qiu, Y. *Building and Environment* **2016**, *104*, 145-151.

(53) Ai, J. *Analytical chemistry* **1997**, *69*, 1230-1236.

(54) Vrana, B.; Schuurmann, G. *Environ. Sci. Technol.* **2002**, *36*, 290-296.

(55) Zhou, S. N.; Zhang, X.; Ouyang, G.; Es-haghi, A.; Pawliszyn, J. *Anal. Chem.* **2007**, *79*, 1221.

(56) Vaes, W. H. J.; Hermens, J. L. M.; Ramos, U.; Verhaar, H. J. M.; Seinen, W. *Anal. Chem.* **1996**, *68*, 4463-4467.

(57) Tang, S.; Zhang, H.; Lee, H. K. *Anal. Chem.* **2016**, *88*, 228-249.

(58) Pawliszyn, J. *Solid Phase Microextraction: Theory and Practice*; Wiley−VCH: New York, 1997.

(59) Lao, W.; Maruya, K. A.; Tsukada, D. *Anal. Chem.* **2012**, *84*, 9362-9369.

(60) van Eijkeren, J. C.; Heringa, M. B.; Hermens, J. L. *The Analyst* **2004**, *129*, 1137-1142.

(61) Heringa, M. B.; Hogevonder, C.; Busser, F.; Hermens, J. L. *J Chromatogr B Analyt Technol Biomed Life Sci* **2006**, *834*, 35-41.

(62) Lee, G.; Park, I.; Kwon, K.; Kwon, T.; Seo, J.; Chang, W. J.; Nam, H.; Cha, G. S.; Choi, M. H.; Yoon, D. S.; Lee, S. W. *Biomed. Microdevices* **2012**, *14*, 375-384.

(63) Yang, C.-K.; Chang, J.-S.; Chao, S. D.; Wu, K.-C. *J. Appl. Phys.* **2008**, *103*, 084702.

(64) Siepmann, J.; Siepmann, F. *Int. J. Pharm.* **2008**, *364*, 328-343.

(65) Shirazian, S.; Pishnamazi, M.; Rezakazemi, M.; Nouri, A.; Jafari, M.; Noroozi, S.; Marjani, A. *Chemical Engineering & Technology* **2012**, n/a-n/a.

164

(66) Gervais, T.; Jensen, K. F. *Chem. Eng. Sci.* **2006**, *61*, 1102-1121.

(67) Derksen, J. J. *Microfluidics and Nanofluidics* **2014**, *18*, 829-839.

(68) Ogawa, A. *Vortex Flow*; CRC Press: Boca Raton, Florida, 1993.

(69) Bird, R. B. S., W. E.; Lightfoot, E. N. *Transport Phenomena*, 2nd ed ed.; Wiley & Sons: New York, 2002.

(70) Datta, A.; Rakesh, V. *An Introduction to Modeling of Transport Processes*, 1st ed ed.; Cambridge University Press: New York, 2010.

(71) Ellis, J. S.; Strutwolf, J.; Arrigan, D. W. *Phys. Chem. Chem. Phys.* **2012**, *14*, 2494-2500.

(72) Thompson, J. A.; Bau, H. H. *J Chromatogr B Analyt Technol Biomed Life Sci* **2010**, *878*, 228-236.

(73) Crank, J. *The Mathematics of Diffusion*, 2nd ed ed.; Oxford

University Press: Oxford, U.K., 1975.

(74) Heringa M.B. , H. J. L. M. TrAC, *Trends Anal. Chem.* **2003**, *22*.

(75) Kopinke, F. D.; Ramus, K.; Poerschmann, J.; Georgi, A. *Environ. Sci. Technol.* **2011**, *45*, 10013-10019.

(76) Minne B. Heringa, D. P., Jon Algra, Wouter H. J. Vaes, and Joop L. M. Hermens. *Anal. Chem.* **2002**.

(77) Vulic, K.; Pakulska, M. M.; Sonthalia, R.; Ramachandran, A.; Shoichet, M. S. *J Control Release* **2015**, *197*, 69-77.

(78) Kramer, N. I.; H., E. J. C.; M., H. J. L. *Anal. Chem.* **2007**, *79*, 6941-6948.

(79) Broeders, J. J.; Blaauboer, B. J.; Hermens, J. L. *J. Chromatogr. A* **2011**, *1218*, 8529-8535.

(80) Liu, C.; Morrison, G. C.; Zhang, Y. *Atmos. Environ.* **2012**, *55*, 347-356.

(81) Mayer, P.; Karlson, U. G.; Christensen, P. S.; Johnsen, A. R.; Trapp, S. *Environ. Sci. Technol.* **2005**, *39*, 6123-6129.

(82) Poerschmann, J.; KOPINKE, F.; PAWLISZYN, J. *Environ. Sci. Technol.* **1997**, *31*, 3629-3636.

(83) Reyes-Garces, N.; Bojko, B.; Pawliszyn, J. *J. Chromatogr. A* **2014**, *1374*, 40-49.

(84) Ramos, E. U.; Meijer, S. N.; Vaes, W. H. J.; Verhaar, H. J. M.; Hermens, J. L. M. *Environ. Sci. Technol.* **1998**, 3430-3435.

(85) Oomen, A. G.; Mayer, P.; Tolls, J. *Anal. Chem.* **2000**, *72*, 2802-2808.

(86) Ouyang, G.; Pawliszyn, J. *Anal. Chim. Acta* **2008**, *627*, 184-197.

(87) Ter laak, T. L.; Busser, F. J. M.; Hermens, J. L. M. *Anal. Chem.* **2008**, *80*, 3859–3866.

(88) Kadam, A. A.; Karbowiak, T.; Voilley, A.; Debeaufort, F. *J. Sci. Food Agric.* **2015**, *95*, 1395-1407.

(89) Liang, Y. *Geochim. Cosmochim. Acta* **2014**, *132*, 274-287.

(90) Chen, Y.; Pawliszn, J. *Anal. Chem.* **2004**, *76*, 5807-5815.

(91) Zhou, N. S.; Zhang, X.; Ouyang, G.; Es-haghi, A.; Pawliszyn, J. *Anal. Chem.* **2007**, *79*, 1221-1230.

(92) Cui, X.; Bao, L.; Gan, J. *Environ. Sci. Technol.* **2013**, *47*, 9833-9840.

(93) Xu, B.; Chen, M.; Hou, J.; Chen, X.; Zhang, X.; Cui, S. *J Chromatogr B Analyt Technol Biomed Life Sci* **2015**, *980*, 28-33.

(94) Zhang, X.; Oakes, K. D.; Hoque, M. E.; Luong, D.; Metcalfe, C. D.; Pawliszyn, J.; Servos, M. R. *Anal. Chem.* **2011**, *83*, 3365-3370.

(95) Booij, K.; Tucca, F. *Mar. Pollut. Bull.* **2015**, *98*, 365-367.

(96) Alam, M. N.; Ricardez-Sandoval, L.; Pawliszyn, J. *Anal. Chem.* **2015**, *87*, 9846-9854.

(97) Siepmann, J.; Siepmann, F. *J Control Release* **2012**, *161*, 351-362.

(98) Xiong, J.; Wang, L.; Bai, Y.; Zhang, Y. *Building and Environment* **2013**, *66*, 65-71.

(99) Liu, Z.; Ye, W.; Little, J. C. *Building and Environment* **2013**, *64*, 7-25.

(100) Endo, S.; Yuyama, M.; Takada, H. *Mar. Pollut. Bull.* **2013**, *74*, 125-131.

(101) Holmgren, T.; Persson, L.; Andersson, P. L.; Haglund, P. *Sci. Total Environ.* **2012**, *437*, 306-314.

(102) Sedahmed, G. H.; El-Taweel, Y. A.; Abdel-Aziz, M. H.; El-Naqeara, H. M. *Chemical Engineering and Processing: Process Intensification* **2014**, *80*, 43-50.

(103) Fu, A. S.; Thatiparti, T. R.; Saidel, G. M.; von Recum, H. A. *Ann Biomed Eng* **2011**, *39*, 2466-2475.

(104) Yang, K.; Wu, J. *Biomicrofluidics* **2010**, *4*.

(105) Munir, A.; Wang, J.; Li, Z.; Zhou, H. S. *Microfluidics and Nanofluidics* **2009**, *8*, 641-652.

(106) Levich, V. *Physicochemical Hydrodynamics*; Prentice Hall: Englewood Cliffs, NJ, 1962.

(107) Thompson, J. M.; Hsieh, C. H.; Luthy, R. G. *Environ. Sci. Technol.* **2015**, *49*, 2270-2277.

(108) Mayer, P.; Tolls, J.; Hermens, J. L.; Mackay, D. *Environ. Sci. Technol.* **2003**, *37*, 184A–191A.

(109) Wang, Y.; O'Reilly, J.; Chen, Y.; Pawliszyn, J. *J. Chromatogr. A* **2005**, *1072*, 13-17.

(110) Zhao, W.; Ouyang, G.; Alaee, M.; Pawliszyn, J. *J. Chromatogr. A* **2006**, *1124*, 112-120.

(111) Ouyang, G.; Cui, S.; Qin, Z.; Pawliszyn, J. *Anal. Chem.* **2009**, *81*, 5629–5636.

(112) Benhabib, K.; ter Laak, T. L.; van Leeuwen, H. P. *Anal. Chim. Acta* **2008**, *609*, 113-119.

(113) Benhabib, K.; Town, R., M; Leeuwen, H. P. *Langmuir* **2009**, *25*, 3381-3386.

(114) Jiang, R.; Xu, J.; Zhu, F.; Luan, T.; Zeng, F.; Shen, Y.; Ouyang, G. *J. Chromatogr. A* **2015**, *1411*, 34-40.

(115) Du, F.; Alam, M. N.; Pawliszyn, J. *Anal. Chim. Acta* **2014**, *845*, 45-52.

(116) Sukola, K.; Koziel, J.; Augusto, F.; Pawliszn, J. *Anal. Chem.* **2001**, *73*, 13-18.

(117) Huang, X.; Ye, H.; Yam, K. L. *Mathematical Problems in Engineering* **2013**, *2013*, 1-10.

(118) Allan, I. J.; Harman, C.; Kringstad, A.; Bratsberg, E. *Chemosphere* **2010**, *79*, 470-475.

(119) Górecki, T.; Yu, X.; Pawliszyn, J. *The Analyst* **1999**, *124*, 643-649.

(120) Semenov, S. N.; Koziel, J. A.; Pawliszyn, J. *J. Chromatogr. A* **2000**, *873*, 39.

(121) Murthy, C. R.; Armani, A. M. *Sensors (Basel)* **2012**, *12*, 14327-14343.

(122) Squires, T. M.; Messinger, R. J.; Manalis, S. R. *Nat. Biotechnol.* **2008**, *26*, 417-426.

(123) Zhang, W.; Stone, H. A.; Sherwood, J. D. *J. Phys. Chem. A* **1996**, *100*, 9462-9464.

(124) Risticevic, S.; Pawliszyn, J. *Anal. Chem.* **2013**, *85*, 8987-8995.

(125) Gionfriddo, E.; Souza-Silva, E. A.; Pawliszyn, J. *Anal. Chem.* **2015**, *87*, 8448-8456.

(126) Martín-Esteban, A. *TrAC, Trends Anal. Chem.* **2013**, *45*, 169-181.

(127) Chen, L.; Xu, S.; Li, J. *Chem. Soc. Rev.* **2011**, *40*, 2922-2942.

(128) Yuan, H.; Mullett, W. M.; Pawliszyn, J. *The Analyst* **2001**, *126*, 1456-1461.

(129) Queiroz, M. E.; Oliveira, E. B.; Breton, F.; Pawliszyn, J. *J. Chromatogr. A* **2007**, *1174*, 72-77.

(130) Song, S.; Wang, L.; Li, J.; Fan, C.; Zhao, J. *TrAC, Trends Anal. Chem.* **2008**, *27*, 108-117.

(131) Hamula, C.; Guthrie, J.; Zhang, H.; Li, X.; Le, X. *TrAC, Trends Anal. Chem.* **2006**, *25*, 681-691.

(132) Balamurugan, S.; Obubuafo, A.; Soper, S. A.; Spivak, D. A. *Anal. Bioanal. Chem.* **2008**, *390*, 1009-1021.

(133) Ruta, J.; Ravelet, C.; Desire, J.; Decout, J. L.; Peyrin, E. *Anal. Bioanal. Chem.* **2008**, *390*, 1051-1057.

(134) Peyrin, E. *J. Sep. Sci.* **2009**, *32*, 1531-1536.

(135) Liu, J.; Wagan, S.; Davila Morris, M.; Taylor, J.; White, R. J. *Anal. Chem.* **2014**, *86*, 11417-11424.

(136) Sivanesan, A.; Izake, E. L.; Agoston, R.; Ayoko, G. A.; Sillence, M. *J. Nanobiotech.* **2015**, *13*, 43.

(137) Lee, W.-B.; Chen, Y.-H.; Lin, H.-I.; Shiesh, S.-C.; Lee, G.-B. *Sensors and Actuators B: Chemical* **2011**, *157*, 710-721.

(138) Płotka-Wasylka, J.; Szczepańska, N.; de la Guardia, M.; Namieśnik, J. *TrAC, Trends Anal. Chem.* **2016**, *77*, 23-43.

(139) Du, F.; Guo, L.; Qin, Q.; Zheng, X.; Ruan, G.; Li, J.; Li, G. *TrAC, Trends Anal. Chem.* **2015**, *67*, 134-146.

(140) Pichon, V.; Brothier, F.; Combes, A. *Anal. Bioanal. Chem.* **2015**, *407*, 681-698.

(141) Li, J.; Chang, K. W.; Wang, C. H.; Yang, C. H.; Shiesh, S. C.; Lee, G. B. *Biosens. Bioelectron.* **2016**, *79*, 887-893.

(142) Sun, C.; Zhang, R.; Gao, M.; Zhang, X. *Anal. Bioanal. Chem.* **2015**, *407*, 8883-8892.

(143) Citartan, M.; Ch'ng, E.-S.; Rozhdestvensky, T. S.; Tang, T.-H. *Microchem. J.* **2016**, *128*, 187-197.

(144) Ilgu, M.; Nilsen-Hamilton, M. *The Analyst* **2016**, *141*, 1551-1568.

(145) Sun, H.; Zu, Y. *Molecules* **2015**, *20*, 11959-11980.

(146) Nie, F.; Xua, Z. K.; Wana, L. S.; Yea, P.; Wu, J. *J. Membr. Sci.* **2004**, *230*, 1-11.

(147) Zewe, J. W.; Steach, J. K.; Olesik, S. V. *Anal. Chem.* **2010**, *82*, 5348.

(148) Shi, Y.; Wang, H.; Jiang, X.; Sun, B.; Song, B.; Su, Y.; He, Y. *Anal. Chem.* **2016**, *88*, 3723-3729.

(149) Zhang, X.; Zhu, S.; Deng, C.; Zhang, X. *Talanta* **2012**, *88*, 295-302.

(150) Huang, Y. C.; Ge, B.; Sen, D.; Yu, H. Z. *J. Am. Chem. Soc.* **2008**, *130*, 8023–8029.

(151) Zhao, Q.; Li, X. F.; Shao, Y.; Le, X. C. *Anal. Chem.* **2008**, *80*, 7586–7593.

(152) Fischer, N. O.; Tarasow, T. M.; Tok, J. B. *Anal. Biochem.* **2008**, *373*, 121-128.

(153) de la Escosura-Muniz, A.; Chunglok, W.; Surareungchai, W.; Merkoci, A. *Biosens. Bioelectron.* **2013**, *40*, 24-31.

(154) Feyzizarnagh, H.; Haushalter, E. F.; Grams, E. K.; Cameron, B. D.; Yoon, D.-Y.; Kim, D.-S. *Industrial & Engineering Chemistry Research* **2015**, *54*, 4072-4077.

(155) Zhao, Q.; Li, X. F.; Le, X. C. *Anal. Chem.* **2011**, *83*, 9234-9236.

(156) Xiang, D.; Shigdar, S.; Qiao, G.; Wang, T.; Kouzani, A. Z.; Zhou, S. F.; Kong, L.; Li, Y.; Pu, C.; Duan, W. *Theranostics* **2015**, *5*, 23-42.

(157) Jolly, P.; Tamboli, V.; Harniman, R. L.; Estrela, P.; Allender, C. J.; Bowen, J. L. *Biosens. Bioelectron.* **2016**, *75*, 188-195.

(158) Li, J.; Zhong, X.; Zhang, H.; Le, X. C.; Zhu, J. J. *Anal. Chem.* **2012**, *84*, 5170-5174.

Copyright
Clearance
Center

RightsLink®

ACS Publications
Most Trusted. Most Cited. Most Read.

Title:	Air Sampling with Porous Solid-Phase Microextraction Fibers
Author:	Jacek Koziel, Mingyu Jia, Janusz Pawliszyn
Publication:	Analytical Chemistry
Publisher:	American Chemical Society
Date:	Nov 1, 2000

Copyright © 2000, American Chemical Society

PERMISSION/LICENSE IS GRANTED FOR YOUR ORDER AT NO CHARGE

This type of permission/license, instead of the standard Terms & Conditions, is sent to you because no fee is being charged for your order. Please note the following:

- Permission is granted for your request in both print and electronic formats, and translations.
- If figures and/or tables were requested, they may be adapted or used in part.
- Please print this page for your records and send a copy of it to your publisher/graduate school.
- Appropriate credit for the requested material should be given as follows: "Reprinted (adapted) with permission from (COMPLETE REFERENCE CITATION). Copyright (YEAR) American Chemical Society." Insert appropriate information in place of the capitalized words.
- One-time permission is granted only for the use specified in your request. No additional uses are granted (such as derivative works or other editions). For any other uses, please submit a new request.

If credit is given to another source for the material you requested, permission must be obtained from that source.

BACK   **CLOSE WINDOW**

ACS Publications
Most Trusted. Most Cited. Most Read.

Title: Calibration for On-Site Analysis of Hydrocarbons in Aqueous and Gaseous Samples Using Solid-Phase Microextraction

Author: Yong Chen, Jacek A. Koziel, Janusz Pawliszyn

Publication: Analytical Chemistry

Publisher: American Chemical Society

Date: Dec 1, 2003

Copyright © 2003, American Chemical Society

PERMISSION/LICENSE IS GRANTED FOR YOUR ORDER AT NO CHARGE

BACK | CLOSE WINDOW

173